DETERMINATION OF HORIZONTAL STRESS IN SOILS

August 1981
Final Report
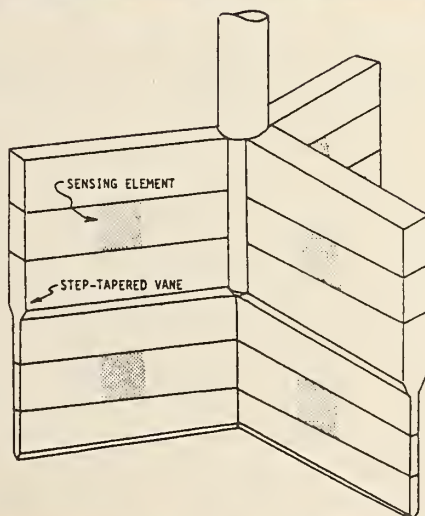
SENSING ELEMENT

STEP-TAPERED VANE

Prepared for
FEDERAL HIGHWAY ADMINISTRATION
Offices of Research & Development
Materials Division
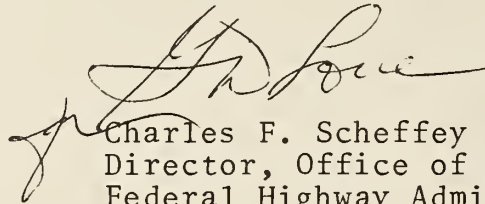Washington, D.C. 20590

FOREWORD

This report presents the results of a 2-year study which led to
the development of a lateral stress sensor and test methods for
determining the horizontal stress in soils in-situ.

The study included laboratory and field tests in several different
soil types and comparisons between lateral stress measurements
obtained with a self boring pressuremeter and the lateral stress
sensor. The results indicate that reliable measurements of lateral
stress can be made quickly and simply.

The work reported resulted from FCP Project 5B Study, 35B2-552,
"Measuring and Testing Techniques for Determination of the In-Situ
State of Stress in Soils," conducted by Soils Systems, Inc.,
Marietta, Georgia. The research was performed under DOT-FH-11-9172,
during the period September 28, 1976, to March 31, 1979.

Copies of the final report are being distributed by the Office of
Research, Materials Division, to other researchers and to appropriate
members of the FCP Project 5B Team.

Charles F. Scheffey
Director, Office of Research
Federal Highway Administration

NOTICE

Technical Report Documentation Page

1. Report No. FHWA/RD-81/118	2. Government Accession No.	3. Recipient's Catalog No.
4. Title and Subtitle Determination of Horizontal Stress in Soils		5. Report Date August 1981
		6. Performing Organization Code
7. Author(s) Dr. N. S. Fox, Dr. R. L. Handy, Gary D. Trott Bernard Remmes, Steven Moldt		8. Performing Organization Report No.
9. Performing Organization Name and Address Soil Systems, Inc. 525 Webb Industrial Drive Marietta, Georgia 30062		10. Work Unit No. (TRAIS) 35B2-552
		11. Contract or Grant No. DOT-FH-11-9172
12. Sponsoring Agency Name and Address Offices of Research and Development Federal Highway Administration U. S. Department of Transportation Washington, D.C. 20590		13. Type of Report and Period Covered Final Report
		14. Sponsoring Agency Code M/0706

15. Supplementary Notes

FHWA Contract Manager: Carl Ealy   (HRS-21)

16. Abstract

This research involves calculating the state of stress in a soil mass by recognizing that disturbance during testing or measuring is inevitable. Thin blades with teflon-diaphragm pneumatic stress cells have been developed for this research to measure soil stresses. Soil stresses on the blade were found to be a function of blade thickness. An exponential relationship between blade thickness and soil stresses was determined to exist except in hard soils with thick (1/4 inch) blades.

Pressuremeter data from two test sites, one in Glacial till and loess, the other in expansive clay, indicated very close agreement with blade stress results. The blade was easier to use than the pressuremeter and because of its statistical advantage (many more test results per day) is more precise.

A three-bladed stepped vane with nine pressure cells has been successfully designed, built, and tested in preliminary trials. Use of this instrument will result in the measurement of a two dimensional soil stress state.

17. Key Words		18. Distribution Statement No restrictions. This document is available to the public through the National Technical Information Service, Springfield, Virginia 22161.
19. Security Classif. (of this report) Unclassified	20. Security Classif. (of this page) Unclassified	21. No. of Pages 205 22. Price

Form DOT F 1700.7 (8-72)   Reproduction of completed page authorized

TABLE OF CONTENTS

LIST OF FIGURES

Page

LIST OF TABLES

INTRODUCTION

Because of increasing emphasis on urban mass transit, in 1976 the
Transportation Research Board prepared a special report (30) on tunnel
construction. The report was a state-of-the-art paper, and recommended
present and future research needs. One such need is to better predict
loads on structural supports in tunnels. Up until now, design of
supports has depended to a great extent on the ability of the engineer
to convert limited geological data into practical information. If the
engineer overestimates loads, the design is uneconomical; if he under-
estimates, yielding in the structure can result. This yielding can
cause excessive ground movement and increase underpinning requirements
for adjacent structures.

Being able to calculate the state of the stresses in a soil mass
is of considerable importance to geotechnical engineers. For example,
a safe and economical design of a pile or deep foundation requires that
the engineer have a working knowledge of the in situ stresses in a
soil mass. The accuracy with which an engineer estimates the lateral
stresses that act upon a retaining wall will affect his final design.
Use of the finite element method of analysis in geomechanics is
severely limited by the engineer's ability to estimate initial in situ
stresses.

A number of schemes have been devised to measure in situ stresses
in soils, illustrated in Figure 1. Hydraulic fracturing consists of
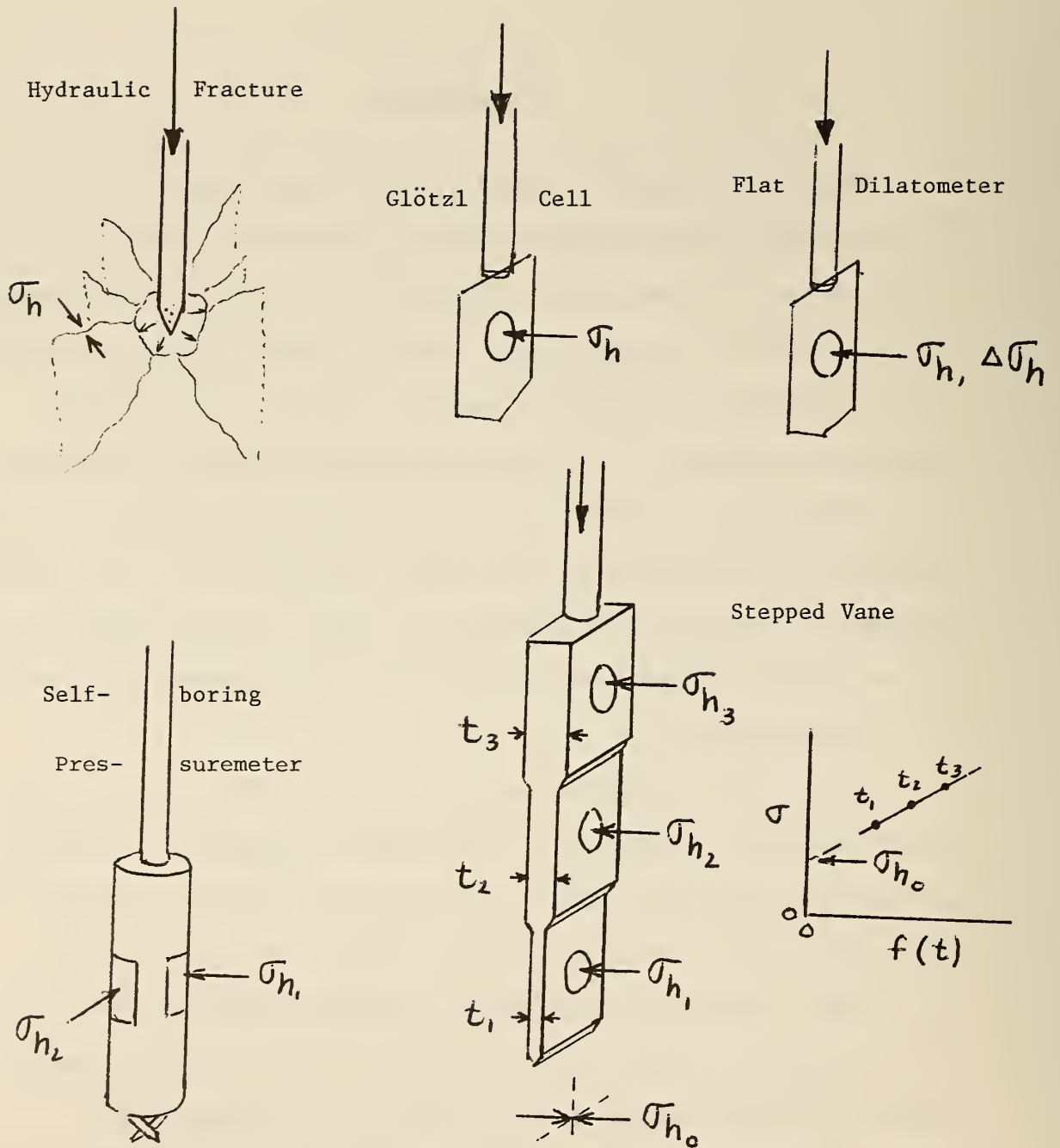
Figure 1. Methods for evaluating horizontal in situ soil stress.

pumping water into a piezometer with gradually increasing pressure while monitoring the pumping rate, a sudden increase in flow being indicative of fracture in the direction of least resistance, i.e. tensile fracture in the direction of the minor principal stress. Errors arise from the disturbance effects from withdrawing a piezometer and the possibility for cavity expansion without fracture. Tensile strength of the soil is taken into account by cycling the pressure and monitoring "closure."

The other devices for measuring in situ soil stress are essentially mechanical with either hydraulic or electrical transducers and readout. These follow one of three patterns: (a) Introduce a thin pressure cell so as to minimize disturbance, but recognize that there has been disturbance and repeat the pressure determinations over a long period of time so as to predict the final pressure at equilibrium: Glötzel cell. (b) Introduce a thin pressure cell and expand it to measure soil response, then in effect by use of empirical data back-calculate for zero thickness: Flat Dilatometer. (c) Introduce a cylindrical pressure cell by making it integral with a soil drill so as to minimize soil disturbance and relaxation, then monitor pressure over a period of time: Self-Boring Pressuremeter.

The problem with most of these methods is the waiting time to reach equilibrium, shown by Tavenas[31] to vary from a few hours for the self-boring pressuremeter to several years for hydraulic fracturing,

Figure 2. Furthermore there is no assurance that the re-attained equilibrium represents the original stress state.

The principle embodied in the research described herein is to recognize that disturbance is inevitable, then vary it in discreet steps, and determine the pressure as a function of disturbance so as to allow an extrapolation of pressure to zero disturbance. This is done with a stepped blade or vane, Figure 1: Pressures σ_{h_1}, σ_{h_2}, σ_{h_3} are measured after insertion of blades of thicknesses t_1, t_2, and t_3. If σ is found to be some continuous function of blade thickness, extrapolation should be possible to find σ_{h_o}, the pressure on a hypothetical blade of zero thickness. The function need not be linear; it must only be continuous. An hypothetical example is shown in Figure 3.

We should note that extrapolation to zero thickness still is not the same as the true undisturbed stress state, since the infinitely thin blade still represents a discontinuity that does not pass through individual soil grains, but pushes them aside. This means a higher-than-original pressure may be determined, the error being largest for dense, granular soils that dilate upon blade intrusion. Dilation or volume increase during shear is a direct evidence for disturbance. We therefore may predict problems with dense sands, as indeed will be shown, but such error should be less in loose sands, and a minimum in soft or moderately firm silts and clays.

It also may be seen that instead of pushing a single blade as in Figure 1, we may assemble several blades into a single instrument so as
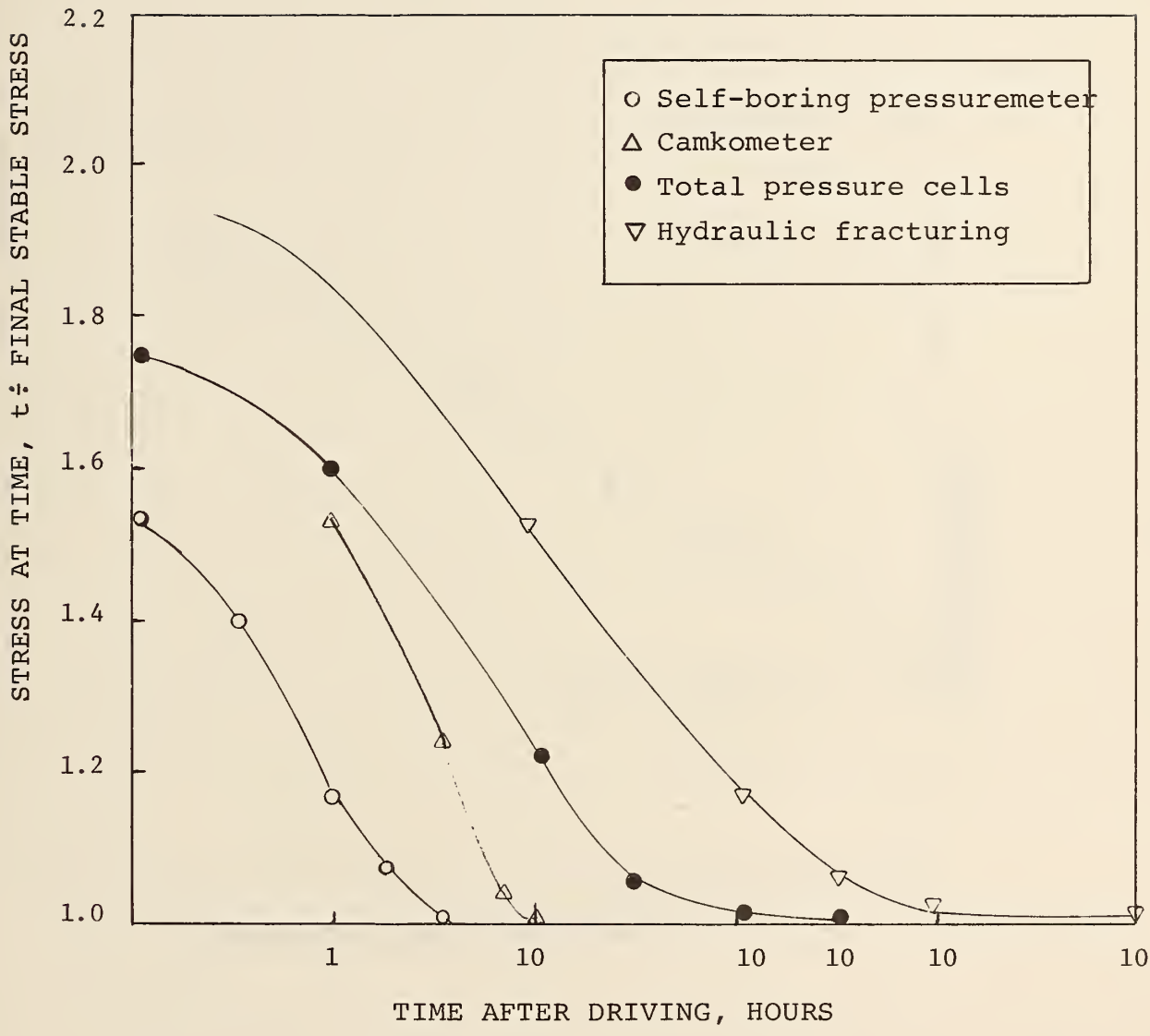
Fig. 2.   Stress relaxation times for various techniques of in
          situ horizontal stress measurement (after Tavenas 31).

5
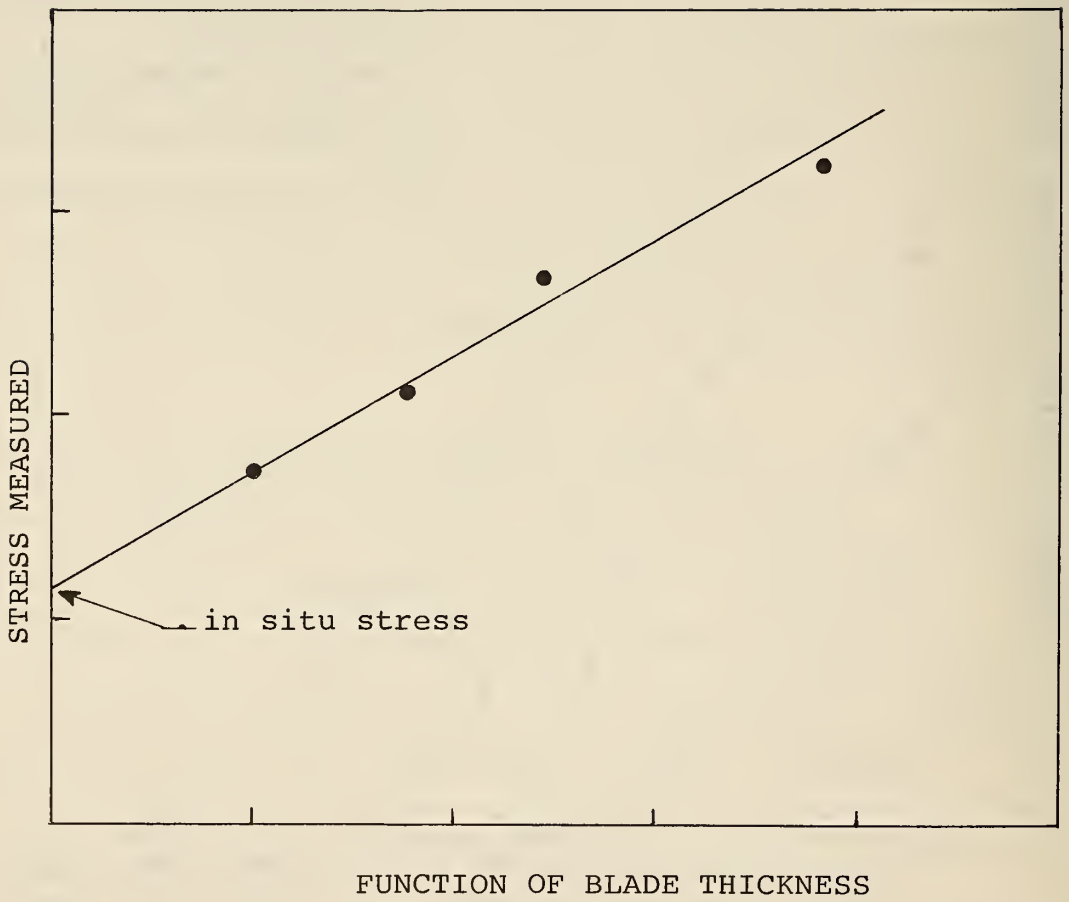
Figure 3. Hypothetical example of extrapolation to
           initial in situ stress.

6

to determine a two-dimensional stress state, Figure 4. This was the

eventual goal of the research.

SENSING ELEMENT

STEP-TAPERED VANE
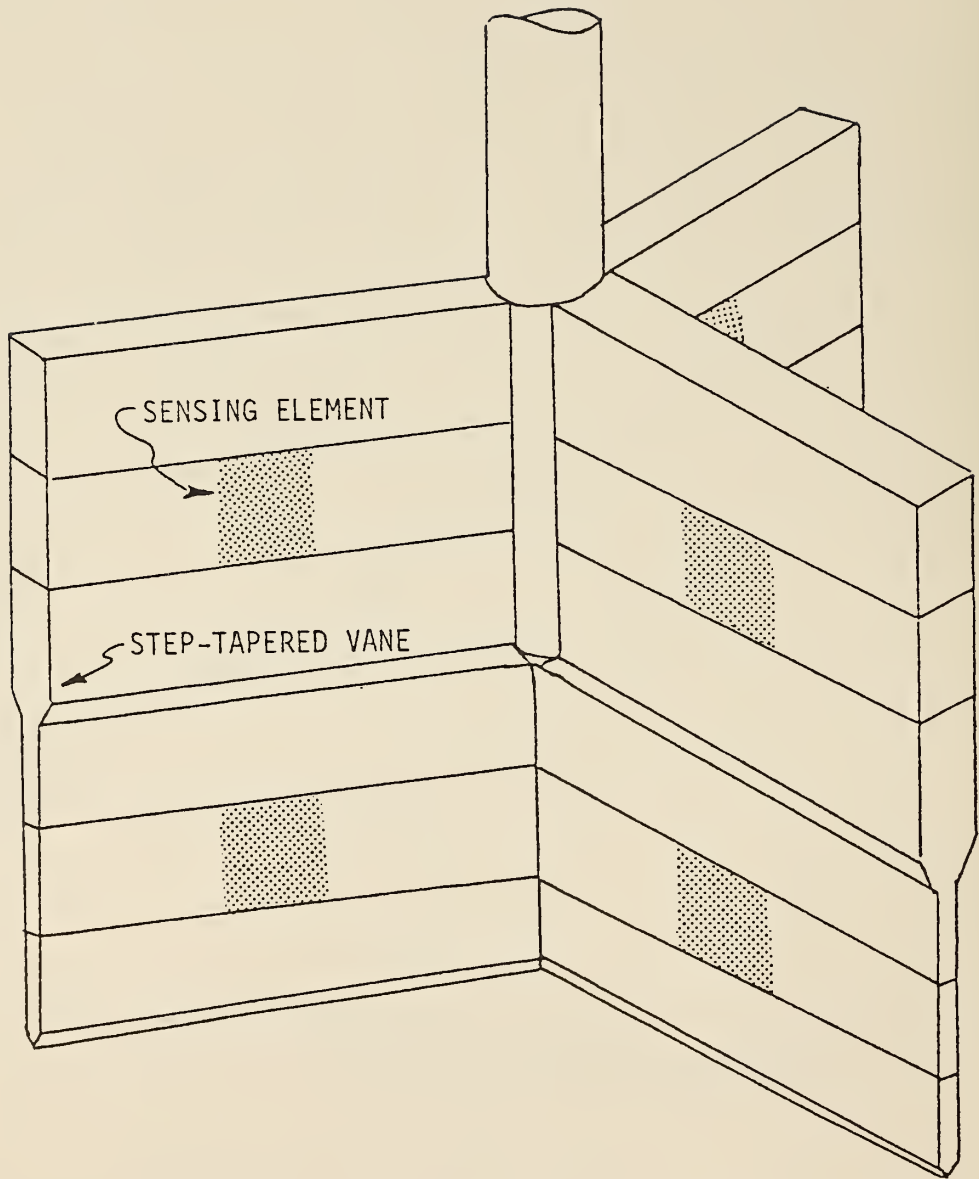
Figure 4. Conceptual drawing of a vane stress sensor.

SCOPE

The primary objective of this research was to determine whether the vane stress sensor method of analysis is in fact an accurate and economical way for stresses in soils to be measured. This objective was pursued in three phases.

The first phase was a literature review and was separated into two sections. Initially, the pertinent references concerned methods of measuring in situ lateral stresses in soils. This section of the literature review is basically a state-of-the-art summary. The second section identifies and reviews critical variables that can be expected to affect the preliminary design of the vane stress sensor. Both sections of the literature review were a basis for developing an experimental program.

The second phase consisted of laboratory testing. The prime concerns of this research phase were to answer questions in specific areas that could influence design of the vane stress sensor (VSS). Some of these areas are as follows:

1) Estimate the amount of soil disturbance from insertion of blade.

2) Find the optimum angle of the leading edge on the blade.

3) Evaluate the effects of blade thickness and surface roughness.

4) Develop a stress cell that could be used on the VSS.

The third phase was the development of a prototype for laboratory and field evaluation.

LITERATURE REVIEW

Determination of Stresses in a Soil Mass

The existing in situ lateral pressure in a soil mass is called the "at-rest earth pressure." This pressure is bounded on the low side by the active pressure and on the high side by the passive pressure of the soil, where the minimum value or active pressure is reached as a result of lateral expansion of the soil prior to failure, and the maximum value or passive pressure is reached as a result of lateral compression of the soil prior to failure (36). Horizontal stress for the at-rest condition is usually expressed in terms of the vertical stress and the coefficient, K_o:

$$\sigma_h' = K_o \, \sigma_v' \qquad (1)$$

where K_o is the coefficient of at-rest earth pressure, and σ_h' and σ_v' are the effective horizontal and vertical stresses, respectively (19).

Accurate determination of the at-rest earth pressure has received increasing attention in geotechnical engineering for several reasons. Analytical techniques such as the finite element method can now handle in situ stresses (20) in making earth pressure predictions. An accurate representation of the stress path in triaxial and plane strain testing requires that specimens be reconsolidated to the initial in situ stress conditions for valid results (32). Other uses of the coefficient of

at-rest earth pressure (K_o) include the design of retaining walls to minimize settlement of adjacent buildings, and to predict friction on piles. The in situ lateral earth pressure is also important in tunnels and bracing systems, where it is necessary to know the initial stress in order to determine how much change in stress may be allowed before failure will occur in the soil mass.

Theoretical Determinations of K_o

The theoretical analysis of the coefficient of at-rest earth pressure has been limited due to problems in modeling real soil behavior. For an ideal linearly elastic isotropic material, the coefficient of at-rest earth pressure (K_o) is related to Poisson's ratio (ν) as follows (1):

$$K_o = \frac{\nu}{1-\nu} \tag{2}$$

Wroth (42) developed a theoretical equation for K_o for overconsolidated soils that have been unloaded only once. The derivation assumes that the stress path upon unloading remains linear, and gives:

$$K_o = K_{nc} \ (OCR) - \frac{\nu'}{1-\nu'} \ (OCR-1) \tag{3}$$

where K_{nc} is the coefficient of earth pressure at rest during normal consolidation of the soil, and OCR is the overconsolidation ratio for the soil. The overconsolidation ratio (OCR) is defined as the ratio of the maximum vertical stress experienced by the soil to the present vertical stress on the soil mass.

For a soil deposit that has been subjected to more than one cycle of loading and unloading due to the deposition and erosion of overlying materials, the existing state of stresses in the soil cannot be accurately predicted through a theoretical analysis (42).

Laboratory Determinations

The direct measurement of K_O in the laboratory requires a testing apparatus in which the soil specimen being loaded can deflect in the vertical direction, but is prevented from straining in the horizontal or radial direction. Also, during testing, vertical shear stresses caused by friction along the sides of the soil specimen must not be allowed to develop (7). Such methods of testing have been found to be very time-consuming and expensive. Also, "undisturbed" samples are required, which are impossible to obtain since stress relief and physico-chemical changes occur during sampling (32). Therefore, a number of researchers have correlated K_O with other soil parameters.

For normally consolidated soils only, several researchers have proposed the following relationships between K_O and the angle of internal friction (ϕ'), of the soil (1):

$$K_O = 1 - \sin \phi' \quad \text{(Jaky)} \tag{4a}$$

$$K_O = 0.9 (1 - \sin \phi') \quad \text{(Frazer)} \tag{4b}$$

12

$$K_o = (1 + 2/3 \sin \phi') \frac{1 - \sin '}{1 + \sin '} \quad \text{(Kezdi)} \tag{4c}$$

$$K_o = 0.95 - \sin \phi' \quad \text{(Brooker and Ireland)} \tag{4d}$$

Brooker and Ireland (10) consider Jaky's equation as an accurate prediction of K_o for normally consolidated sands, whereas their equation should be used for cohesive soils.

Another important factor influencing K_o is the horizontal stress which may be induced as a result of previous loading. Thus, K_o should be proportional to the overconsolidation ratio. As shown in Figure 5, a high overconsolidation ratio will dictate a high value for K_o regardless of soil type.

A different approach suggested by Spangler and Handy (29) is to attribute K_o to intergranular sliding friction. A rearrangement of their equation gives:

$$K_o = \frac{1 - \sin \phi_s}{1 + \sin \phi_s} \tag{5}$$

where ϕ_s is the angle of sliding friction, normally ranging from 10 to 30 degrees. This equation ignores interlocking effects which add to ϕ', their argument being that volume change work or dilatancy is needed for interlocking effects to occur.

If K_o is dependent on just the material properties of a soil, changes in its value can occur only when there is a subsequent change
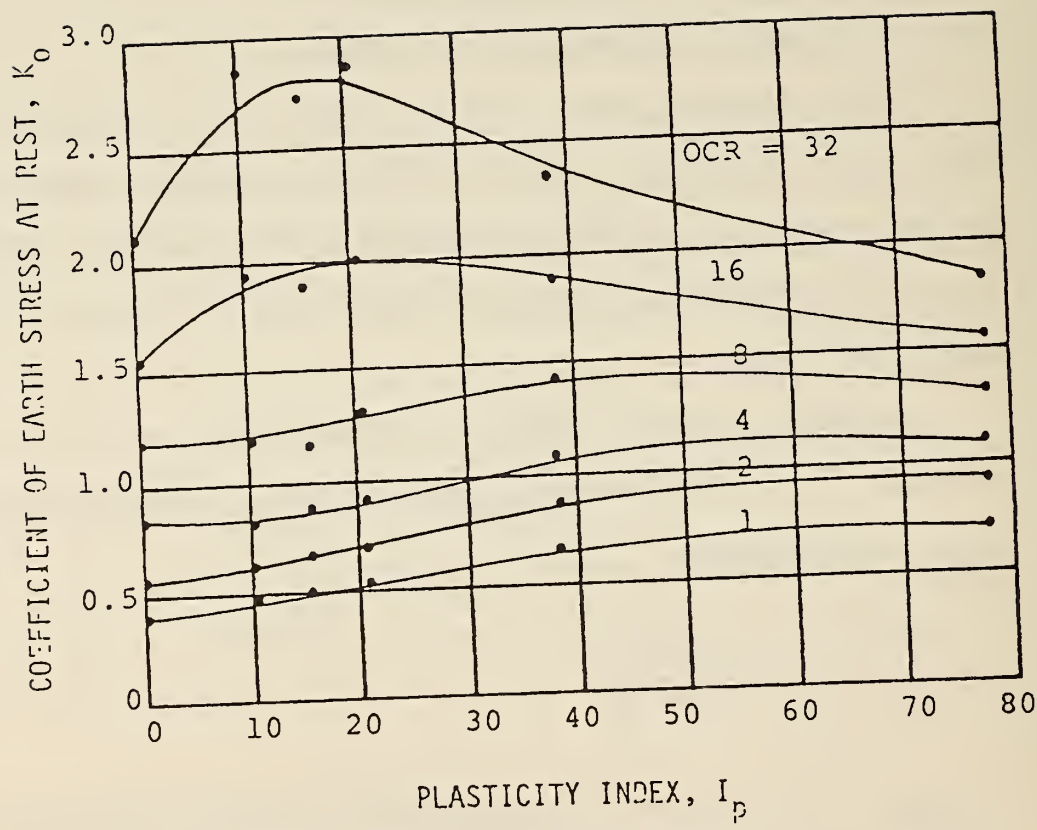
Figure 5. K_o as a function of overconsolidation ratio (from Brooker and Ireland (10)).

14

in material properties. This means that K_o will stay constant through the entire depth of a uniform soil deposit. But an investigation by Massarsch, et al. (20) indicated considerable variations of K_o close to the dry crust, and the general decrease of K_o with depth below a level of 5 meters even though there was no material change. These variations may be caused in part by the seasonal fluctuations of the water table. Therefore, it can be concluded that no rigorous method has been developed that will determine K_o through analytical or laboratory methods for soils.

In Situ Evaluation of K_o

In recent years attention has been focused on the evaluation of K_o by measuring the total horizontal stress in situ. Basically, the techniques available for such measurement can be divided into two general classes.

(1) Hydraulic fracturing; and

(2) Measurement of the horizontal total stress with a stress cell.

The hydraulic fracturing method of measuring horizontal stresses in clay deposits was suggested by Bjerrum, et al. (8), while they were investigating the problem of in situ permeability tests. The hydraulic fracturing technique has been described by Massarsch, et al. (20). It consists of inserting a piezometer into a cohesive soil, and after allowing the excess pore pressures to dissipate, forcing water into the soil and causing a crack to form in soil at the piezometer tip. This

15

crack is assumed to develop vertically, which means that the hydraulic fracturing method is limited to soils with a K_o value less than 1.0. A falling head permeability test is then performed with the quantity of water flow being monitored. As the head decreases, a sudden reduction in flow will occur which indicates closure of the crack. The head at which the crack closes should be related to the lateral stress and can usually be found by plotting piezometer pressure versus flow.

The assumptions made in the hydraulic fracture method have been described by Massarsch, et al. (20) and are summarized as follows:

(1) The direction of the crack is vertical and the direction of the minor principal stress is horizontal.

(2) The direction of cracking is controlled only by the horizontal stress. Factors such as varves, fissures, pockets of highly permeable materials, cementation, etc., that could affect the direction of cracking are ignored.

(3) The small, but possibly significant tensile strength of the clay is neglected.

Another shortcoming of this method would be its usage in metastable soils, such as loess. These soils are known to collapse upon saturation, which would undoubtedly cause erroneous results. Therefore, the hydraulic fracturing method would not be applicable in such soils.

Two procedures have been developed to measure the total horizontal stresses in soils using stress cells. The first method, proposed by Massarsch (19), is limited to usage in low shear strength material.

This method consists of pushing a Glötzl pressure cell, a spade-like very thin cell filled with oil, into the soil mass. By taking pressure readings from the cell, a plot of horizontal stress versus time can be constructed. After approximately one week, the excess pore pressure generated by the insertion of the cell will dissipate, and eventually an "equilibrium" pressure will be reached. The equilibrium pressure is assumed to be the same as the initial in situ pressure.

Another approach used by Marchetti (43) is similar except that the pressure cell is expanded to give a measure of deformation modulus. An empirical relationship is established between the horizontal stress index K_D and K_o. On the basis of empirical data fits, $K_o = (0.67\ K_D)^{0.47} - 0.6$ for noncemented and insensitive clays and noncohesive sands, and the overconsolidation ratio OCR $= (0.5\ K_D)^{1.56}$ for uncemented cohesive soils only. The test thus requires empirical correlations for particular soils.

The other method that uses total stress cells was developed independently by Baguelin, et al. (3) and by Wroth (42). Their methods use self-boring cylinders with total stress sensors mounted on the exterior. The Wroth device is shown in Figure 6. Since the apparatuses are self-boring, the disturbance caused by the introduction of the
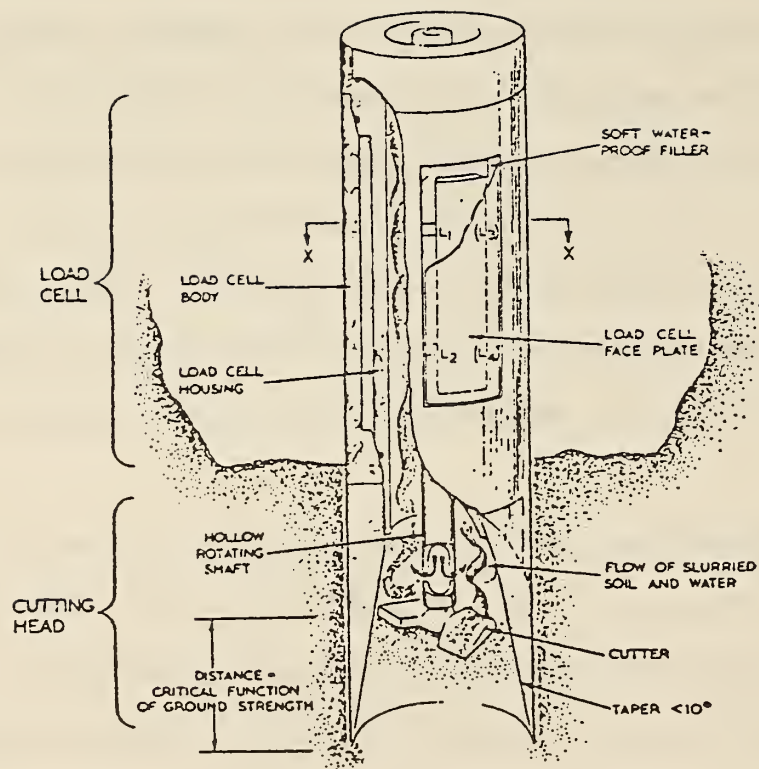
Figure 6. "Camkometer" self-boring pressuremeter (from Wroth (42)).

apparatus into the soil mass is assumed to be negligible.

Baguelin, et al. (4) have studied the effect of disturbance caused by insertion of their self-boring apparatus. They concluded that degree of disturbance does not affect the equilibrium values of lateral stress that are eventually obtained, but considerable time may be necessary before "equilibrium" is reached and the in situ lateral stress is measured. In a recent state-of-the-art paper, Wroth (42) stated that under favorable conditions, the radial displacements to be expected by insertion of the self-boring apparatus is less than 0.5 percent of the radius of the cylinder. Ideally, no disturbance should occur, but this condition is impossible to achieve since shearing forces will always occur on the exterior of the self-boring cylinder or, alternately, the borehole must be larger than the probe.

The self-boring apparatus has been used in both soft and stiff soils with reasonable success (42). The usage in stiff soils gives the self-boring method a distinct advantage over the Glötzl cell, which can be inserted only in soft soils. A major limitation of the apparatus is gravel or rock fragments, which when encountered will cause the boring apparatus to jam.

Although the self-boring apparatus seems to be one of the most promising methods of determining the state of stress in a soil mass, it still creates a disturbed zone around the sensors. The disturbance has been found to be quite significant, particularly in a sensitive highly plastic clay (21). Therefore, although the self

boring apparatus is perhaps the best method now available, it does not give a final answer to the problem of determining the in situ state of the stresses in soil (31).

Penetration Mechanics

Disturbance

The insertion of a vane by pushing into soil will cause a shear zone to develop around the vane blades. This zone may be similar to one of the three types of shear failure that have been proposed for pile foundations. The three modes of shear failure described in the literature are: general shear failure (Caquot,and Terzaghi); local shear failure (Terzaghi, DeBeer,and Vesic); and punching shear failure (DeBeer,and Vesic) [37].

General shear failure is characterized by the existence of a well-defined failure pattern that starts downward at the tip of a pile and bends outward and upward to the ground surface (40). This type of shear failure can occur only in piles that are relatively short and near the surface. Therefore a general shear failure would not be expected to be a common failure mode for a vane stress sensor inserted to depth-to-thickness ratios greater than 30.

Local shear failure as described by Vesic (40) is characterized by a clearly defined failure pattern that develops only immediately below the pile. The pattern consists of a wedge and slip surfaces, which start at the bottom of the pile just as in the case of general

20

shear. Because of the compressibility of soil, the slip surfaces

dissipate in the soil mass and do not reach the surface.

The punching shear failure pattern is not so easily recognized

(40), but may dominate deep pile shear behavior. An investigation

by Vesic (37) indicates that in sands, only punching shear occurs for

rectangular piles when a depth-to-base ratio of eight is exceeded.

Through his investigation Figure 7 was developed, which indicates

the types of failure that can be expected to develop at different

relative depths. It has been concluded that pile in sands for the

most part give a punching failure (15). Therefore a punching shear

failure probably develops around the blades on the VSS provided the

blades are inserted into a soil mass past a critical depth.

The meaning of various failure modes can be seen by reference to

Figure 8. The general shear plastic zone proposed in Figure 8a is

probably incorrect because of the assumption that the soil above the

failure surface A-B, can be replaced by a surcharged loading that does

not have any strength. The general shear pattern shown in Figure 8b

requires that the plastic zone extend from the point of initiation

beneath the pile, through a radial zone away from the pile, and then

move back upward toward the pile's exterior surface. Local shear

would be a partial initiation of either of these failure modes, Figure

8c. Vesic (37) found in his investigation on pile behavior that sand

did not move through a radial zone and return to the pile surface, and

Baligh and Scott (6) made the same observation in clay.
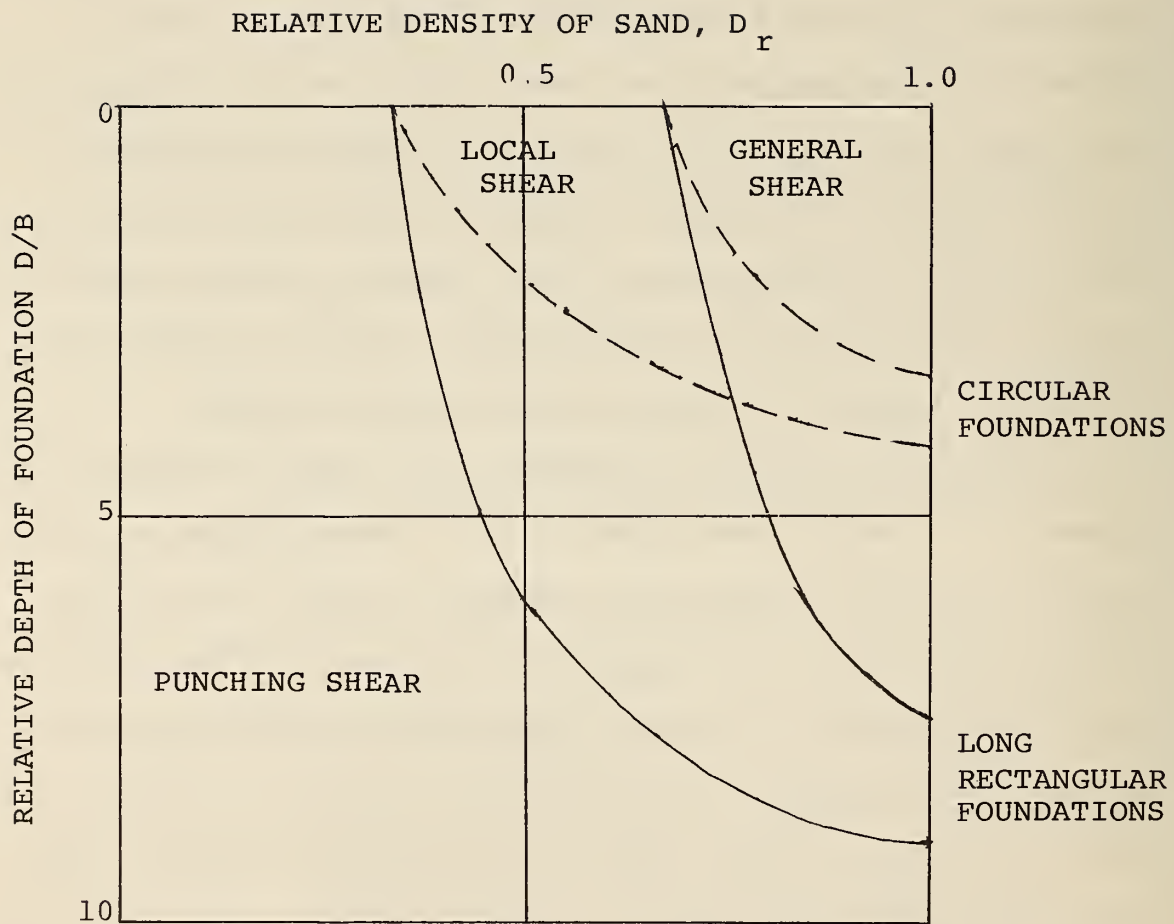
Figure 7. Foundation failure modes (from Vesic (37).
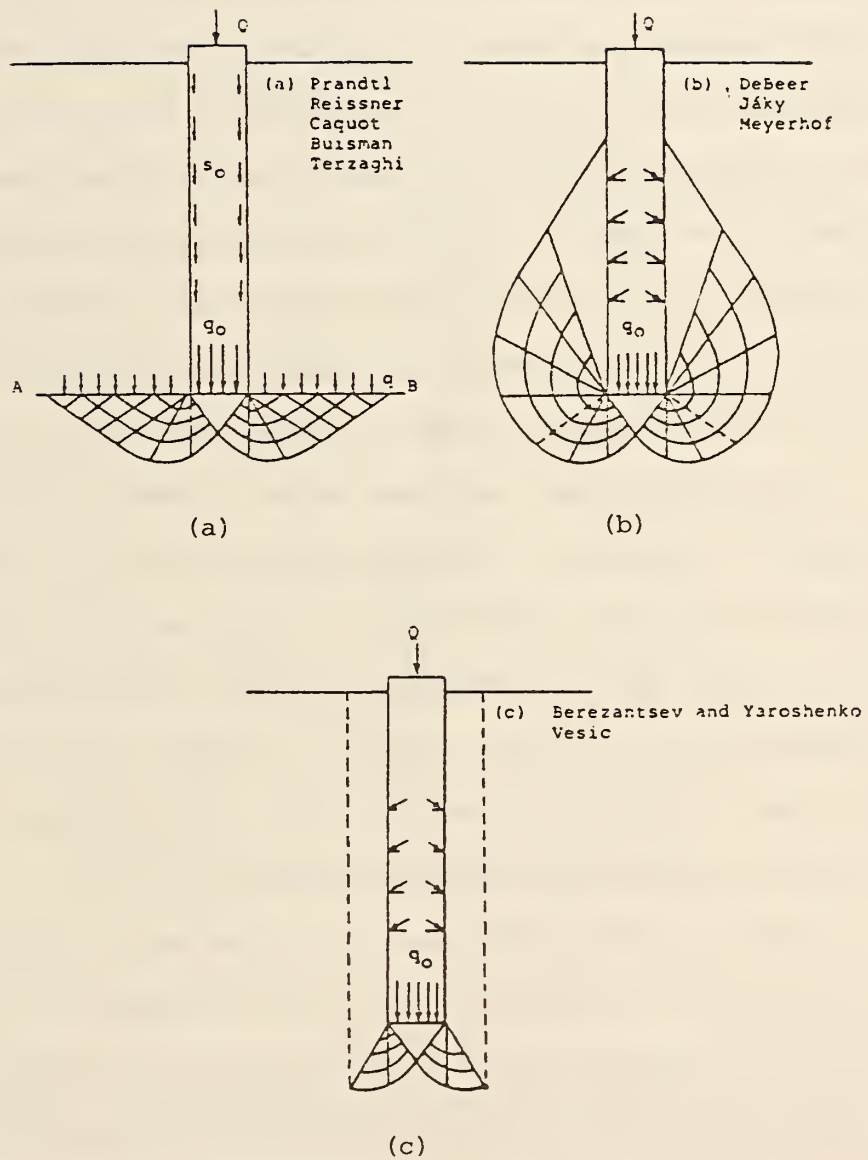
Figure 8. Assumed plastic zones under deep foundations (from Vesic (39)).

Punching shear is nicely illustrated by the study by Robinsky, et al. (27) on model friction piles in sand. The general displacement envelope was described as an elongated bulb, and the sand revealed a complex variation in density illustrated in Figure 9. The zone of displacement beneath the pile point has approximately the shape of a truncated cone extending downward and outward from the tip. This cone-shaped, vertical compression and two-dimensional horizontal expansion were found to take place accompanied by radial downward translation. As the pile is advanced and moves through the previously compacted zone, sand movement is induced downward along portions of the pile wall, causing a sleeve of loose sand to form around the pile.

These studies found that the process of sand displacement and compaction resulted in a seemingly erratic pattern of high and low densities which apparently cause a complex system of arching to occur. Kezdi (15), and Sanglerat (28) have observed the same type of arching effects. It is not possible to predict what effect arching will have on the VSS from these studies, but an awareness of this phenonenon possibly developing is important.

Numerous investigations have been conducted to determine the radial extent of disturbance caused by the insertion of a pile. Vesic (39) developed a theoretical analysis that indicated the radius of the plastic zone is dependent primarily on the rigidity index of the soil. The size of the disturbed radial zone has been studied by numerous investigators and can be expressed as a function of the pile
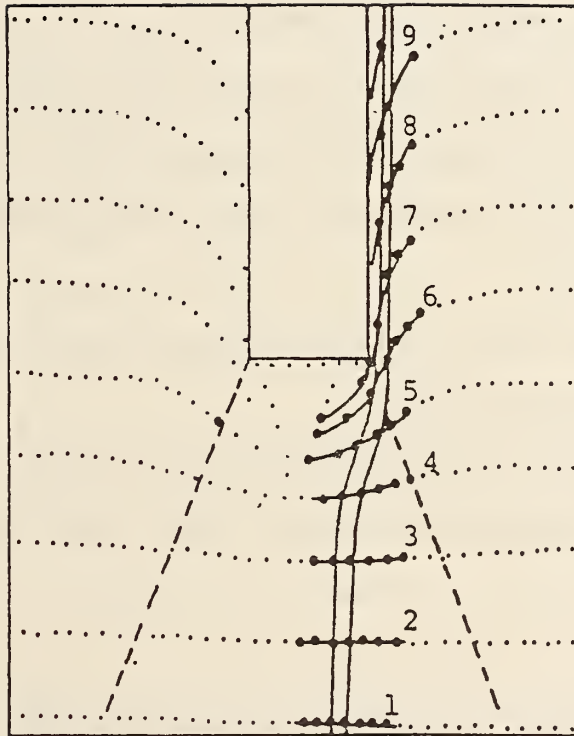
Figure 9. Sand displacement around a pile (from Robinsky and Morrison (26)).

diameter. Meyerhof (23) experimentally found that the diameter of the disturbed zone in sand is approximately six times the diameter of the pile. A pile pushed into saturated clay will cause remolding at a distance of roughly one pile diameter (25).

The following conclusions relating to the proposed vane stress sensor can be made from the preceding discussion on disturbance caused by a pile being advanced in a soil mass:

(1) Inserting a VSS into a soil mass will probably cause a punching shear pattern to develop around the vane blades, provided the VSS is inserted to a depth greater than approximately 10 times the blade thickness.

(2) Arching in sand around the VSS might cause some problems in measuring the in situ stresses.

(3) The horizontal extent of disturbance out from the surface of the VSS caused by insertion into a soil mass should be less than 6 times the thickness of the blades and will vary depending on the soil.

Wedge Shape

The force necessary to insert the Vane Stress Sensor can be substantially decreased by a wedge-shape leading edge, which also should influence the degree of disturbance. Therefore, the effect of the wedge on the shear pattern that develops over the vane surface must be investigated. The two wedge parameters that will probably affect the shear zone, are the wedge angle and whether the wedge is smooth or rough.

Baligh and Scott (6) did a study on the insertion of wedges of various angles into modeling clay. They found that if the coefficient of friction on the wedge surface is larger than a critical value, the wedges are considered rough. This value was found to be so low that unless extraordinary efforts are made, all wedges can be assumed to be rough.

Meyerhof studied the effect on the bearing capacity of shallow foundations by varying the wedge angle. These results indicated for wedge angles equal to or greater than 60°, the bearing capacity factors were not affected by changes in wedge angle. When approximately this same wedge angle was exceeded in Baligh and Scott's studies with clay, a dead zone was found to be about 75°. Therefore, use of a trial wedge angle of approximately 60° for the VSS would appear desirable since the resistance to penetration should not appreciably change for greater wedge angles.

Pore Pressure

Excess pore pressure will develop due to insertion of the vane stress sensor. Overconsolidated soils generally develop negative excess pore pressure when sheared, whereas positive pore pressure will develop in normally consolidated soils (6, 41).

If a plot is made of the measured total stress as a function of blade thickness for an overconsolidated soil immediately after

insertion of the vane stress sensor, the plot could resemble Figure 10. Such a plot should be indicative of negative pore pressure developing as a result of dilatant shear, or positive pore pressure as a result of soil compaction. It therefore would be advantageous to mount a piezometer on the device to measure pore pressures and isolate this effect from the total disturbance effects hypothesized in Figure 3. A pore pressure device was developed for use at the tip of a cone penetrometer by Wissa, et al. (41).

Stress Cell Location

The total bearing capacity (Q_t) of a pile (12) is usually expressed in terms of skin friction (Q_s) acting on the pile, and point resistance (Q_p):

$$Q_t = Q_p + Q_s \tag{6}$$

The development of skin friction on a pile is dependent on two variables, and can be expressed as follows:

$$Q_s = \sigma' \tan \phi_s \tag{7}$$

where σ' represents the effective normal stress on the pile exerted by the soil, and ϕ_s is the angle of skin friction. The lateral stress acting on a pile is not uniformly distributed over its length. Therefore, a study of this distribution can give some insight as to where the stress cell should be mounted on the vane stress sensor.
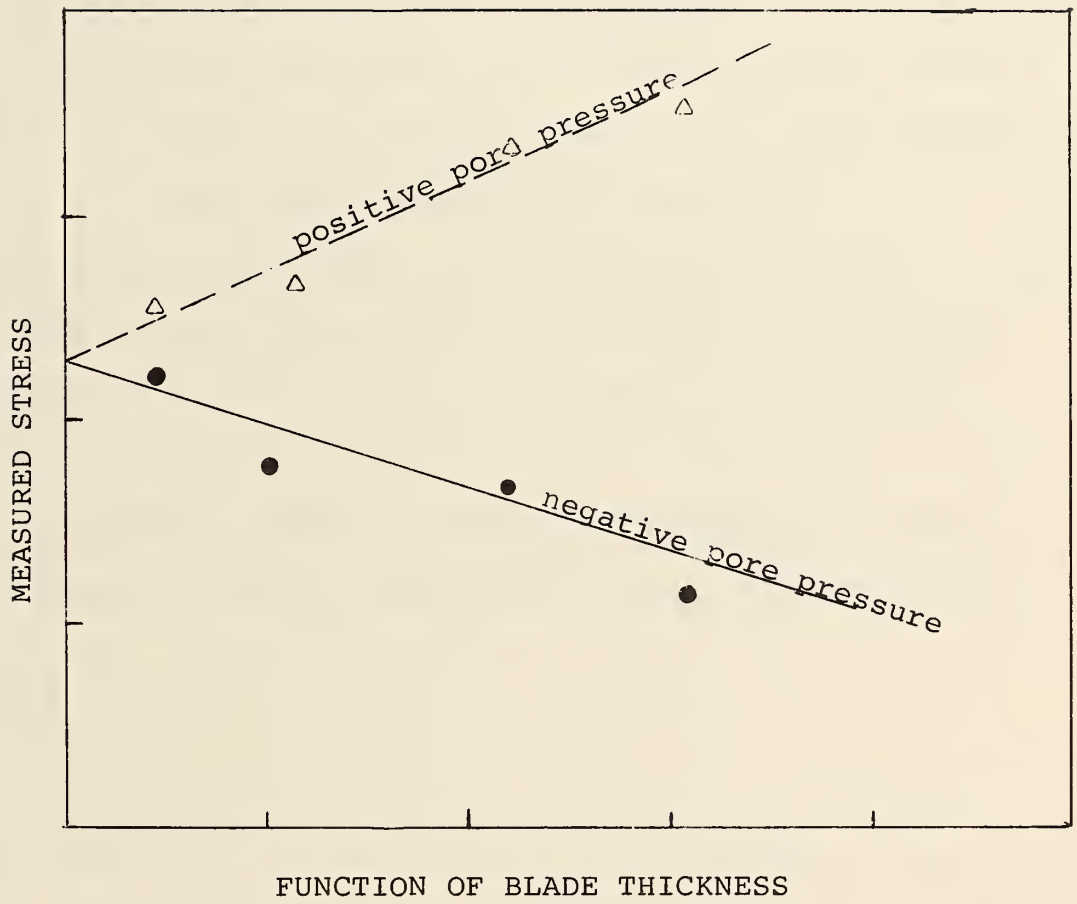
Figure 10.   Representation of possible pore pressure
effects in soil.

Numerous investigations have been performed to evaluate the soil properties that affect stress distribution on a pile. Vesic (39) found that the principle parameters affecting the lateral pressure on a pile are strength and volume change characteristics of the soil expressed by the rigidity index. Broms and Silberman (9) found that relative density of the sand has a large effect on the skin friction that develops. As yet, however, the exact distribution of the lateral stress cannot be predicted from soil properties alone.

The lateral stress in sands does not continue to increase indefinitely with depth, but instead reaches a constant value (37) at a depth of approximately 15 times the pile diameter. The results indicate that the stress cells on the VSS should be installed at a distance of 15 blade thicknesses below the top of the vane. By doing this the reproducibility of the results should be enhanced.

INVESTIGATIVE PROCEDURE

The Vane Stress Sensor method of analysis is based on the premise that extrapolation to a zero blade thickness effect is possible. If this is not the case, the feasibility of the vane stress sensor is questionable. Therefore a laboratory testing procedure was set up to test this premise.

Material Properties

There are two extreme soil types -- noncohesive soil such as a sand, and cohesive soil such as a homogeneous clay. Both were used in the initial research.

Sand

The sand initially selected to represent a noncohesive soil was a washed well-graded river sand. The gradation of the sand is shown in Figure 10. The uniformity coefficient was determined to be 6.25, and the specific gravity of the material was 2.66.

The maximum and minimum densities of the sand were determined by following ASTM (1) test procedure D2049-69, with the following modifications. Instead of using a mold 15 cm in diameter by 15.5 cm in height, a standard Proctor mold, which is 10 cm in diameter and 11.6 cm high, was used to determine minimum relative density of the sand. The maximum relative density was determined by using a mold 10 cm in diameter with

Figure 11. Grain size curve of sand used in this project.

32
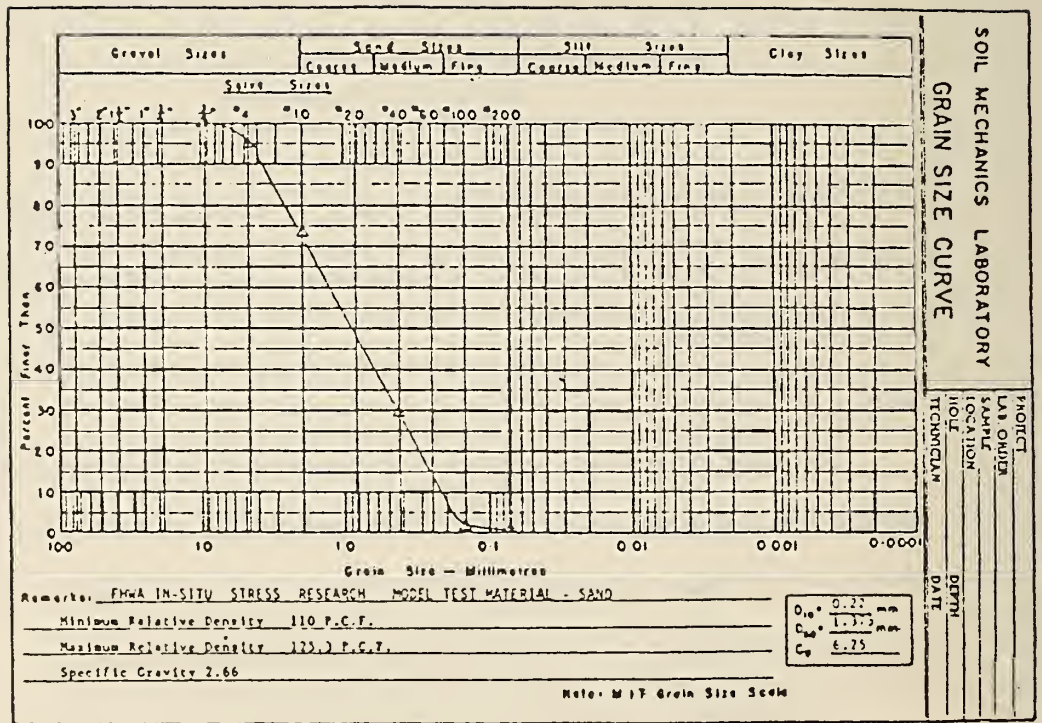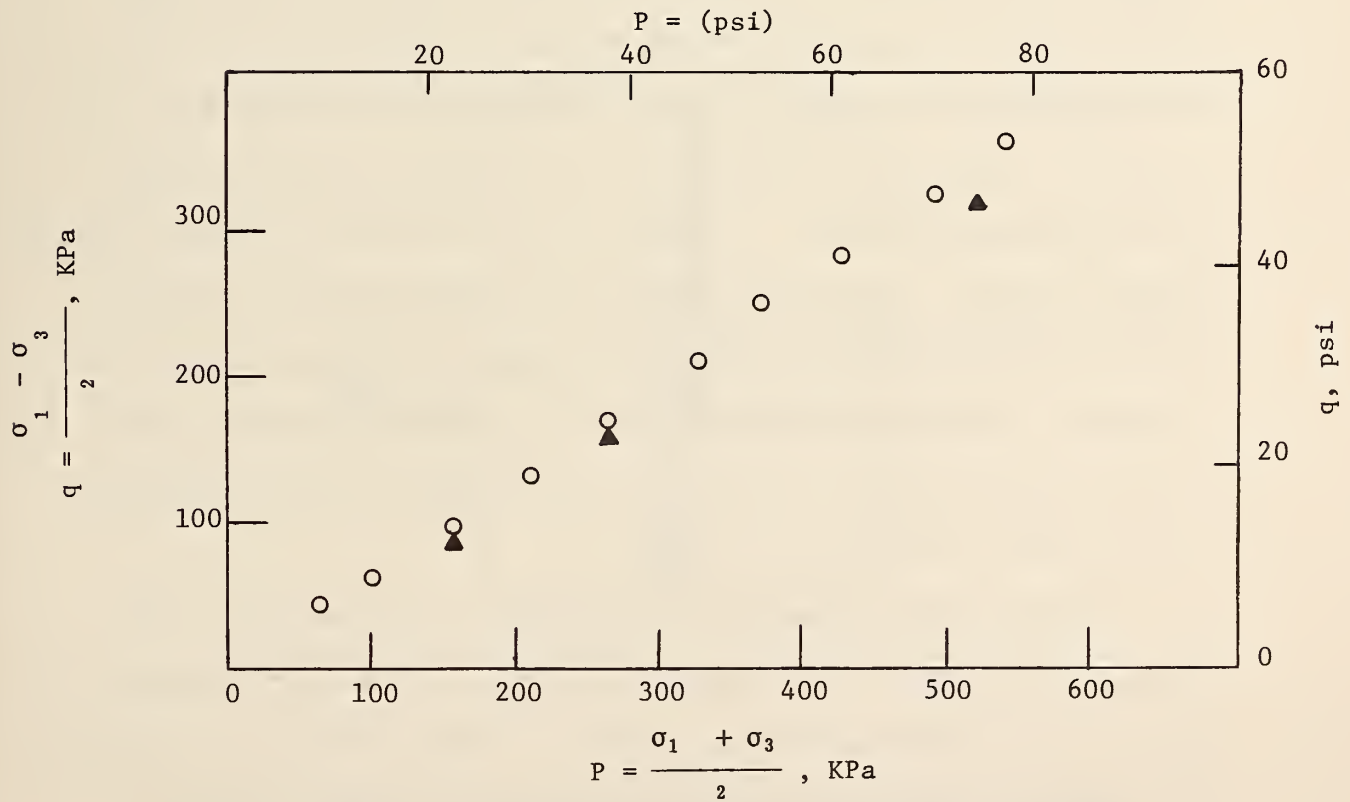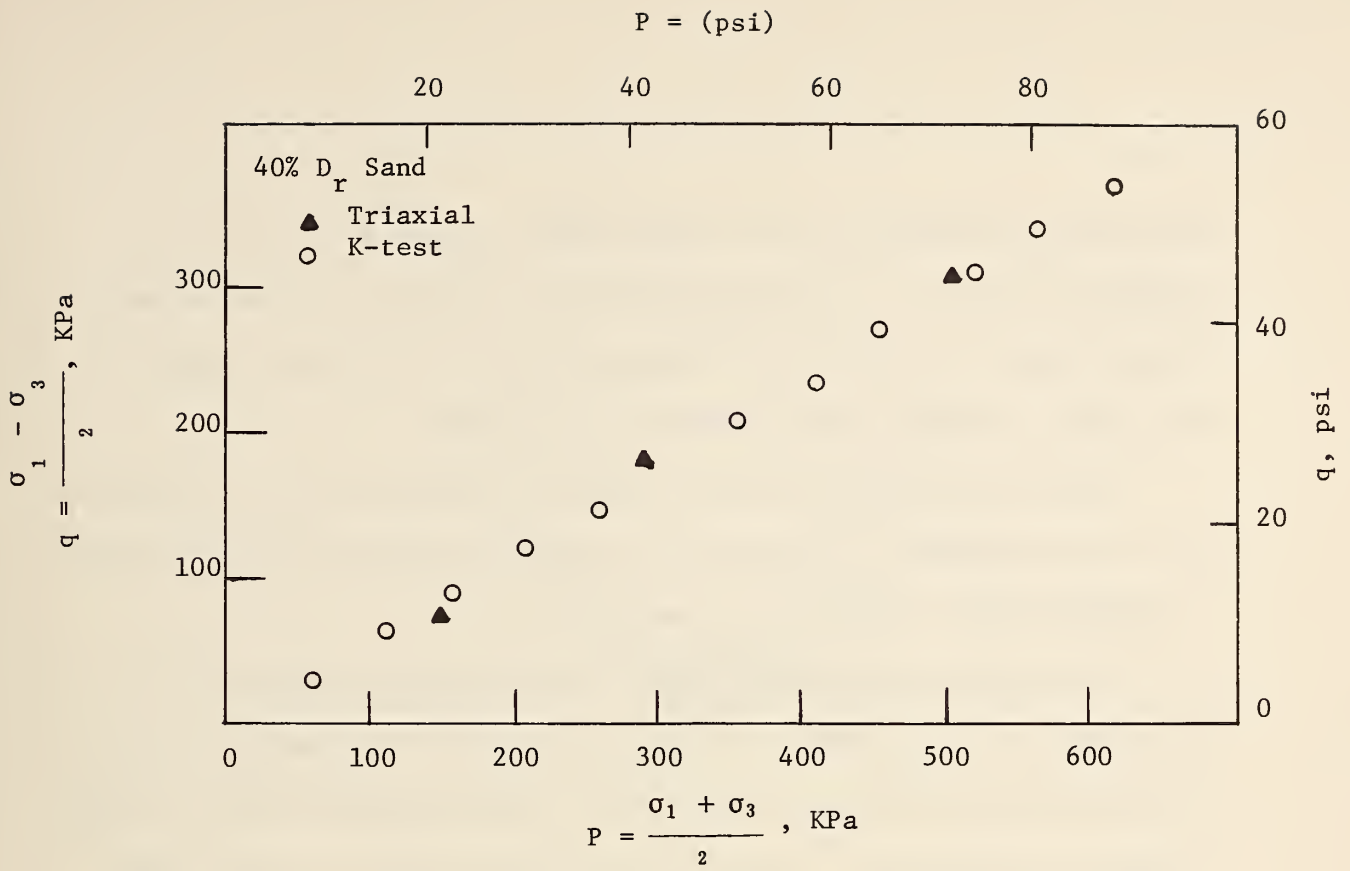
Figure 12. Shear strength test results for sand.

1 psi = 70.31 gm/sq cm

33

the sand being compacted to a final height of 10 cm $\pm$ .25 cm. The

maximum density of the sand was found to be 2.00 g/cc and the minimum

density was 1.76 g/cc. These values, as was expected, are close to

one another because of the gradation of the sand.

Maximum and minimum relative densities normally are not encountered

in a natural deposit. Therefore, all testing was done on sand compacted

to either 40% or 75% relative density, D_r.

The shear strengths of the sand at both testing densities were

determined by two different testing methods. The first method consists

of running a set of three triaxial tests (consolidated drained) on sand

samples of each density. Figure 12 shows the results of these tests.

It should be noted that this is not a graph of normal stress versus

shearing stress, but rather a stress path method (17) of plotting test

results. A functional relationship exists between the internal angle

of friction and the slope of the best-fit line through the triaxial points

on the p-q plot. This best-fit line was determined through a least

square fitting method, and the resulting internal friction angles were

calculated. The dense sand had a friction angle of 41° with a corre-

lation coefficient of 0.998, while the loose sand had a friction angle

of 39.5° with a correlation of 0.994.

The other shear strength testing method is the Iowa K-Test (18),

diagramed in Figure 13. This apparatus consists of a split cylindrical mold

with a piece of Teflon covering the split. When a soil sample is placed in

the mold and loaded in the vertical direction, it begins to deform

in both the vertical and radial directions.
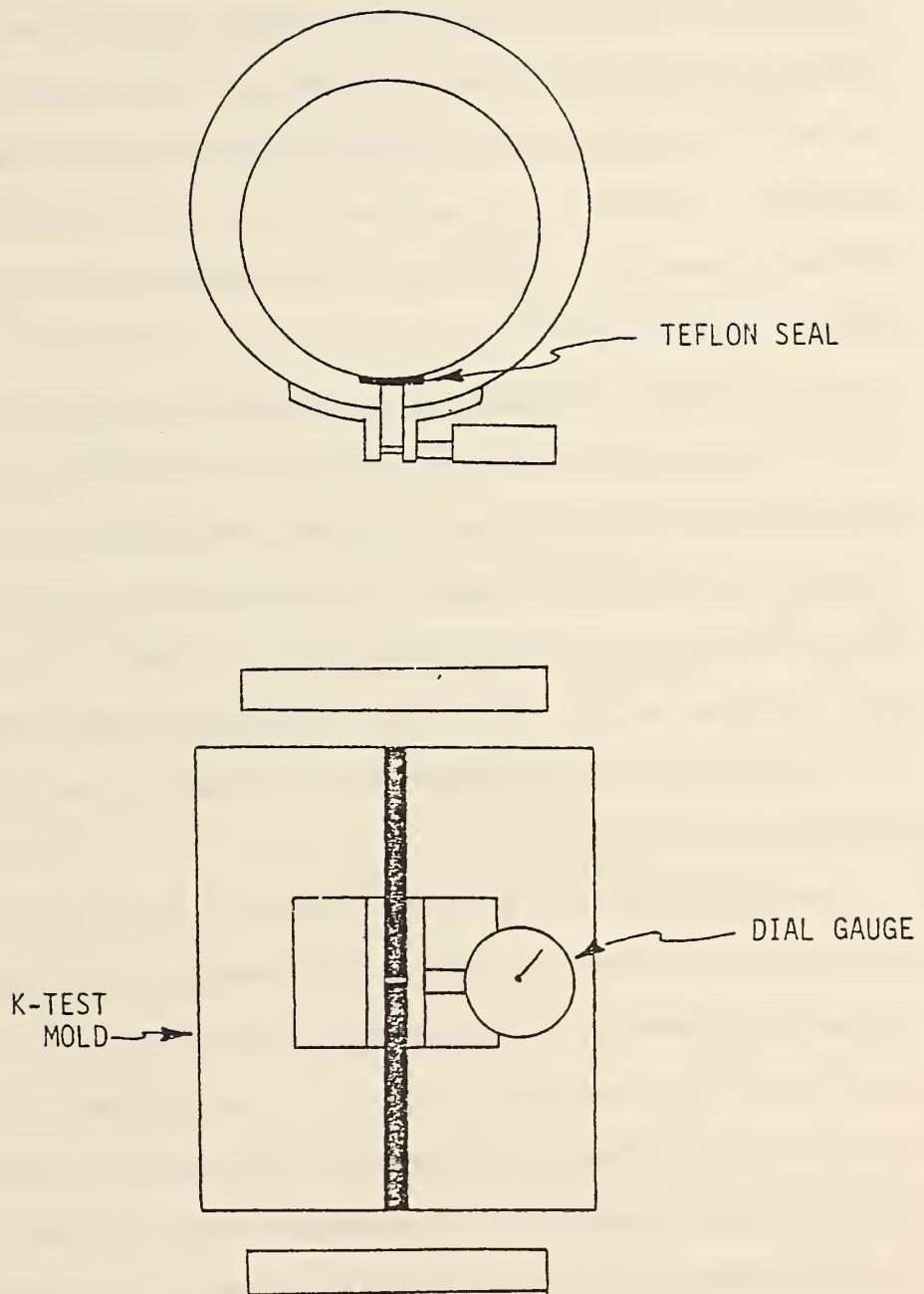
Figure 13. The Iowa K-Test mold (from Lutenegger (18)).

This causes expansion of the mold which can be monitored with a dial gauge. Since the relationship between radial stress and mold deflection has been previously determined, it is possible to determine the radial stress acting on the soil sample at predetermined vertical stresses. The sample is considered to always be in shear, so the shear strength parameters of the sample can be determined through Mohr-Coulomb failure criteria.

K-Tests were performed on sand samples in both the dense and loose state. The results of these tests are plotted on the p-q graphs in Figure 12 with the radial and top platen stresses considered to be principal stresses. The angle of internal friction for the dense sand was 41.6° with a correlation coefficient of 0.999, and the loose sand had a friction angle of 39.0° and a correlation coefficient of 0.999. These values are in close agreement with triaxial test results, as may be seen in Figure 12.

The soil-to-steel friction is another property that can be determined from the K-Test. This is done by setting a soil specimen to be tested on a pressure cell. A difference in stress is noted between the stress at the top of the specimen and the bottom of the specimen. This difference in stress is caused by side friction occurring between the mold and soil specimen. It is assumed that a uniform gradient of friction exists across this interaction surface. By assuming this gradient and knowing the stress (radial stress) acting normal to this interface, it is possible to calculate the friction angle of soil on steel.

36

K-Test results on a dense sand gave a friction angle of soil on steel equal to 17.5° with a correlation coefficient of 0.984 (10 data points). The loose sand had a soil to steel friction angle of 16.5° with a correlation coefficient of 0.994 (10 data points used).

Modeling clay

Modeling clay was used by Baligh and Scott (6) in their laboratory work on wedge penetration into clay for the following reasons: it has high cohesive strength, normally is homogeneous, and approaches rigid-perfectly plastic behavior. These same characteristics were desirable in this research, so a modeling clay manufactured under the commercial name Roma Plastilina was selected to represent a clay soil. The modeling clay was available in two colors, white or gray, but it was available in only one consistency.

The bulk density of the clay was determined by the following method of testing: the clay was compacted into a standard Proctor mold (944 cc) in three lifts. Each lift received 25 blows from a 4.5 Kg hammer dropped 46 cm. A density of 1.55 g/cc was determined through this method, and all subsequent testing was done on modeling clay molded in this same way.

In order to evaluate the effect of different cohesive material strengths on the ability of the vane stress sensor to perform properly, it became necessary to change the consistency of the commercially available modeling clay. This was done by adding mineral oil (0.7% by weight)

37

to the clay. This increased the cohesive strength of the clay
and allowed testing on modeling clay with two different consistencies.

X-ray diffraction technique was used to determine the modeling
clay mineralogy. A copper x-ray tube was used in the analysis with a
nickel filter. The x-ray trace of the clay is shown in Figure 14. Trace
A was run on a sample of untreated clays. By observing the 2θ angles at
which peaks occur, it was possible to identify the presence of kaolinite
(11) in the clay sample. But, at the lower 2θ angles peaks were observed
that were not characteristic of kaolinite. A second x-ray trace was made
on a clay sample that had been heated to a temperature of 400°F for four
hours to remove organic matter. The trace for this sample, Figure 14,
indicates the low 2θ peaks disappeared and the clay is composed of one
clay mineral, kaolinite. The clay in its commercial form also contains
some organic compounds.

Shearing strength of the material was determined by the same
methods of testing used for sand. A set of three triaxial tests
(unconsolidated undrained) were performed on the softer commercial
form of modeling clay. The test indicated an internal friction angle
of 4° and 3 psi (21 KPa) cohesion, the correlation coefficient being
0.998 for this data. The K Test also gave these same values for ϕ and
c, with a correlation coefficient of 0.961. A K Test of the stiff
clay gave a friction angle of 8° and a cohesion of 4 psi (28 KPa),
with a correlation coefficient of 0.998.

Heated 400° C

20 · (degrees)
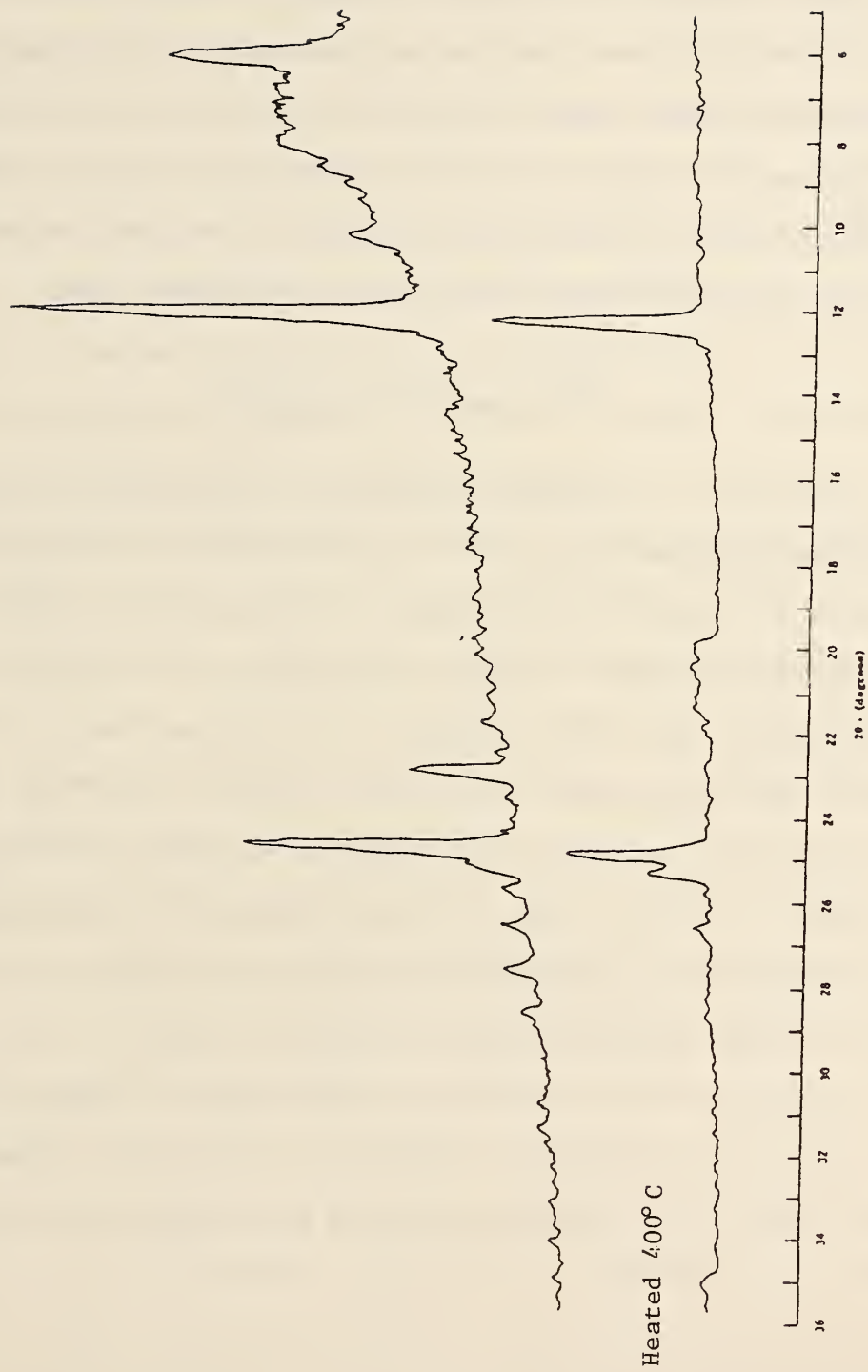
Figure 14. X-ray diffraction traces of modeling clay.

39

The soil-to-steel friction parameters were calculated for
each modeling clay consistence in the same way as for the sand tests.
Results indicated an adhesion term of soil-on-steel was present in
the modeling clay test, the friction angles being 6° and 5° with an
adhesion of 3 KPa and 2.5 KPa respectively for the stiff and soft
clay. Both had correlation coefficients greater than 0.94.

Blade Insertion Into Sand

The purpose of laboratory testing was to determine the amount of
disturbance and resulting stress increase caused by the insertion of
a rigid steel blade into a soil mass. The ideal soil mass would be
semi-infinite, but this of course is impossible. Two possibilities
were available that could approximate a semi-infinite mass, one being
a box of large dimensions, and the other being an Iowa K-Test mold.

The box had two major shortcomings in this type of testing. If
the sides of the box are rigid a boundary condition is inevitable. The
other problem is the development of friction forces along the sides
of the box when vertical or lateral loads are applied to the soil mass.

Selection of an Iowa K-Test mold substitutes an elastic yielding
boundary but with an inherent high modulus of elasticity compared to
that of soils. This high modulus should cause higher stress changes

to occur when a rigid inclusion is inserted into a soil specimen contained in the mold. Therefore usage of a K-Test mold should exaggerate the error and be a conservative step. The main advantage of using a K-Test mold instead of a box is that the mold expands in the lateral direction, more-or-less simulating confinement in a semi-infinite mass. Therefore, the K-Test mold was selected for laboratory testing. A second advantage is that the lateral stress at all times may be monitored from expansion of the mold, allowing a ready evaluation of the stress effects from blade insertion.

The rigid inclusions used to represent a vane stress sensor are steel blades 6 inches long, one or two inches wide, and 1/8 in., 3/16 in., or 1/4 in. thick. The blades were tapered at one end by an apical angle of 45°, 60°, or 90°. The surface of each blade was either ground smooth or sanded rough with 60 grit emery cloth. No attempt was made to use scaling laws in the design of these blades. Previous researchers (38) have found that conventional dimensional analysis of model tests in sand fail. Scale effects have to be assessed in a different way, because they relate to changes in intrinsic properties of the material.

The testing procedure used is outlined in the following steps:

1. The K-Test mold was expanded by inserting a soft rubber specimen and compressing it under load. When the mold reached a specific lateral deflection, a metal bar was slipped into the mold slit. Then the rubber specimen was unloaded allowing the K-Test mold to tighten on the metal bar, which kept the mold from reaching its initial

41

unstressed state. Therefore a certain known stress is locked into the mold. The rubber specimen is then removed.

2. The mold is placed on a pressure cell, as shown in Figure 15. Sand is poured into the mold and compacted to a predetermined relative density, either 40% or 75%, by tapping the mold. All sand tests had final sample heights of 4 in.

3. The mold and pressure cell are transferred to a loading machine. A stationary Teflon disc was clamped on top of the sand (Figure 15). The metal bar in the mold split is removed, causing a lateral and vertical pressure to be applied to the sand, since it is completely enclosed in the mold. The lateral reading of the mold is noted and is used in calculating the initial lateral stress. Also, the base pressure gauge reading was recorded.

4. It was initially assumed that blade penetration rate would not be a significant factor in sand test. Therefore a seemingly reasonable value of 0.0275 cm/sec was selected for test blade insertion in all sand tests. At blade depth penetration increments of 0.25 in. blade load, mold lateral deflection, and base pressure were recorded until the test blade reached a depth of penetration equal to 3.5 in.

5. The blade was then extracted at a rate of 0.0275 cm/sec. The same readings were taken in this step as in step 4, and at the same depths. This was done until the blade was completely extracted. Then the sample was extruded from the mold.

This laboratory testing procedure was modified when special horizontal layer samples were made to investigate the amount of disturbance caused by
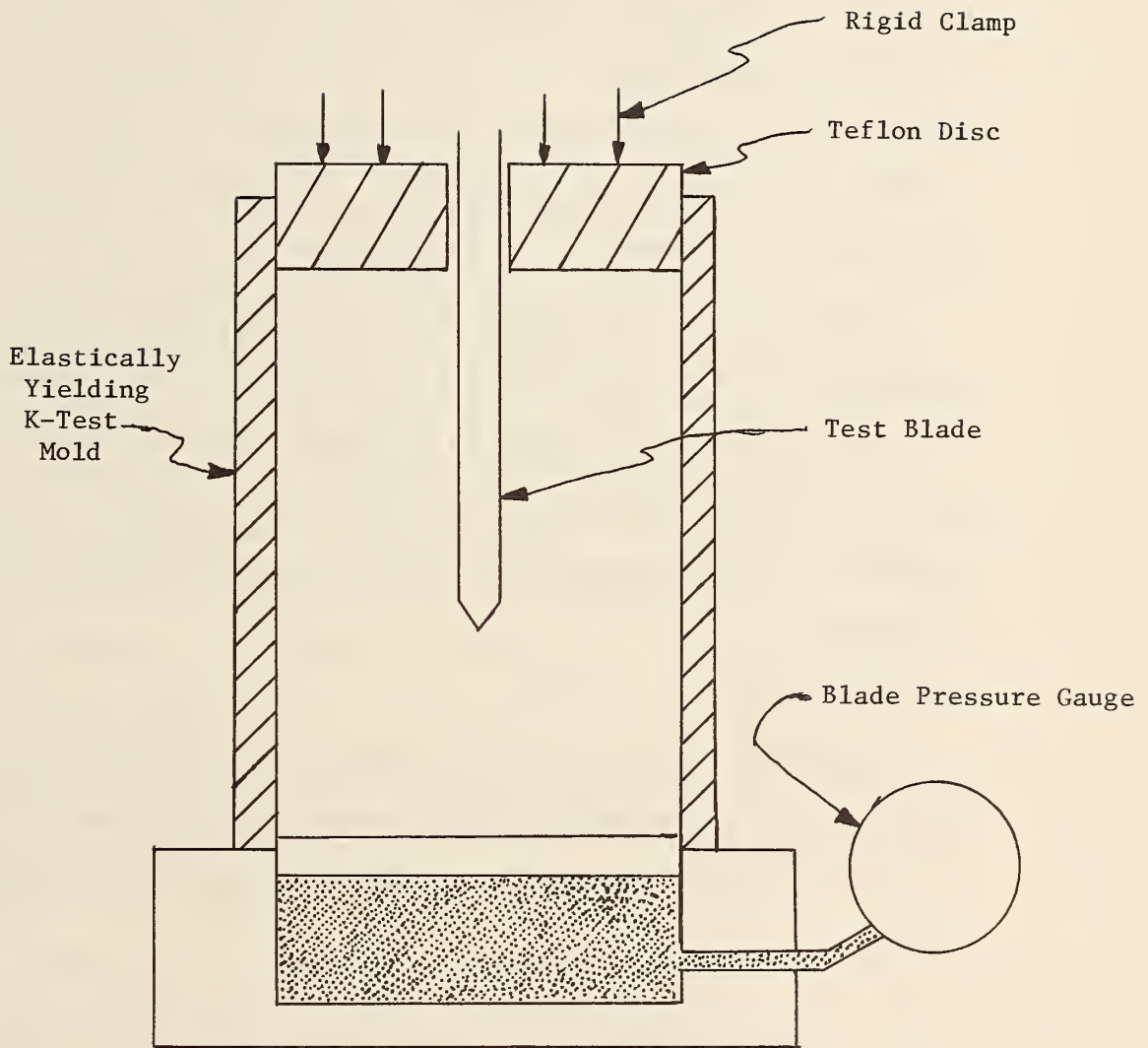
Figure 15. Laboratory testing apparatus.

blade insertion. Sand layered samples were constructed in the K-Test mold

with sand containing 1% by weight portland cement. Initially a natural colored

sand layer approximately 0.5 in. in height was placed in the mold.

Then a 1/4 in. thick layer of sand with a small amount of lamp black

mixed into it was placed in the mold. This stacking procedure was

followed until a sample 4 in. high had been constructed.

After the blade had been removed from the layer samples, the

samples were saturated with water and allowed to set 24 hours. At the

end of this period the sample was extruded from the K-Test mold and

sliced at predetermined vertical planes. Each sample was then photo-

graphed so that measurements on amounts of disturbance could be

recorded.

Data reduction

Two methods for data reduction were available from blade insertion

tests in the K Test mold. The first, based on the blade skin friction,

uses the following equation to obtain an average lateral stress on the

blade:

$$\bar{\sigma}_b = \frac{F_s}{A_b \tan \phi_s} \qquad (8)$$

where

$\bar{\sigma}_b$ = average lateral stress on blade

ϕ_s = angle of friction for soil-steel interface (from K-Test data)

A_b = area of blade in soil

F_s = pulling force on blade.

During insertion of the blade, the load acting on it is composed of F_s plus a force F_b exerted against the bottom of the blade. While pulling the blade, F_s is equal to the total force acting on the blade. The calculated F_s for each case, pushing or pulling, have been found to be unequal by numerous investigators (9, 35, 36). This is probably because downward friction from the blade adds to the overburden pressure, with a consequent increase in the lateral pressure on the blade. Conversely, the friction developing during pulling acts opposite to the overburden pressure close to the loaded blade. Due to uncertainties in estimating the bottom resisting forces, only blade loads recorded during pulling were used in calculating the lateral stress on the blade.

The second method for data reduction was simply to compare the K-Test mold stress after blade insertion to the stress before blade insertion.

A problem in data reduction was that in order to define the functional relationship between blade thickness and lateral stress, all variables except blade thickness should be held constant. It was found that the initial lateral stress on different samples varied by as much as 2 psi. Therefore, a nondimensional ratio of lateral stress on blade or mold to initial lateral stress on sample before

testing was defined and called λ. This allowed plotting of a graph with blade thickness on the abscissa and λ on the ordinate. An extrapolation of data points to a blade of zero thickness ideally should give a λ of one.

Blade Angle

The literature indicated that a blade apical angle of 60° would probably minimize disturbance effects caused by blade insertion, but it was deemed advisable to perform some laboratory checks before the major portion of laboratory testing was undertaken. All of these tests were done with smooth-finished blades 2 in. wide and 1/8 in. thick. The results are shown below.

Blade Angle	D_r, Sand Density	λ	
		Blade	Mold
45°	40%	14.84	10.17
60°	40%	2.12	2.84
60°	75%	9.41	8.65
90°	75%	14.21	16.78

As can be seen from the results, λ was minimized when the blade had an angle of 60°. This is in agreement with previous researchers, and all subsequent sand tests were done on blades with 60° tapered ends.

Mold effects

In all testing, data were reduced by assuming a uniform distribution of stress across the surface of the blade. To test this assumption,

46

a special blade was fabricated as shown in Figure 16. The dimensions of the blade were 7 x 2 x 1/8 in. One side of the blade was ground down so that six pieces of steel tape covered with a layer of shim stock would lay flush on the blade surface and would maintain the initial blade thickness of 1/8 in.

Four pieces of the steel tape had the same dimensions, 6 x 0.25 x 0.005 in. The other two pieces had a width of 0.5 in. The tapes were laid side-by-side against the blade surface, the two wider strips being at the outside, and a layer of 0.005 in. shim stock was placed over them and epoxy glued to the blade just above the angle taper.

This blade was inserted into a K-Test mold containing sand at 40% relative density. The previously described procedure for blade insertion was followed; then when the blade reached the final penetration depth of 3.5 in., the strips were pulled sequentially a distance of approximately 0.050 in. The maximum force encountered for each tape was recorded during the pulling operation.

Later, this same blade was inserted into a small box 2ft. x 1.5ft. x 4 in. in dimensions filled with sand at 40% relative density. Again the strips were pulled with the maximum resisting force on each recorded.

Two tests each were run in the K-Test mold and in the box. The results of these tests are shown in Figure 17, with a plot of strip location as the abscissa and the ratio of pulling force per inch ÷ maximum force per inch width as the ordinate.

47

EXPOSED FRICTION STRIP   SHIM COVER STOCK

Figure 16.   Photographs of special stripblade with friction strips.
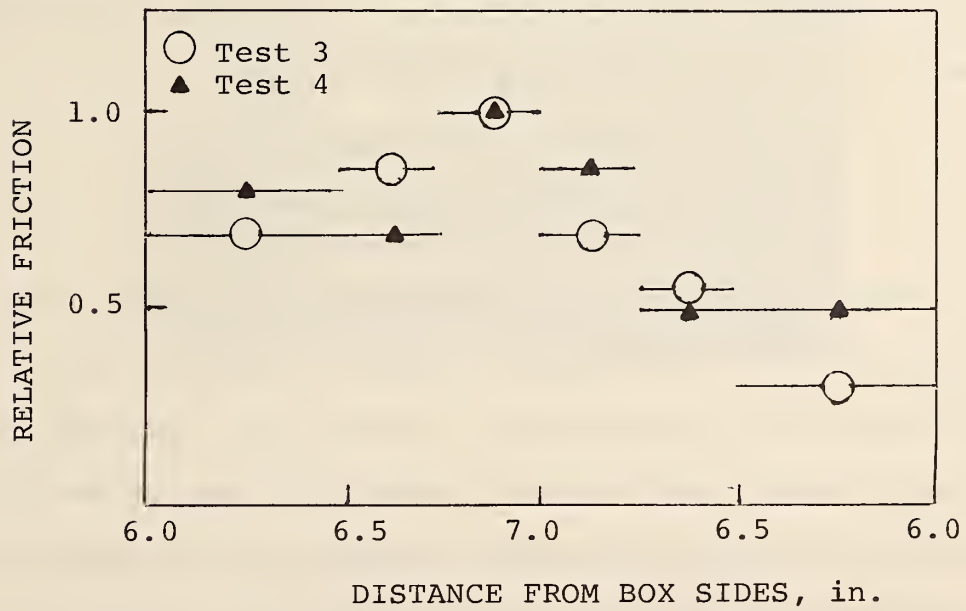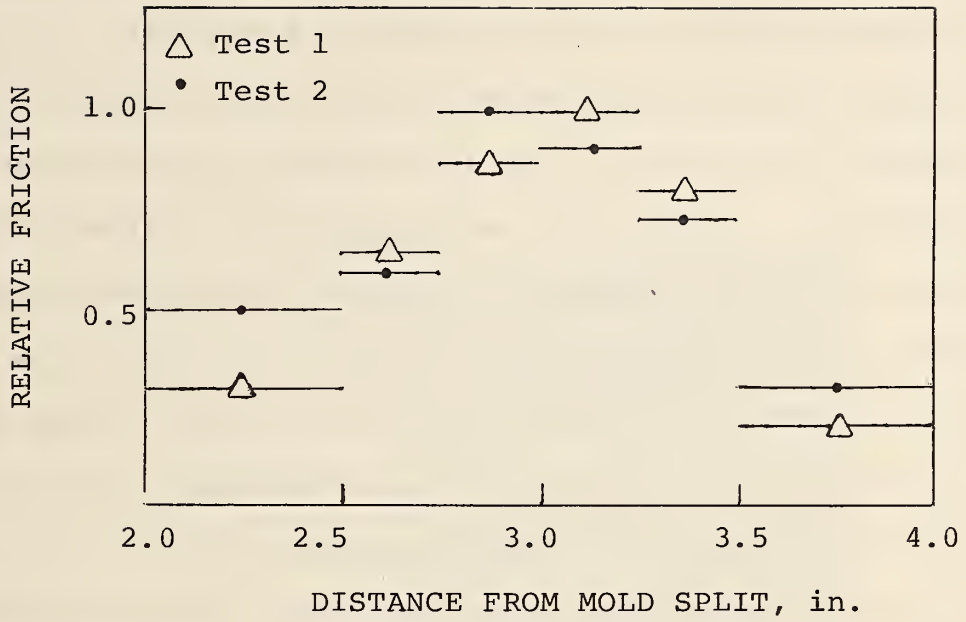
Figure 17. Test Results from special "tape" blade in sand.
1 in = 2.54 cm

The top plot in Figure 17 shows the results when the special blade was inserted into sand confined by a K-Test mold. In test 1, the first tape pulled was the one farthest from the mold split, whereas in the second test, the tape closest to the mold split was pulled first. By doing this, error introduced by pulling sequence would be averaged. The plots for these two tests indicate a non-linear stress distribution across the blade. The data points on the side of the blade nearest the mold split are closer to being equal in value than the other points. This is probably due to the way in which the mold opens when the blade is inserted into it, allowing more soil movement to occur on the half space closest to the mold split causing a more uniform stress distribution to develop. The plot of data points from box tests 3 and 4, Figure 17, indicate a more uniform distribution of stress across the blade, by avoiding assymetrical loading conditions in the K Test mold.

Blade Insertion Into Modeling Clay

Modeling clay tests followed the general procedure outlined for sand tests, with the exception of sample preparation. The clay was not compacted in the K-Test mold. Instead it was compacted in a standard Proctor mold, extruded, wrapped in a sheet of aluminum foil and slipped into the K-Test mold. Aluminum foil was used to increase the overall volume of the specimen, resulting in a higher initial
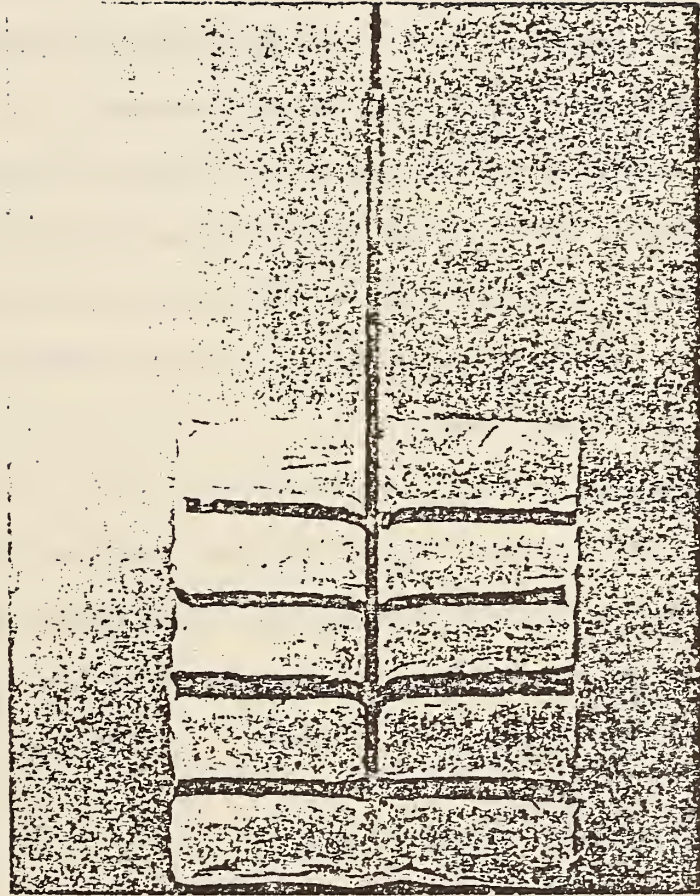
Figure 18.   Photograph of a layered modeling clay specimen
with a metal blade inserted into it.

lateral stress.

Some layer samples were constructed with the low consistency clay. This was done by compacting two specimens, one gray and one white, and slicing them into "biscuits" approximately 0.5 inches in height. The biscuits were stacked in alternating colors to a height of 4.5 inches. Care was taken in this stacking process to make sure the samples retain a right circular cylinder shape.

Figure 18 contains a photograph of a layer clay specimen sliced open to expose a 1/8 in. blade that has been inserted into it. Normally the blade would be extracted so that the stress acting on its surface could be calculated, this specimen being prepared for illustrative purposes only.

Data reduction

Because the friction between clay and steel was found to be dependent on two parameters, namely friction angle and adhesion, the equation used in clay test data reduction was:

$$\bar{\sigma}_b = \frac{F_s - \alpha A_b}{A_b \tan \phi_s} \tag{9}$$

where

$\bar{\sigma}_b$ = average lateral stress on blade

ϕ_s = angle of friction for soil-steel interface

α = adhesion for soil-steel interface

A_b = area of blade in soil

F_s = shear force acting on blade surface

The definition of the dimensionless term λ is the same as in the sand tests.

Rate of Penetration

Creep and pore pressure are two physical phenomena common in clay, and have a time-dependent behavior. Therefore the penetration rate at which a blade is inserted into a clay specimen became more important than it was during sand testing, and a short investigation was done to determine a rate by which changes from the initial stress regime would be minimized.

Previous research work on cone penetration rates indicated that a tenfold increase or decrease in rate was necessary to significantly change resistance value of penetration in a clay deposit (16). Therefore tests were performed at three penetration rates on the low consistency clay. A smooth blade 2 in. wide and 1/8 in. thick with a taper angle of 60° was used in all three tests. The results are summarized below.

Penetration Rate (cm/sec.)	λ	
	Blade	Mold
0.00275	6.17	2.12
0.0275	4.32	1.41
0.275	11.15	5.5

53

The results indicate the rate previously used in sand testing is also optimum for clay testing, so this rate was used throughout the remaining laboratory tests.

Blade Angle

The optimum angle for the blades used in clay testing was determined by a procedure similar to that used in sand. Three blades with differing angles on their tips were inserted into low consistency clay specimens. The blades all had a smooth finish, a width of 2 in. and a thickness of 1/8 in. The results of these tests are listed below.

Angle	λ	
	Blade	Mold
45°	0.78	1.94
60°	4.32	1.41
90°	6.11	4.58

The selection of the optimum angle was not as clear-cut as it had been in the penetration rate selection. The mold λ values indicate a 60° angle causes the least stress increase, but a 45° angle produced the lowest blade λ. If λ is calculated correctly, it seems reasonable that no λ would be less than one, since a lower value would indicate a decrease in stress due to the insertion of the blade. This could only occur by developing a negative pore pressure. Therefore, because of the questionable blade λ value calculated for the 45° angle, more weight was placed on the mold λ values. These values suggest the 60° blade is optimum, and this was used in all subsequent clay tests.

STRESS SENSOR DESIGN

The pneumatic stress sensor used in this research was devised
by Dr. R.L. Handy and Dr. E. G. Ferguson and introduced in February
1977 (13). To evaluate the workability of the proposed sensor, the
following laboratory investigation was undertaken. The perfected
sensor then was incorporated into a metal blade for further laboratory
testing in sand and modeling clay.

Model Test

Procedure

The initial laboratory set-up used in developing the stress cell
was designed by Dr. Glen Ferguson, then Chief Engineer for Soil
Systems, Inc. It consists of a needle valve, pressure gauge, sensor
simulator, air lines, and two consoles. Each console was equipped
with a pressure regulator, pressure gauge, and air tank.

The set-up is shown in Figure 19. Console 1 was used to supply
air at a constant pressure through line 1 (approximately 7 ft in
length) to a needle valve. The pressure in this line was kept at
either 60 psi or 80 psi, and is indicative of a "tank pressure."
The needle valve was used to regulate the air flow through line 2
(approximately 1.5 ft in length) to the sensor. A pressure
gauge was placed between line 2 and the needle valve, so that
calibration of the sensor could be attained. Later, for reasons
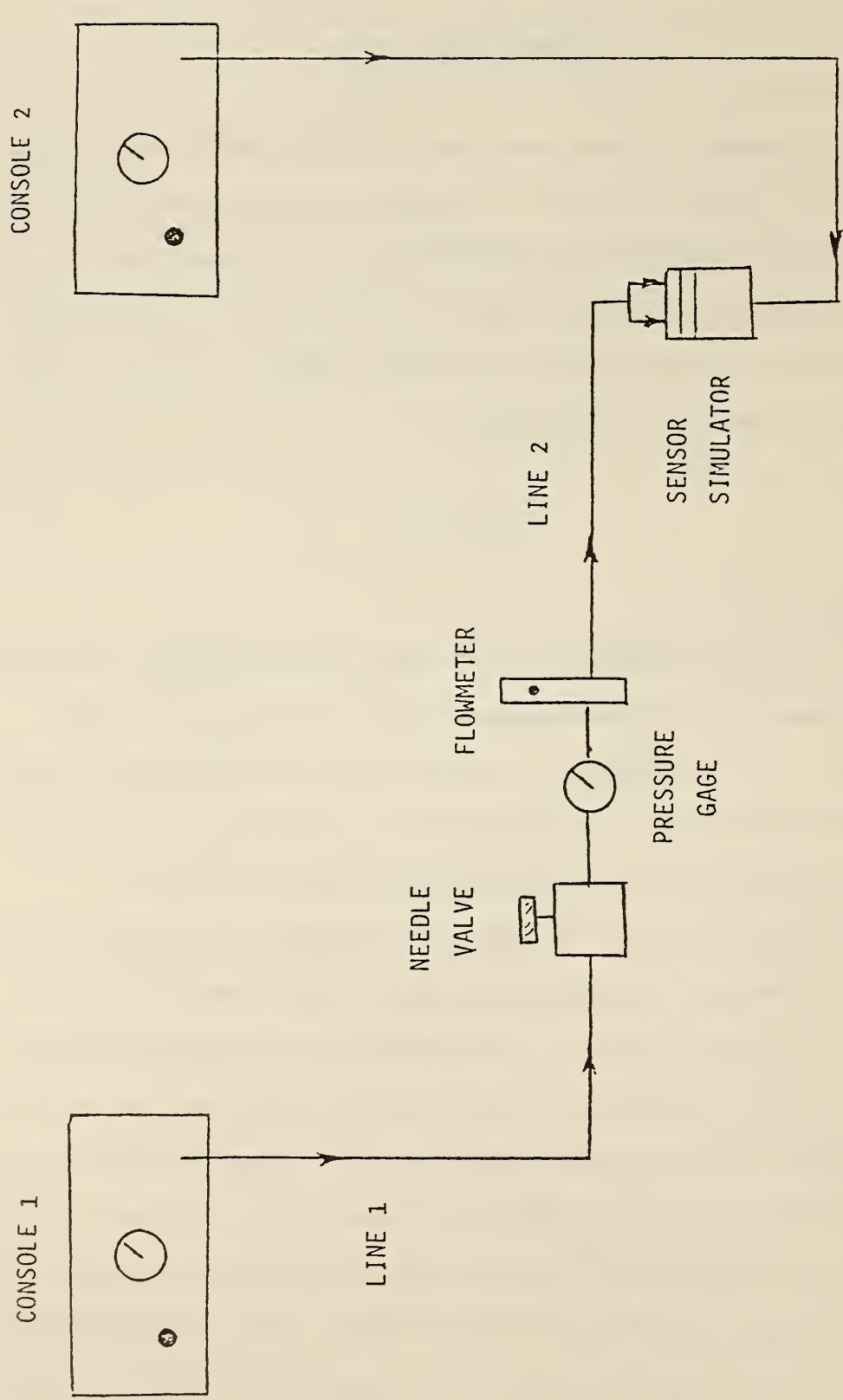
Figure 19. Schematic of laboratory set-up used in testing gas-flow pressure sensor concept.

56

yet to be discussed, a flow meter was placed between the pressure
gauge and line 2. Console 2 was used to supply a constant air
pressure to the soil simulator chamber. The consoles were standard
equipment for the Iowa Borehole Shear Tester manufactured by Handy
Geotechnical Instruments, Inc., Ames, Iowa.

The sensor simulator pictured in Figure 20 was designed to give
maximum flexibility in changing sensor membranes and also to allow
pressure applied on the sensor to be adjustable. The simulator
consists of the sensor body, which had two air inlets each of which
enter into separate inlet chambers. Between the inlet chambers was
an exhaust chamber that was open to the atmosphere. Covering the
sensor body was a diaphragm such as shim stock. The diaphragm was
held firmly against the sensor body with a hold-down disc. An air-
tight gasket was placed between the hold-down disc and the soil simula-
tor chamber. The soil simulator chamber was used to simulate the pressure
of a soil mass. The soil simulator chamber had an air inlet that
allowed the pressure in it to be varied, consequently the pressure on
the sensor was also varied.

The sensor simulator operates in the following manner:

1. The pressure in the soil simulator chamber is increased and
held at a predetermined value. This causes the diaphragm to seal
tightly against the sensor.

2. Air is forced into the sensor inlets causing air in the inlet
chambers to increase in pressure. The pressure increase continues until
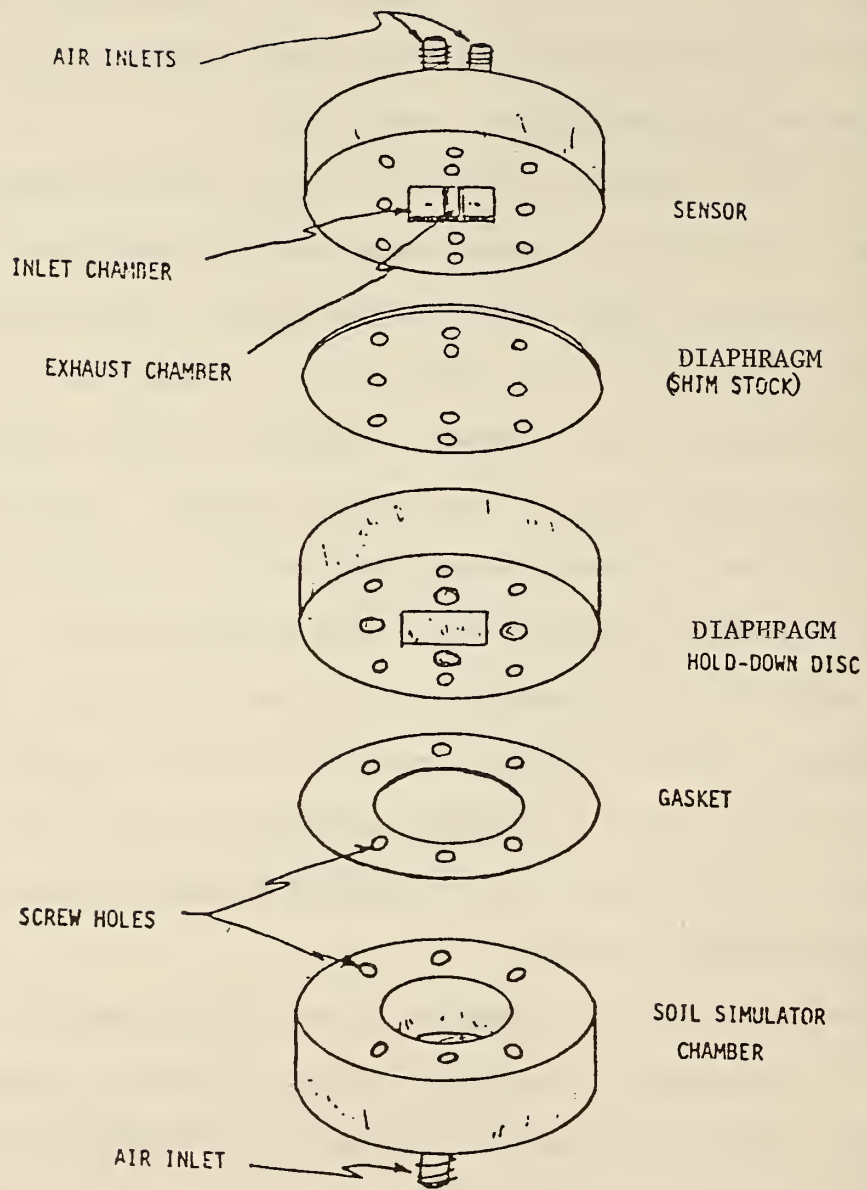
Figure 20. Drawing of sensor simulator used to evaluate the pneumatic stress cell

it just exceeds the soil simulator chamber pressure. At this time the diaphragm bulges out away from the sensor. The air in the inlet chamber rushes into the exhaust chamber, resulting in a pressure drop in the inlet chambers.

3. The pressure drop will cause the diaphragm to collapse to its original position against the sensor body. This will reseal the inlet chambers allowing the pressure in them to again increase, thus beginning the same cycle of events over again. This cyclic operation of filling the inlet chambers with air and then after pressure build up allowing them to exhaust, gave the sensor a "fluttering" effect.

A specific testing procedure was set up in hopes of answering the following questions:

1. Can the gas-flow pressure sensor be taken from concept to a working model?

2. If so, what diaphragm material should be selected for the sensor?

3. Does the length of air lines have any effect on the sensor calibration?

To answer the first question, 0.002 in. thick brass shim stock was placed in the sensor simulator. Console 2 was set at 10 psi, thus applying the same pressure onto the sensor by way of the soil simulator chamber. At this time console 1 was set at 60 psi, and the needle valve slowly opened. The pressure in line 2 was increased until it reached a maximum value of approximately 14 psi. At this point the sensor started fluttering. The fluttering was indicated by an audible

hissing, due to gas being exhausted into the atmosphere, and an oscilla-
tion of the pressure gauge needle. Maximum and minimum readings
indicating the pressure in line 2 during both bulging and return of the
diaphragm were taken.

After the maximum and minimum pressure readings had been recorded,
the pressure in the soil simulation chamber was increased in increments
of 10 psi. At each increase, the pressure in the line to the sensor was
also increased until the sensor again began "fluttering." During this
time the maximum and minimum gauge pressures were recorded. This process
continued until the limiting tank pressure was reached. The results
of this test were plotted with the soil simulator chamber pressure on the
abscissa and the sensor pressure on the ordinate. Remarkably linear
plots were observed from these results. Therefore, it was concluded the
stress sensor concept could be turned into a functional sensor that would
be easy to calibrate.

Selection of the best material for the diaphragm was done in a trial-
and-error process. Basically it involved trying different materials (e.g.,
steel, brass, and aluminum) and different thicknesses to arrive at the
presumably best membrane. A plot of soil simulator pressure versus
sensor pressure was made for each type of shim stock tested. An
example is shown in Figure 21.

The effect of varying line lengths was investigated on both line 1
and line 2. Initially, a twenty-five foot extension was added to line
1. A new calibration was performed on the sensor, and compared to the
previous calibration curve.
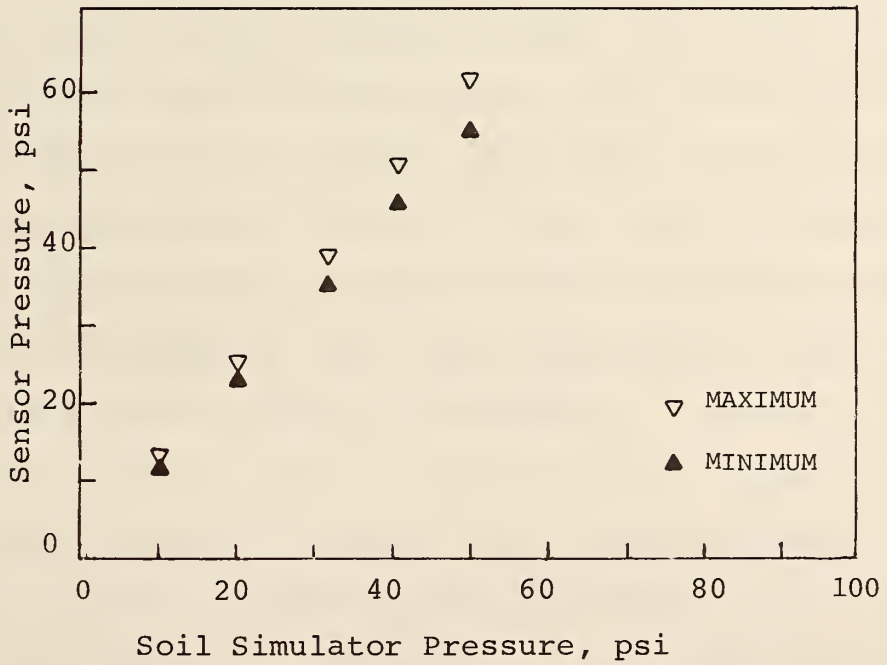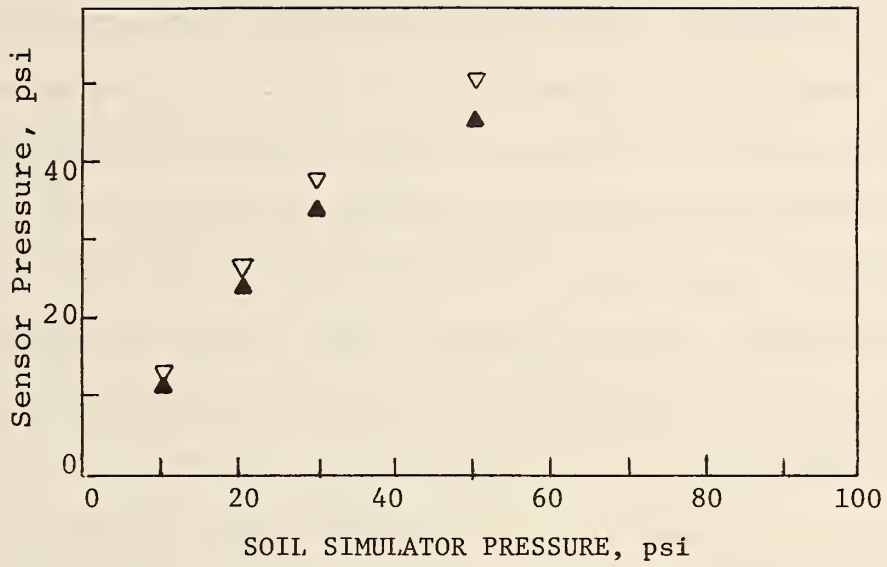
Figure 21.   Typical plot of results obtained from
          a steel diaphragm performance test
              1 psi = 70.31 gm/sq cm

This same method was to be used when a 25 ft extension was placed on line 2. When line 2 was increased in length, no oscillation of the pressure gauge could be observed. The audible fluttering noise of the sensor was heard, but the compressibility of the air in the longer line caused the previously observed pressure gauge fluctuation to be non-existant. This meant that the operator would not know the sensor had begun fluttering; instead he probably would continue increasing the pressure in line 2, which would only result in an increase in the sensor response rate.

The use of a remotely-located pressure gauge to monitor the pressure at which a sensor began oscillating was questioned. One alternative would be to measure the pressure with a transducer that was located close to the sensor; another was to make an electrical contact between the sensor membrane and the sensor body such that when the sensor started fluttering a break in the circuit would result. Either of these ideas, if implemented, would require electrical lines to be placed "down the hole" when the vane stress sensor was used. Also, the electrical circuit breaker idea could cause an anode to develop which might result in considerable corrosion to the stress sensor. An alternative was devised to solve the fore-mentioned problem.

By reasoning that after each cycle (that is pressure build-up then release) a surge of air would take place in line 2, it should be possible to detect the "surge" with an air flowmeter. A flowmeter with a range of 0-100 ft^3/hr was placed after the pressure gauge as pictured in

Figure 20. The addition of the flowmeter made it possible to construct a plot similar to Figure 20, even though line 2 had been increased in length by 25 ft.

Preliminary Diaphragm Selection

Test results on different diaphragm materials were compared by a least-square line fitting method applied to data points. A summary of test results can be found in Table 1. The constants "c" and "d" represent the slope and intercept of the previously mentioned line. Correlation coefficients, r, of the lines were used to check the strength of the relationship between the two pressures.

Three materials initially were tried as sensor diaphragms, their pertinent properties being listed in Table 2. Aluminum shim stock used in the sensor was found to be inadequate because yielding occurred at low stresses, making calibration impossible. Both brass and steel shim stock at equivalent thickness produced approximately the same constants "c" and "d". Steel was tentatively selected as a sensor membrane due to its high modulus of elasticity and low coefficient of thermal expansion. Also, the sensor membrane is repetitively "fluttered" so a material such as steel with a high endurance limit is needed.

Membrane thickness selection was governed by two criteria: the thickness should be maximized for durability, but the maximum thickness will be limited by the requirement that the diaphragm be flexible enough to properly seal against the sensor body. Three different thicknesses of shim stock were tested; results are summarized in Table 1.

Table 1. Summary of Diaphragm Test Results

1 in = 2.54 cm , 1 psi = 70.31 gm/sq cm

Number	Material	Thickness (in.)	Tank Pressure (psi)	Gauge Reading (Max/Min)	c	c	r	Trials
B1	Brass	.001	60	Max.	1.22	3.22	0.999	2
			60	Min.	1.13	2.32	0.994	2
			80	Max.	1.23	2.20	0.999	2
			80	Min.	1.13	1.85	0.998	2
B2	Brass	.002	60	Max.	1.29	-0.11	0.998	2
			60	Min.	1.11	1.82	0.998	2
			80	Max.	1.21	1.50	0.999	2
			80	Min.	1.07	2.73	0.998	2
B3	Brass	.005	60	Max.	1.20	2.75	0.998	2
			60	Min.	1.12	2.75	0.998	2
			80	Max.	1.20	2.45	0.999	2
			80	Min.	1.06	3.40	0.999	2
B4[a]	Brass	.002	60	Max.	1.19	1.25	1.000	1
			60	Min.	1.06	2.75	1.000	1
			80	Max.	1.19	1.55	0.999	1
			80	Min.	1.06	3.00	0.999	1
B5[b]	Brass	.002	60		1.10	10.50	0.997	1
			80		1.18	9.65	0.998	1
S1	Steel	.002	60	Max.	1.24	0.87	0.999	2
			60	Min.	1.09	2.00	0.999	2
			80	Max.	1.24	0.63	0.999	2
			80	Min.	1.07	2.23	0.998	2
S2	Steel	.005	60	Max.	1.17	0.125	1.000	2
			60	Min.	1.05	0.375	0.999	2
			80	Max.	1.16	0.29	0.999	2
			80	Min.	1.03	1.09	1.000	2

a Additional 25 ft. air line added between console 1 and needle valve.

b Additional 25 ft. air line added between pressure gauge and sensor simulator.

Table 2.   Average properties of selected enginnering materials.
           1 in = 2.54 cm, 1 ksi = 70.31 kg/sq cm

Material	Modulus of Elasticity (1000 ksi)	Coefficient of Thermal Expansion $(10^{-6}$ in/in./F)	Endurance Limit (ksi)
Aluminum	10.3	12.5	6–11
Brass	15	9.8	7–20
Steel	29	6.6	24–32

The 0.005 in. shim stock did not seal properly on the sensor body, and air leaked from one inlet chamber to the exhaust chamber when this thickness was tested. Both the 0.001 in. and 0.002 in. thicknesses appeared to work properly. Therefore it was suggested that the thicker of the two (0.002 in.) be used in future sensors.

In all sensor tests high correlation coefficients were obtained. Since the data points used in the least-square line fitting method were normally from two independent trials, high correlation coefficients should give some indication that calibration of the sensor is highly reproducible.

Line length effects were studied in tests B4 and B5. The B4 test had a 25 ft extension on line 1. The effect of this increase in line length was fairly insignificant. But the B5 test, which had a 25 ft. extension on line 2, showed an increase in the "d" coefficient (see Table 1). This increase, though significant, is probably due to frictional resistance in line 2 and the air experiencing density changes in the line during sensor operation. It should be noted that in this test

maximum and minimum pressure gauge readings were not recorded. Instead, only a single reading could be taken since no oscillation of the pressure gauge was observed. Actuation of the sensor in this test was indicated by oscillation of the ball in the flowmeter. This method of sensor calibration was found to be extremely precise.

Blade-Mounted Sensors

Since encouraging results were attained in testing the stress sensor concept and in selecting a sensor diaphragm, it was decided to continue the study with soil contact rather than air contact. A new stress sensor was designed and mounted on a steel blade. The overall blade dimensions are 7.0 x 2.0 x 1/8 in. The blade had a smooth finish and a 60° angle taper on its bottom. The blade, like all previously used blades, was made of cold-rolled steel.

The sensor was located 3.8 cm from the bottom of the blade on center. Intake and exhaust lines were machined into the blade on the side opposite the sensor. After machining, these lines and the sensor were covered with a layer of shim stock.

The sensor was made circular in shape to avoid stress concentrations at corners. The overall diameter of the sensor was one inch, which is equal to one half the blade width. The inner chamber was used as an exhaust chamber, while the outer chamber was equivalent to the inlet chambers used in the model stress sensor tests.

66

Results from the stress sensor development phase of this study indicated that steel shim stock 0.002 in. thick would be the optimum material for a sensor membrane. Initial attempts were made to cover the stress sensor with this grade of shim stock by silver soldering them together. Unfortunately, heating the thin piece of steel caused it to develop weak spots that probably would oxidize in a short period of time, rendering the sensor useless. Therefore, stainless steel was used instead of cold-rolled steel, and epoxy-cemented into place. Although no testing was done during the preliminary selection tests on stainless steel, it was felt that its physical properties were sufficiently close to those of cold-rolled steel that the sensor should perform properly.

One further modification was done to the testing apparatus before any testing was done with the sensor blade. The flowmeter previously used was replaced with a purge meter that had a range of $0.2 - 3.5 \text{ ft}^3/\text{hr}$. to increase the sensitivity of the apparatus.

The sensor blade was calibrated in a cell filled with water. Pressure in the water cell was increased in increments of 5 psi to 50 psi, and at each increment the pressure into the blade inlet chamber was increased until the purge meter indicated the sensor had begun fluctuating. This pressure was recorded. A plot was made of blade sensor pressure versus water cell pressure. A straight line was fit to the data points using a least square method, this resulted in a high correlation coefficient (1.00) indicating the sensor should be very precise.

Only two tests were performed with the new blade. One of the tests was done with the low consistency modeling clay confined by the K-Test mold. The previously established procedure for clay testing was followed in this test, except for taking a pressure reading with the sensor before the blade was removed from the specimen.

The results of this test are summarized in Table 3. The initial mold σ_3 indicated in the table was defined as the lateral stress acting on the specimen before insertion of the blade. Final σ_3 mold is equal to the stress on the specimen at the soil-mold contact during the time the stress sensor was being actuated. Blade σ is the lateral stress acting on the blade calculated from pulling force, and sensor σ is the pressure measured by the sensor membrane.

Table 3. Summary of test results using a blade with steel diaphragm stress sensor

1 psi = 70.31 gm/sq cm

| Material | Mold σ_3 (psi) | | Blade σ (psi) | Sensor σ (psi) |
	Initial	Final		
Soft Clay	4.57	5.42	40.74	11.06
Sand	4.27	13.24	18.67	10.52

Results of the modeling clay test indicate a significant difference between the calculated blade lateral stress and the sensor pressure reading. Since only a small increase in mold stress occurred due to insertion of the blade, it would seem unreasonable to expect a 10 fold

68

increase in stress around the blade due to its insertion. One reason for the discrepancy between calculated blade σ and sensor σ is the assumption the friction angle and adhesion of soil on steel measured for the mold apply to the blade.

A test was also performed on sand compacted to 40% relative density with the new blade. The same general procedure was followed in this test as was previously outlined in initial sand test. The results of this test also are indicated in Table 3, and are in closer agreement than in the clay test. As shown in Figure 16, the stress at the blade center is of the order of two to three times higher than at the edges, and this difference is accentuated by the K-Test mold. It should be mentioned that it was not anticipated that the agreement of data in Table 3 would be close, because of the high K-Test mold elastic constant compared to soil, the stress concentrations and discontinuities in the mold, and the indirect means for assuming the blade σ from pulling force.

Further Sensor Designs

Preliminary tests with the steel diaphragm stress sensors indicated two rather serious problems: sealing of the diaphragm, and puncturing when testing in dense sands. Any hole in any diaphragm renders the device useless, and replacement of the stainless steel was inconvenient and required long setting times.

The search for a material that would resist puncturing by sand grains ended with the choice of Teflon-TFE. The flourocarbon resin

69

film 0.010 in. in thickness was found to be tough enough and also provided a good seal between the pressure and exhaust chambers of the sensor. Figure 22 shows photographs of a sensor with and without the Teflon diaphragm. The diaphragm is held in place by a brass press-ring, and is supported from behind by a porous brass plate. The diaphragm and press-ring are both flush with the surrounding surface of the blade.

Calibration

Initial calibration tests of the stress sensor were performed in a cell filled with water, increments of pressure being applied to the water and thus to the external surface of the sensor. The stress at each pressure increment was determined by the sensor and the resulting data set was plotted.

The water cell calibration method was time-consuming and difficult to perform but was felt satisfactory when stainless steel diaphragms were being used. However, with the ease of replacement of Teflon-covered sensors, a more convenient calibration method was considered necessary. For this purpose a small chamber that clamps to the blade is placed over the sensor, and pressure is applied to the chamber. The sensor stress corresponding to each chamber pressure is evaluated and plotted. A typical calibration plot for the sensors on the stepped vane is shown in Figure 23. All three plots have high correlation coefficients.

The calibration plots are virtually unchanged when the Teflon diaphragms are replaced. A statistical analysis of variance of many calibration tests with different diaphragms indicated that the slopes and intercepts were essentially constant at a 95 percent confidence

Figure 22. Photographs of teflon diaphragm stress
sensor
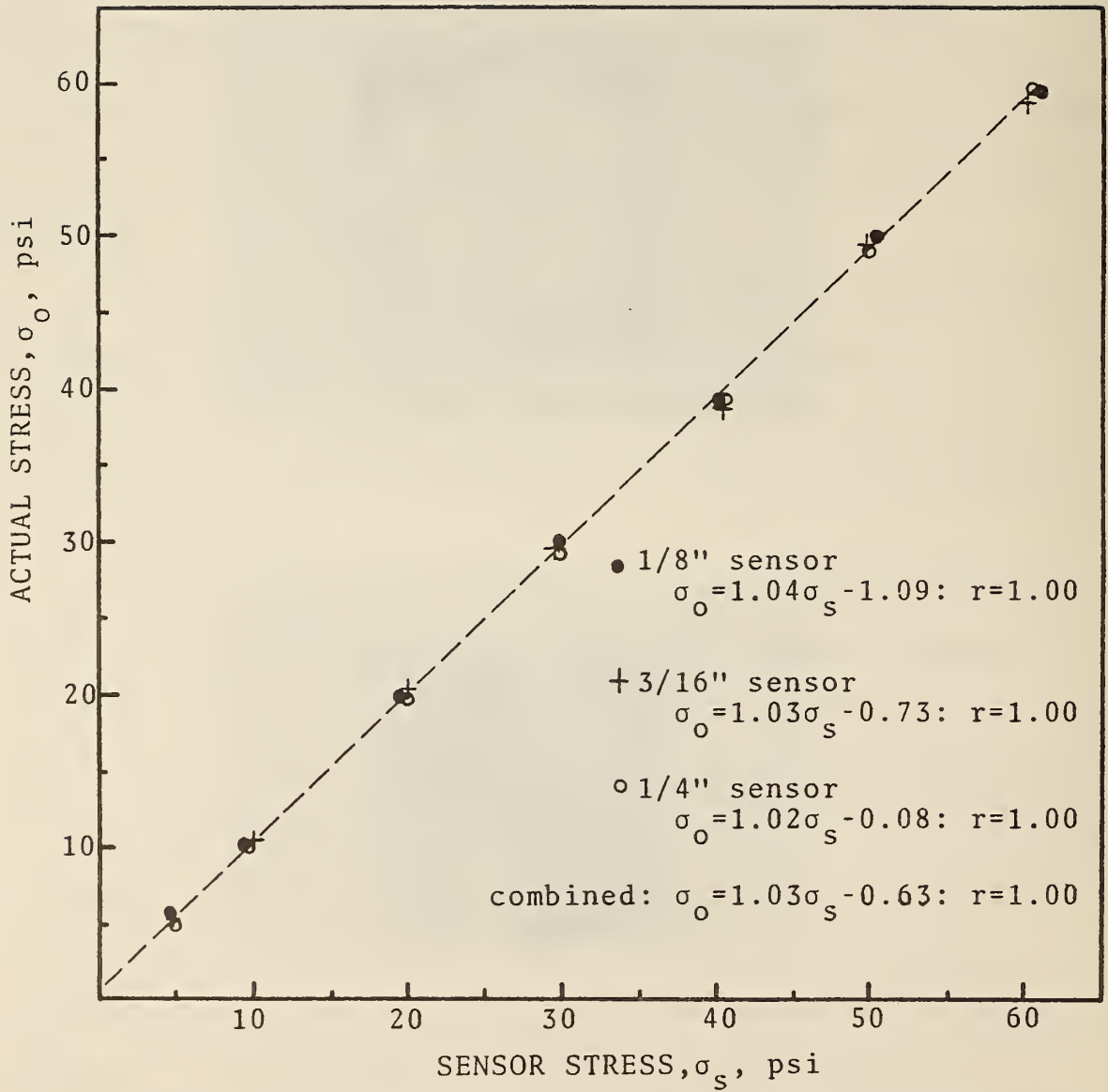
Figure 23. Calibration plots for the teflon diaphragm stress
sensors of the stepped VSS device.

1 psi = 70.31 gm/sq cm

72

interval. Only periodic calibration checks are thus required when diaphragms are replaced correctly.

In calibration tests it was found that the rate at which pressure is applied to the sensor prior to leakage has an effect on the results, too fast a rate causing the diaphragm to lift at an erroneously low pressure. A very slow rate is therefore preferable. However, a rapid test also is desirable. Therefore a uniform rate of approximately one psi/sec was chosen as a convenient yet slow enough rate. Any rate can be employed as long as the calibration is determined using the same rate as in the test.

Extensive tests using Teflon diaphragms have been favorable. Even in dense sand the diaphragms resist damage, and with the press-ring fit, damaged diaphragms can be replaced rapidly with a minimum of equipment. The only problem encountered has been in the field in very cold weather the brass press-rings loosen due to thermal contraction. This problem can be alleviated by use of rings with a thermal coefficient of expansion the same as that of the blades, or by using a flush-head screw to hold the ring in place, Fig. 24 shows three sensors mounted on a stepped blade.

Peripheral Equipment

The support system required to operate the stress sensor is shown in Fig. 25. Gas flows through a regulator and pressure gauge and goes to the sensor. A flowmeter in the return line then detects when the diaphragm lifts and vents into the exhaust chamber of the sensor. The
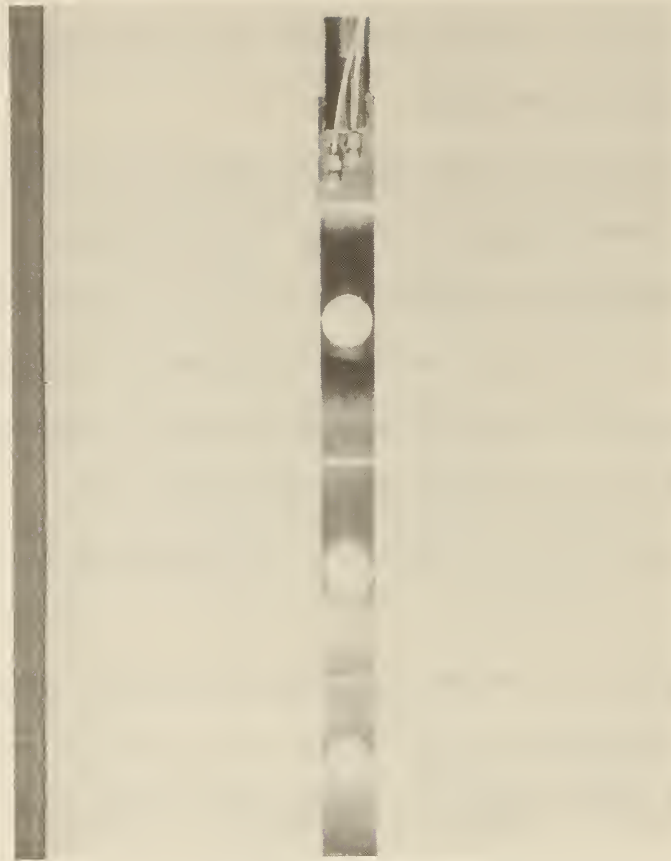
Figure 24.   Photographs of blade with teflon diaphragm
             stress sensors.
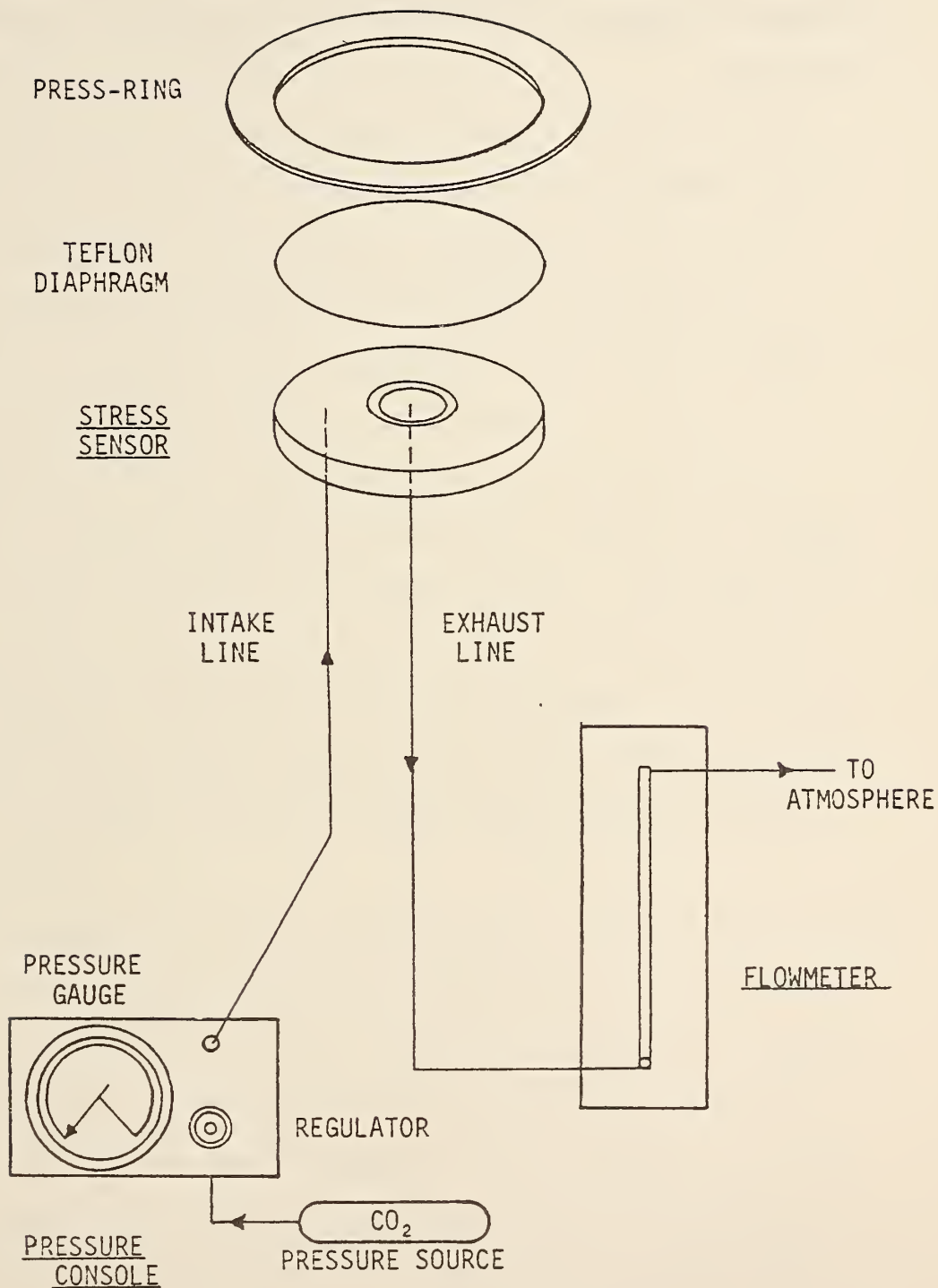
Figure 25. Schematic of stress sensor pressurizing system

flowmeter in turn vents to the atmosphere. The set-up is quite satisfactory

although the flowmeter is very sensitive to any surges in operator application

of pressure.

LABORATORY TEST RESULTS

Disturbance in Layered Specimens

One assumption basic to the proposed method of extrapolating to
obtain the soil in situ stress is that a functional relationship exists
between the thickness of a blade and the disturbance its insertion
causes. To evaluate this assumption layered sand or modeling clay
specimens were constructed, tested, then sliced open to allow visual
observation of disturbance caused by blade insertion.

All testing was done in accordance with previously outlined pro-
cedures. At the end of testing the specimens were sliced open perpendi-
cular to the width of the blade at the mold centroid. Photographs were
taken of the exposed specimen cross section. Later, measurements were
taken on the photos to define the limits of disturbance. For the purpose
of this study, disturbance was defined as the total distance from each
blade face to the point at which horizontal layers deviated from their
original position.

A total of eight layered sand specimens and six layered clay specimens
were constructed to evaluate disturbance caused by blade insertion into
sand confined by a K-Test mold. Six of the sand specimens were compacted
to a relative density of 40%, while the other two were at 75% relative
density. Testing was done on 40% relative density specimens with rough
and smooth blades, 1/16, 1/8, and 1/4 in. in thickness. The two denser
specimens were used in tests with 1/8 in. thick, both rough and smooth
blades. All test blades had angle tapers of 60% and were 2 in. in width.

Loose sand. The results of the 40% relative density sand tests are shown in Figure 26. A straight line was fit to each set of data points using a least square method. The equation of the line fitting the smooth blade points was:

Disturbance = 3.08 (Blade Thickness in inches) + 0.0385   (10)

with a correlation coefficient of 0.999. The equation for the rough finish blade test was:

Disturbance = 3.26 (Blade Thickness) + 0.274   (11)

With a correlation of 0.997. These high correlation coefficients strongly suggest that disturbance caused by blade insertion varies linearly with its thickness.

It is interesting to note the intercept values of both lines, which indicate disturbance from an infinitely thin blade. The smooth blade line had a very low intercept while the rough blade line had a high intercept with the ordinate. The only major difference between the set of tests was the finish on the blades. Therefore it seems logical to assume more grain interlocking occurred on the rough blade surfaces, causing a large constant disturbance to occur. This insinuates that a set of tests done with very smooth blades should have a best-fit line with an intercept that approaches zero, because its finish would mini-mize interlocking effects on disturbance.

Dense sand. Disturbances in the dense sand tests were found to be larger than in the loose sand tests. The smooth blade test results showed

78
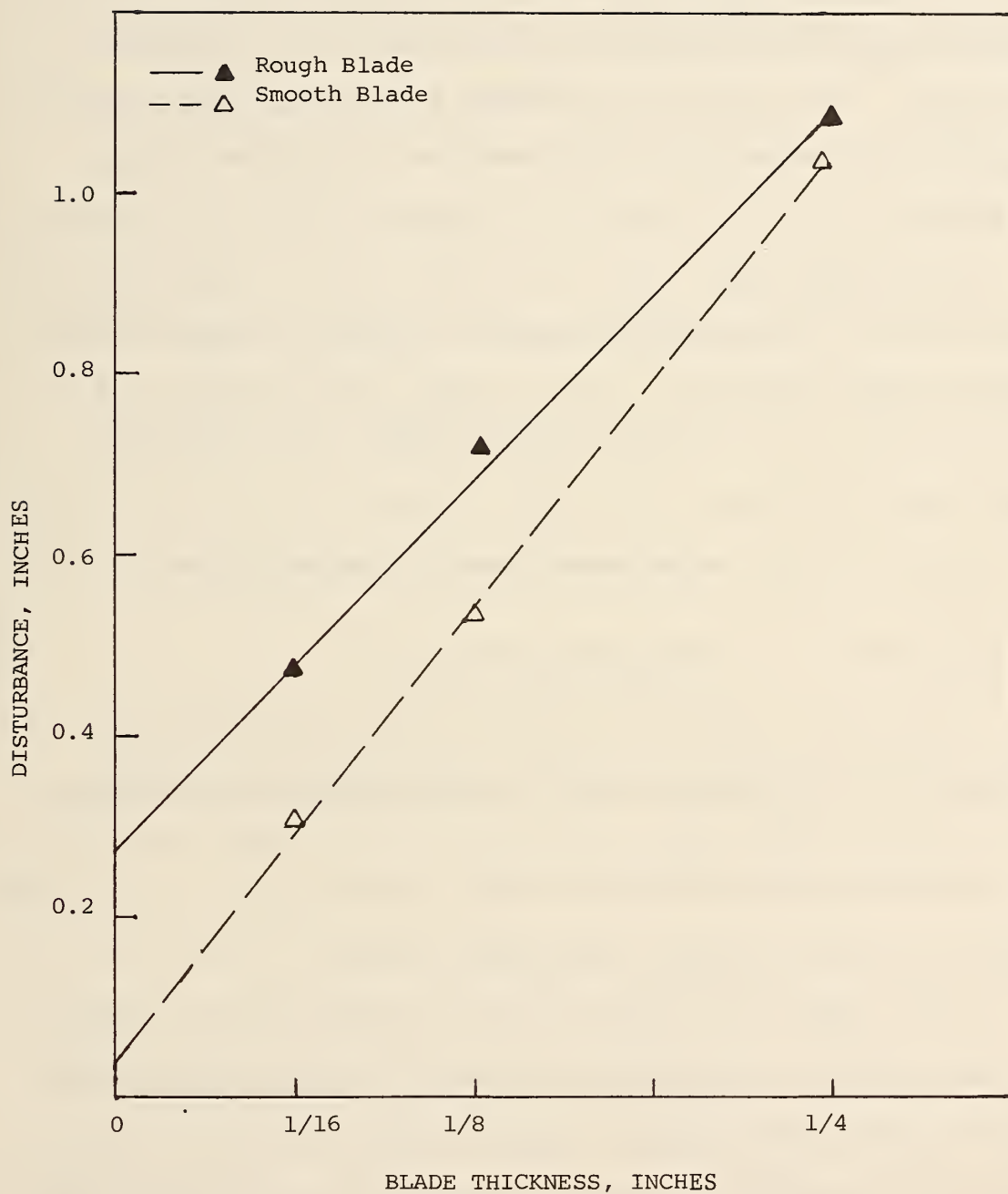
Figure 26. Measured disturbance in 40% relative density sand
specimens.

1 in = 2.54 cm

a 75% increase in disturbance, whereas the rough blade tests resulted in only a 40% increase in disturbance. But the actual values of disturbance of each test were found to be very close, 0.90" and 0.98", respectively. These results indicate that a disturbance limit may be approached which cannot be exceeded regardless of the blade surface roughness.

Low consistency clay. Tests using both smooth and rough blades were performed on the clay layer samples. Figure 27 is a plot of blade thickness versus disturbance. As can be seen, the data points tend to be in a straight line, the same as was observed in the layered sand test.

The best-fit line to the smooth blade data was as follows:

Disturbance = 1.96 (Blade Thickness) + 0.055   (12)

A correlation coefficient of 0.999 was calculated for this line. The equation of the line that best fit the rough blade data points was,

Disturbance = 2.06 (Blade Thickness) + 0.051   (13)

with a calculated correlation coefficient of 0.985.

The intercept of the smooth blade line was found to have a higher value than the rough blade intercept, which is a reversal of what was found in sand disturbance tests. However, the values differ by only 8% and with the correlation coefficient computed from the rough blade data is low, below the 0.10 significance level.

80

Also shown in Figure 27 are average smooth blade data points obtained by first slicing sections of the smooth blade layer specimens at approximately 1/4 in. increments beginning at the mold centroid, and measuring disturbance on each section.

Resulting disturbance data are shown in Figures 28 and 29. These measurements were then averaged for each blade thickness and plotted in Figure 27.

The line best fitting the average data points is:

$$\text{Disturbance} = 2.10 \text{ (Blade Thickness)} + 0.016 \qquad (14)$$

with a correlation coefficient of 0.999. This line comes closer to a zero intercept, indicating probable mold effects.

Stress Concentration

Linear elastic theory based on Mindlin's derivation (15) indicates an extremely large increase in stress will result when a blade is inserted into a semi-infinite mass. This also will reflect in an increase in total stress in the K-Test mold, which simulates an elastic continuum. The amount of this increase is simply predicted by assuming that blade insertion in the K-Test mold causes an increase in the overall stress related to volume of the blade. The test results reveal that these pre-dicted stresses did not develop to such high magnitudes, probably due to plastic behavior around the blade and soil densification occurring in the specimen. If the soil were to undergo zero volume change, calculations
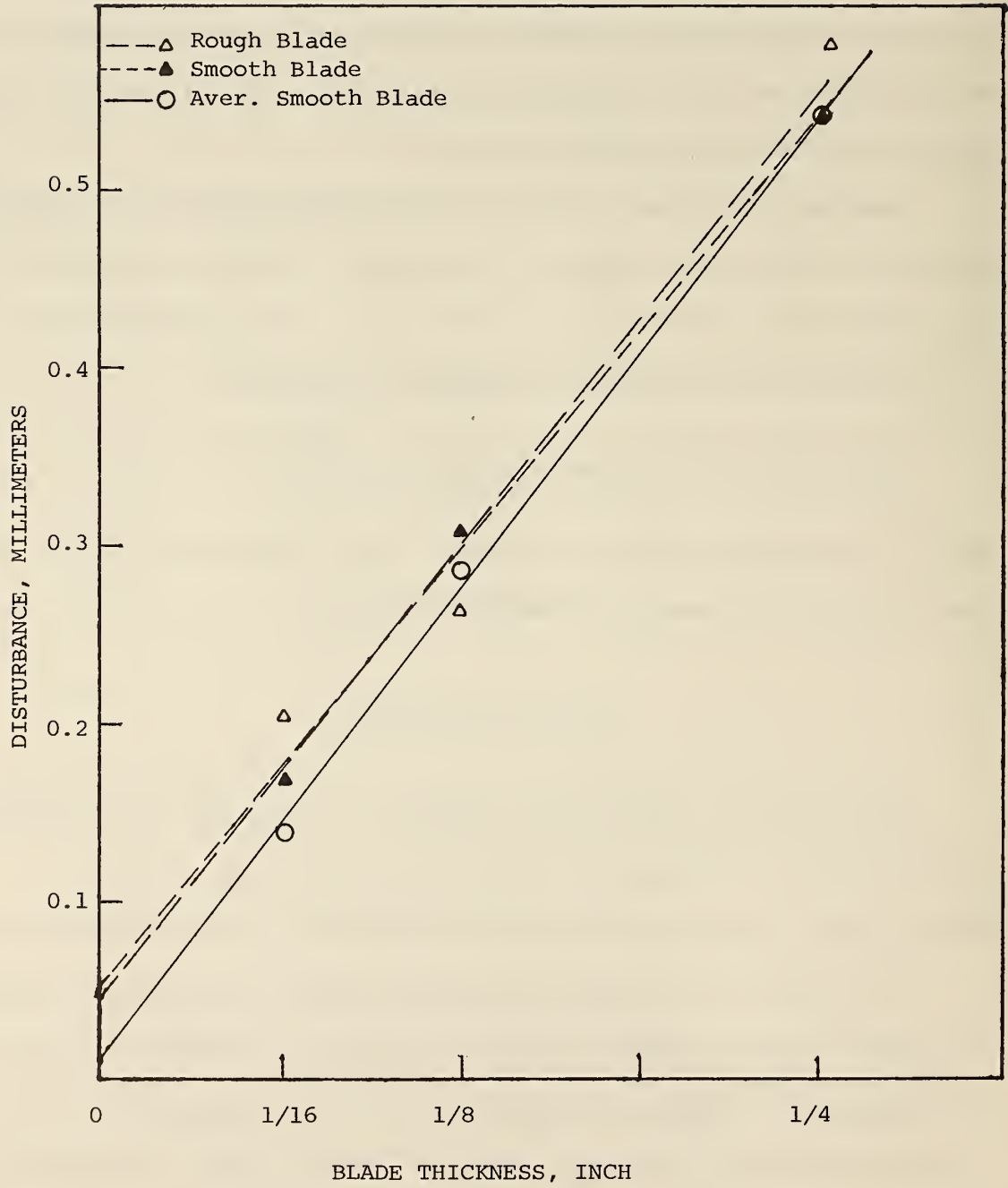
Figure 27. Measured disturbance in the low consistency
clay specimens
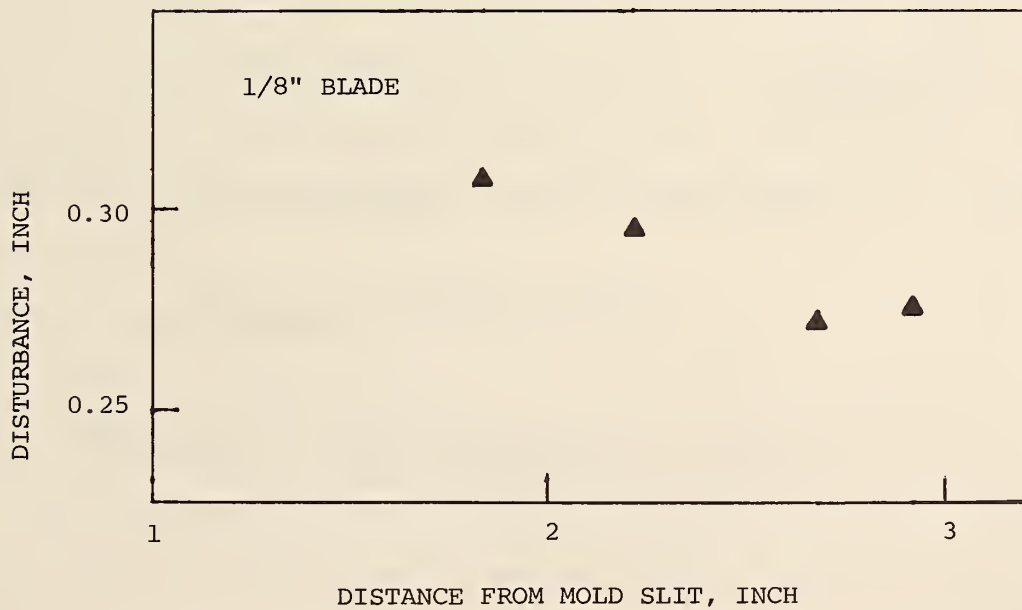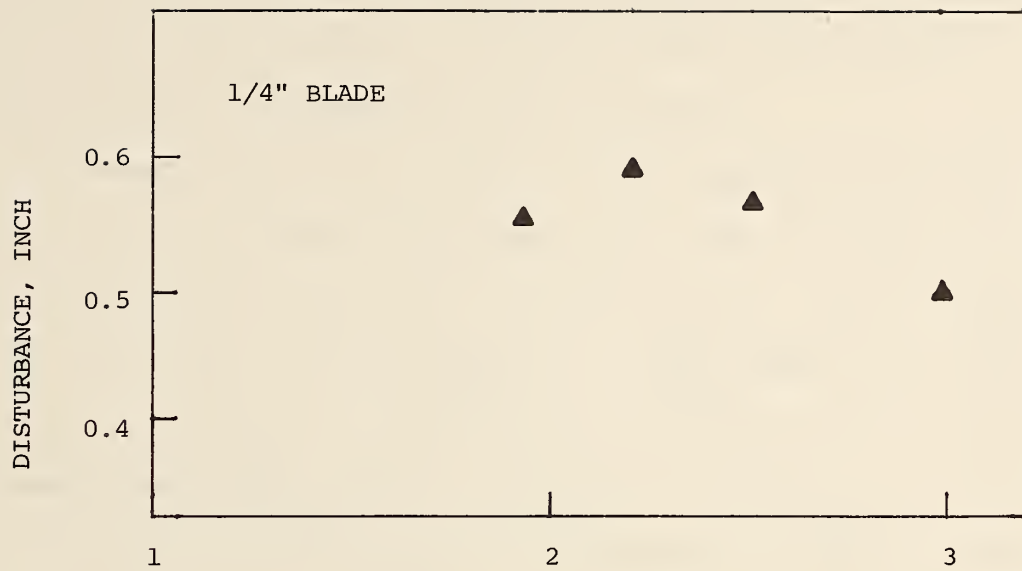
1 in = 2.54 cm

Figure 28. Plots of disturbance as a function of location
in the low consistency clay.
1 in = 2.54 cm
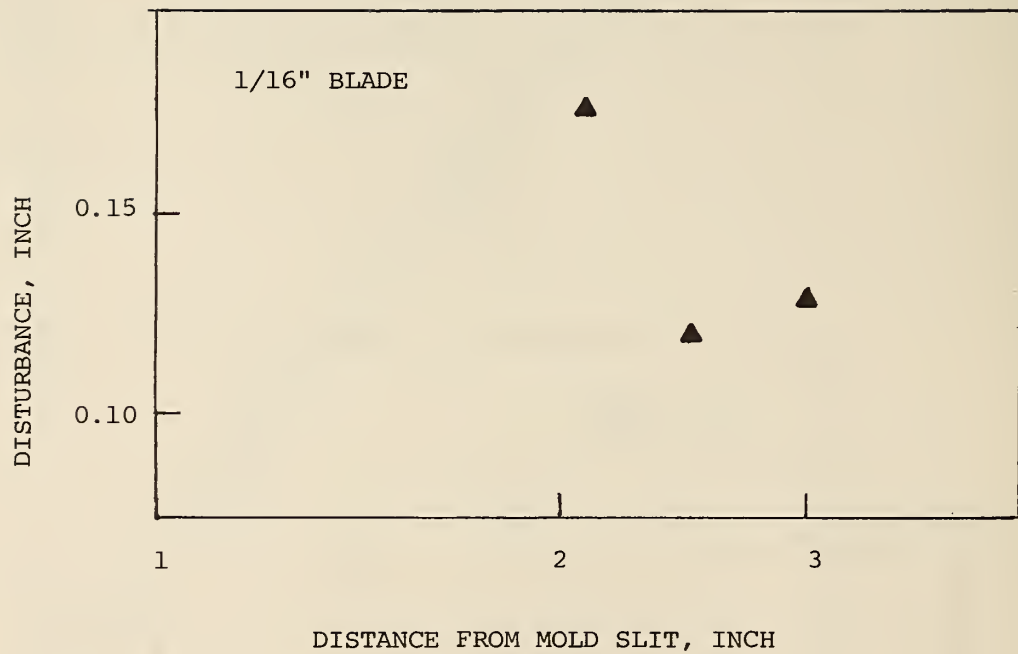
Figure 29. Plots of disturbance as a function of location in the low consistency clay.

1 in = 2.54 cm

show that the mold stresses should have been approximately 5 to 6 times greater than actually measured for both the sand and for the clay. Typical data plots are presented in Fig. 30 and 31.

The testing done on sand compacted to 75% relative density gave lateral stresses and stress ratios about three times as high as in the 40% relative density sand tests. Since the gradation, shear strength, and friction of soil on steel values do not significantly differ between all tests, it is logical that the three-fold increase is due to differing soil compressibilities.

Most testing was done with 2-inch wide blades. Tests were performed in 40% relative density sand or soft clay with smooth one-inch wide blades. Results were approximately equal to those observed with a 2-inch wide smooth blade, indicating that the soil densification occurs mainly normal to the blade.

In the clay tests the blade stresses appear to increase as the blade is extracted, and blade lateral stresses plot above mold stresses. Only initial (3 in. penetration depth) blade data points were used for extrapolation purposes.

Stress vs. Blade Thickness

A list of all tests performed with sand specimens is given in Table 4. The results of these tests are plotted in Figures 32 through 36. Each figure has two plots, one with lateral stress as the ordinate and the other with stress ratio, λ as the ordinate. All plots have blade thickness as the abscissa. It should be noted that 1/4 inch blade
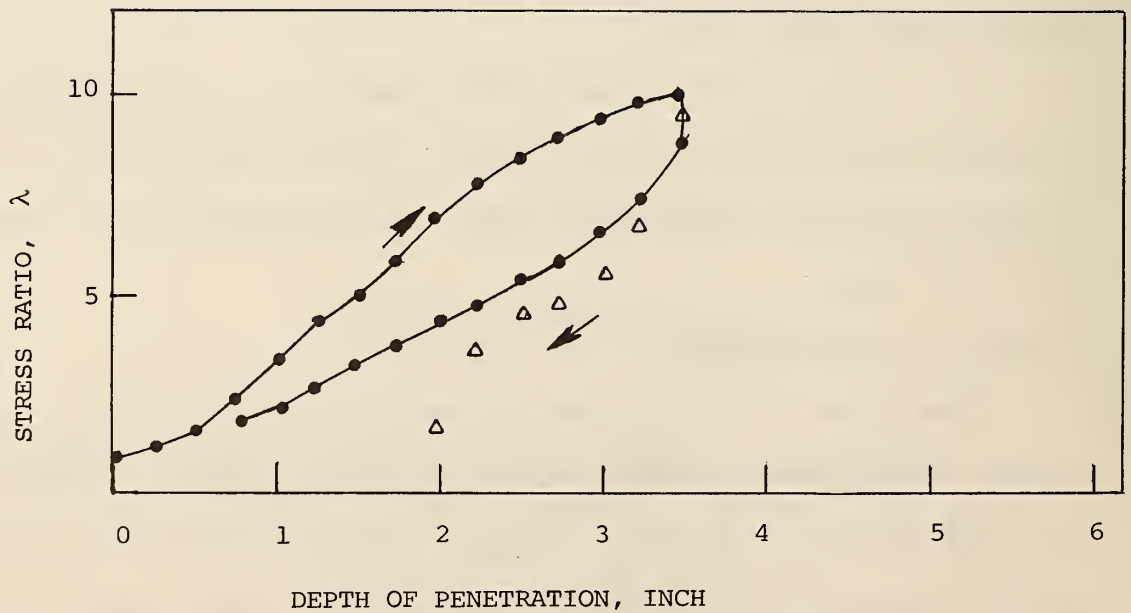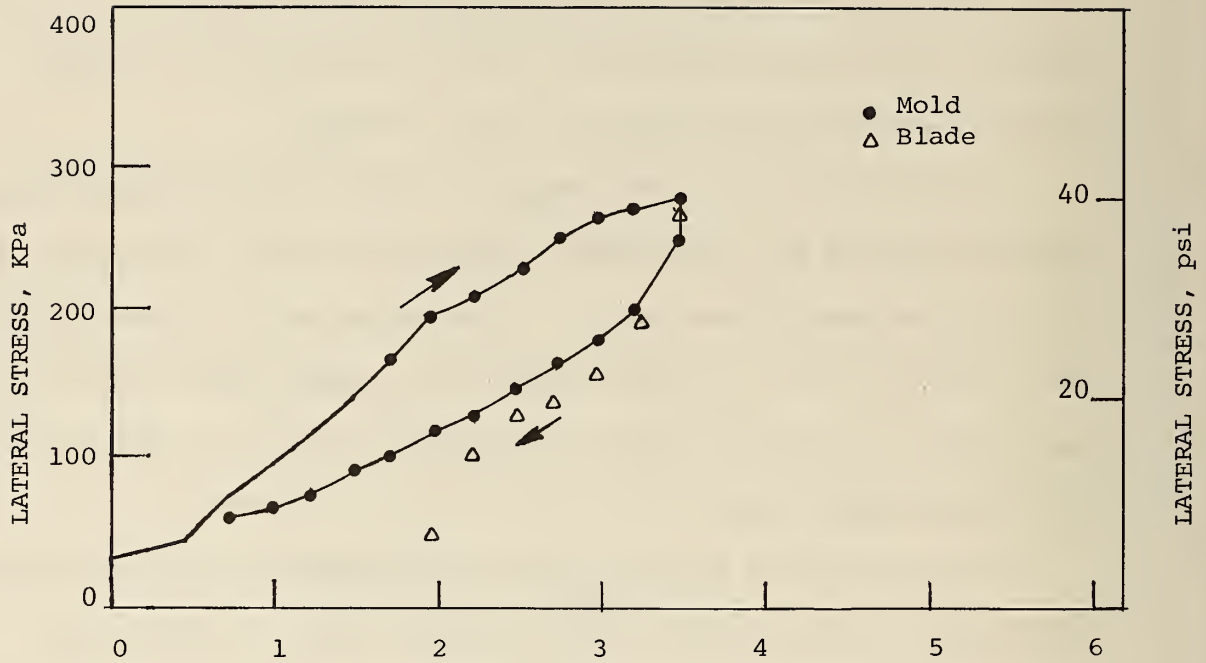
Figure 30. Test results from 1/8 in. thick smooth blade inserted
into a 75% D_r sand specimen.

1 in = 2.54 cm , 1 psi = 70.31 gm/sq cm
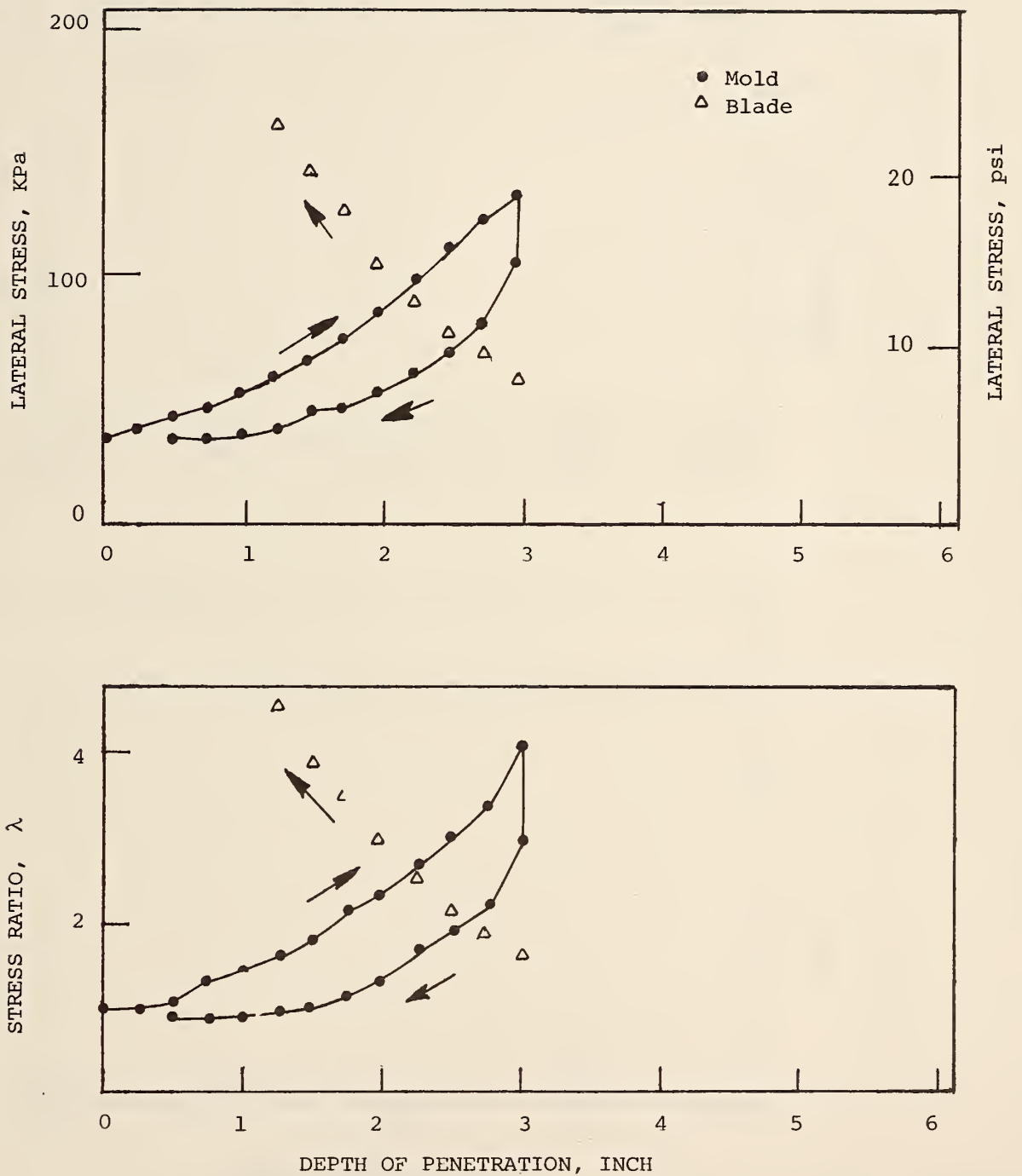
Figure 30. Test results from 1/8 in. thick smooth blade inserted into a low consistency clay specimen.

1 in = 2.54 cm , 1 psi = 70.31 gm/sq cm

87
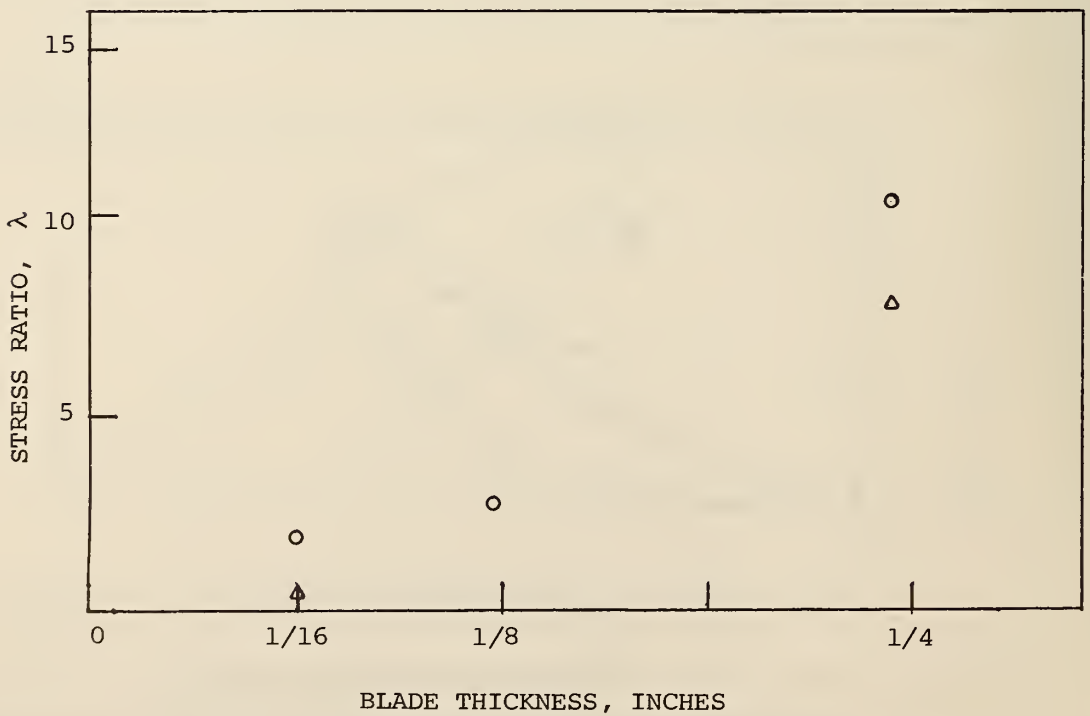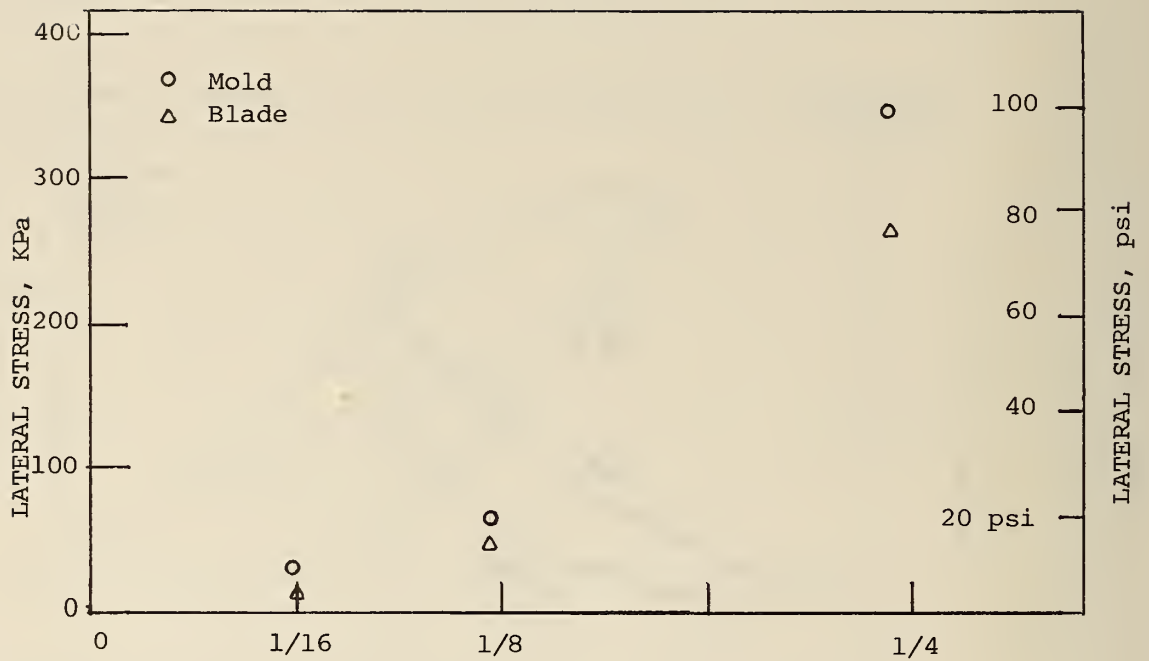
Figure 32. Test results from 2 in. wide smooth blades inserted into 40% D_r sand specimens.

1 in = 2.54 cm , 1 psi = 70.31 gm/sq cm
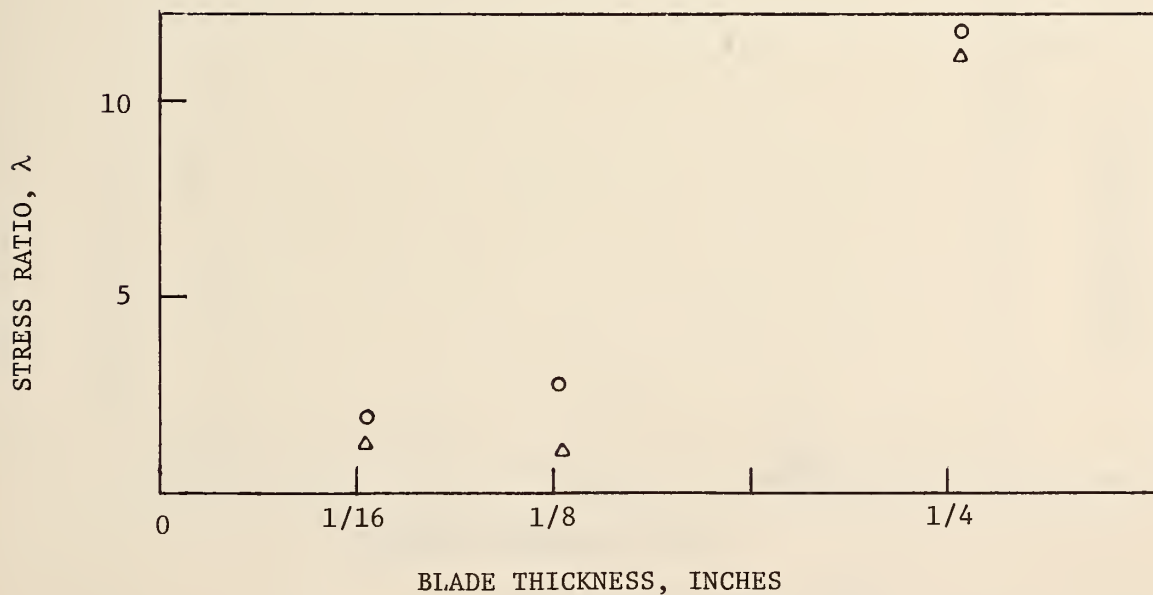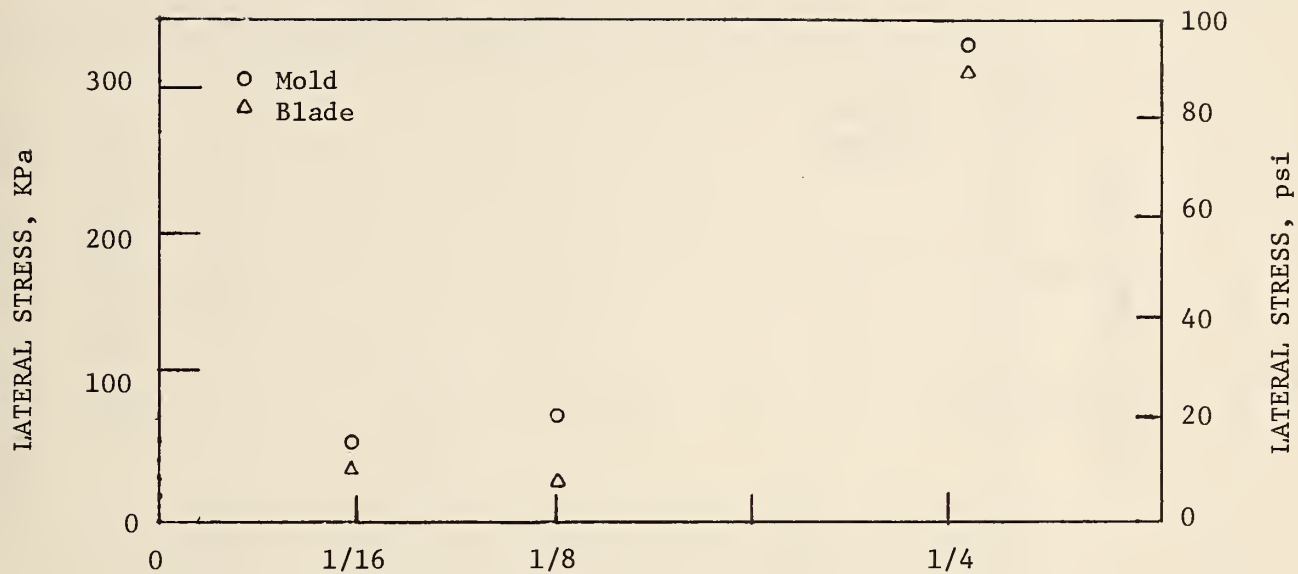
Figure 33. Test results from 2 in. wide rough blades inserted
into 40% D_r sand specimens.
1 in = 2.54 cm., 1 psi = 70.31 gm/sq cm
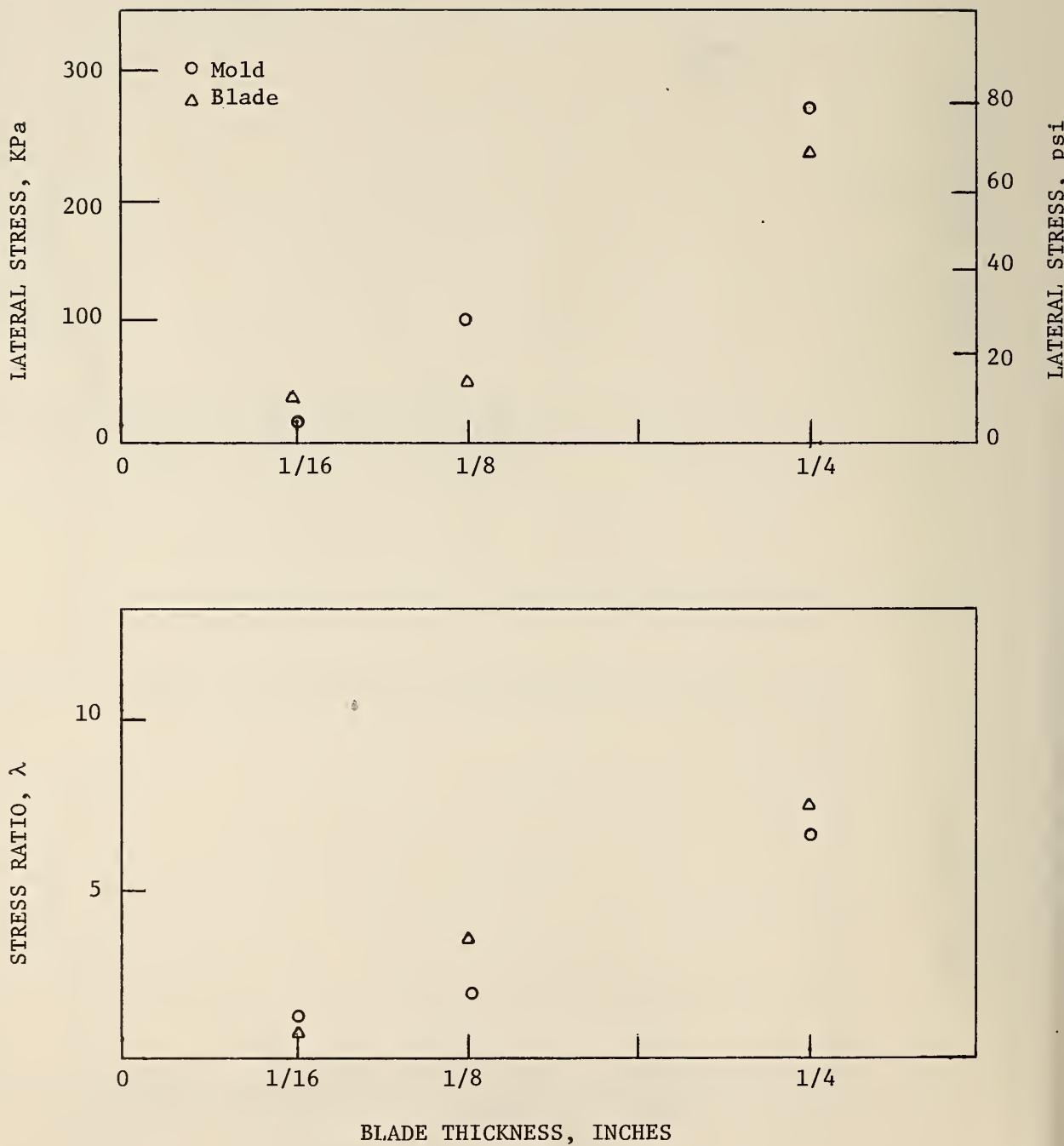
Figure 34. Test results from 1 in. wide smooth blades inserted into 40% D_r sand specimens

1 in = 2.54 cm , 1 psi = 70.31 gm/sq cm
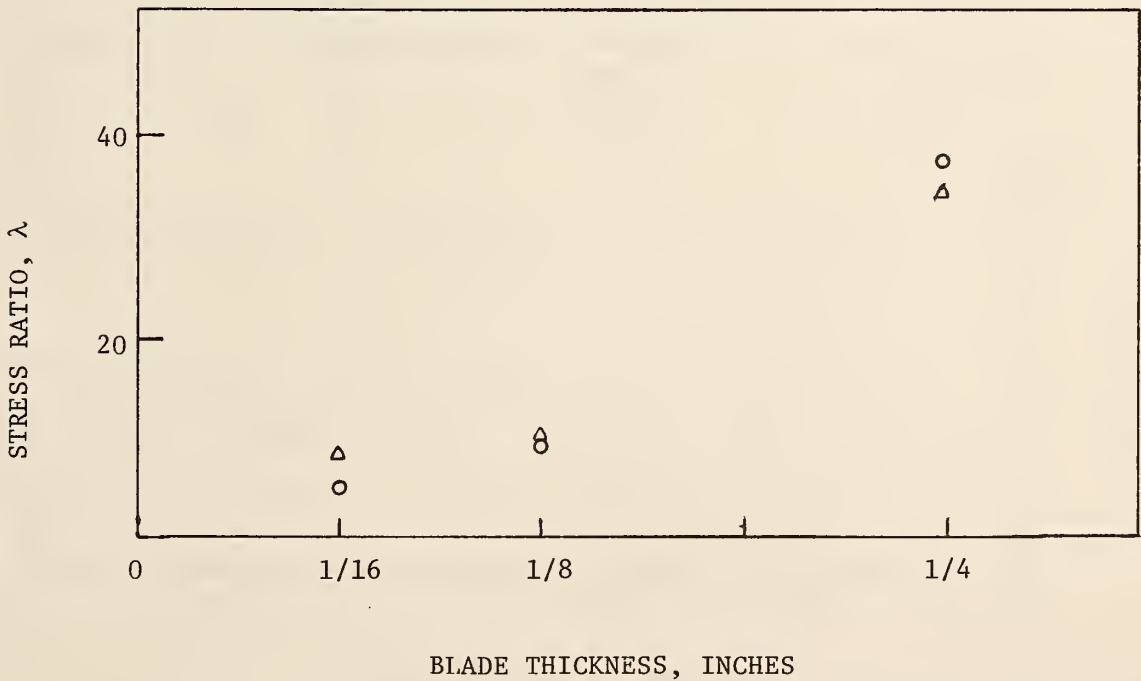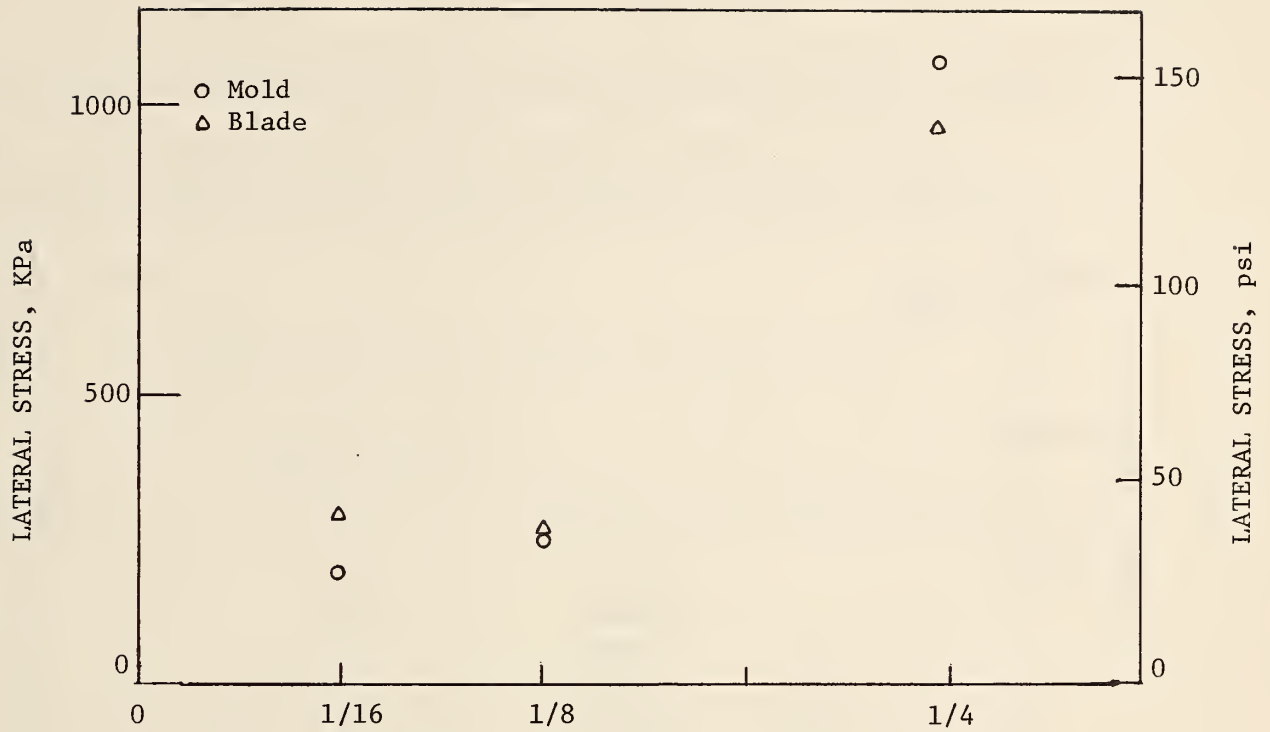
Figure 35. Test results from 2 in. wide smooth blades inserted into 75% D_r sand specimens.

1 in = 2.54 cm , 1 psi = 70.31 gm/sq cm
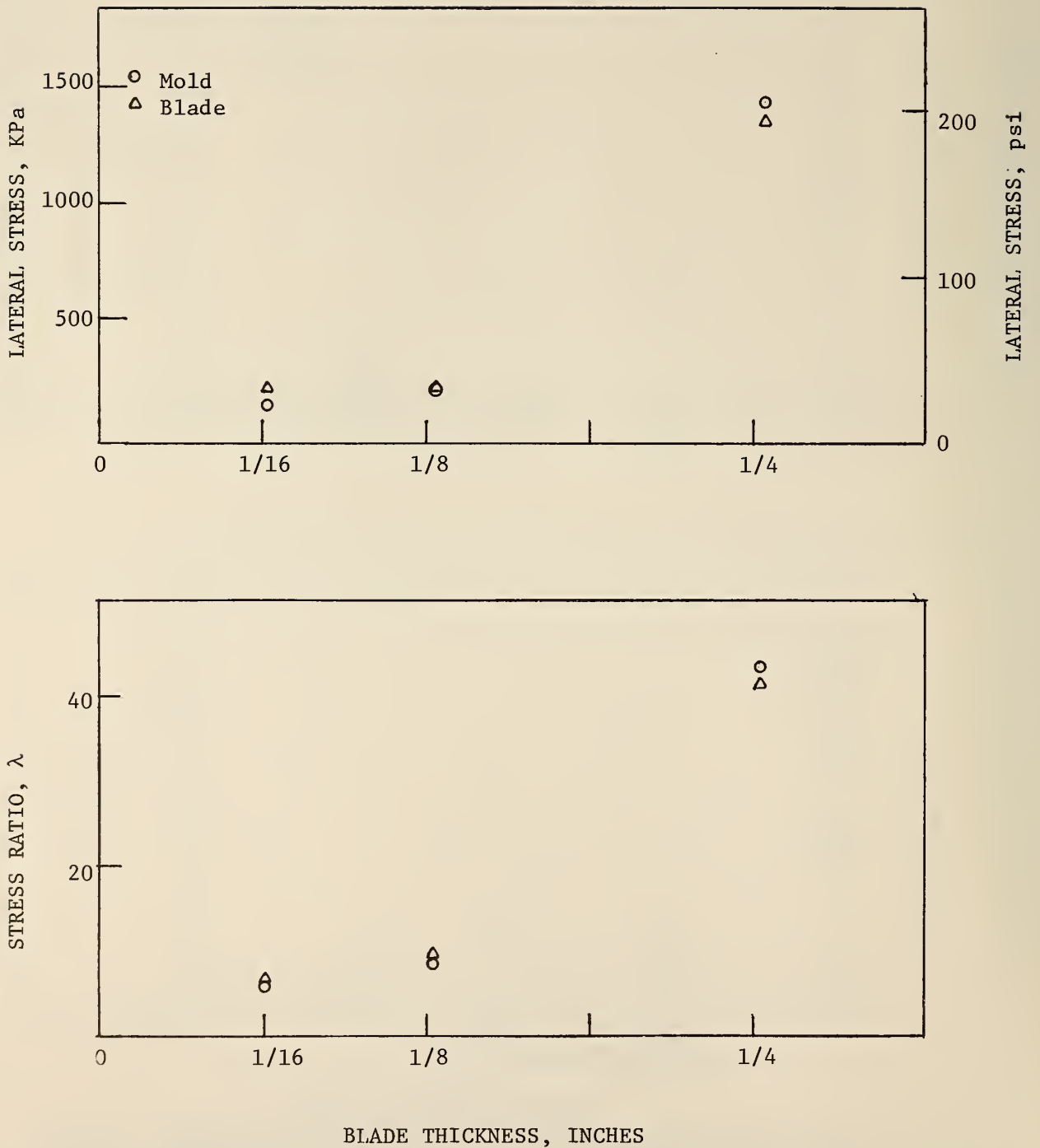
Figure 36.   Test results from 2 in. wide rough blades inserted
into 75% D_r sand specimens.

1 in = 2.54 cm , 1 psi = 70.31 gm/sq cm

data points for the 75% density tests were extrapolated from a 1.5 inch

depth of penetration to a 3.5 inch penetration depth so that all

plotted values would represent lateral stresses and stress ratios at

the same depth.

Table 4. List of sand tests used in extrapolation procedure.
1 in = 2.54 cm

Blade[*]	Blade Width Inch	Blade Surface	Relative Density %
A	2	smooth	40
B	2	smooth	40
C	2	smooth	40
A	2	rough	40
B	2	rough	40
C	2	rough	40
A	1	smooth	40
B	1	smooth	40
C	1	smooth	40
A	2	smooth	75
B	2	smooth	75
C	2	smooth	75
A	2	rough	75
B	2	rough	75
C	2	rough	75

[*] Blade thicknesses: A, 1/6 in.; B, 1/8 in.; C, 1/4 in.

Visual inspection of these graphs indicates they cannot be

described with a straight line fit. When this is done correlation

coefficients are low, and the intercept of the line is usually a nega-

tive number. As will be discussed later, exponential curves gave the

best fit.

A listing of all tests performed in modeling clay is in Table 5, and the results of these tests are plotted in Figures 37 through 40.

Table 5. List of clay tests used in extrapolation procedure.
             1 in =. 2.54 cm

Blade*	Blade Width (inch)	Blade Surface	Clay Consistency
A	2	smooth	soft
B	2	smooth	soft
C	2	smooth	soft
A	2	rough	soft,
B	2	rough	soft
C	2	rough	soft
A	1	smooth	soft
B	1	smooth	soft
C	1	smooth	soft
A	2	smooth	stiff
B	2	smooth	stiff
C	2	smooth	stiff

*Blade thicknesses are the same as in Table 4.

Lateral stress plots of clay data were unpredictable. Since the final lateral stresses on the blade and mold were less than those encountered in sand, the initial lateral stress became more important, which would account for the apparently random behavior of these plots. The plots of stress ratio versus blade thickness are more consistent, and all plots except for the 1 in. wide blade seem to follow a general exponential function.
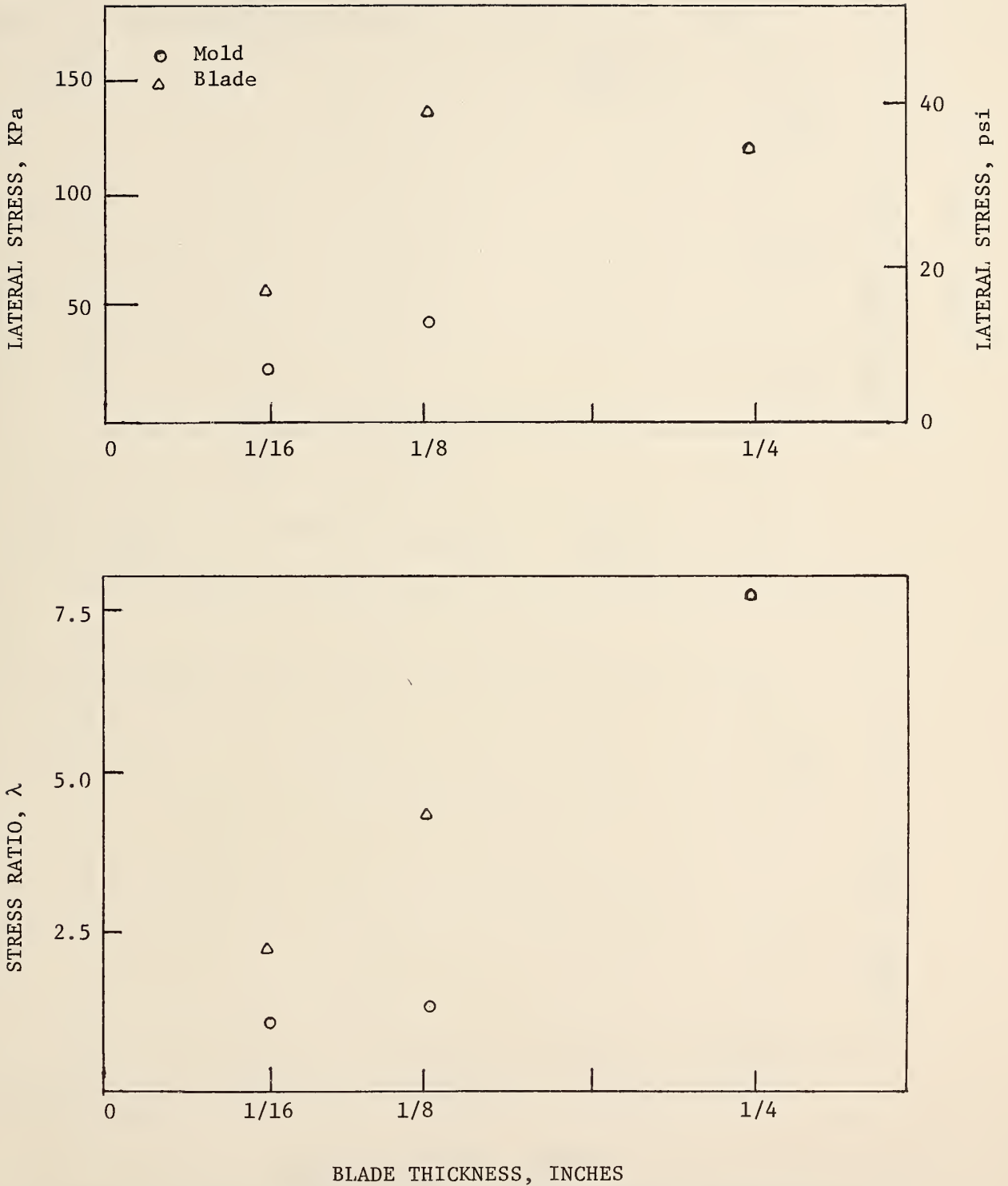
Figure 37.   Test results from 2 in. wide smooth blades inserted
into low consistency clay specimens.

1 in = 2.54 cm , 1 psi = 70.31 gm/sq cm
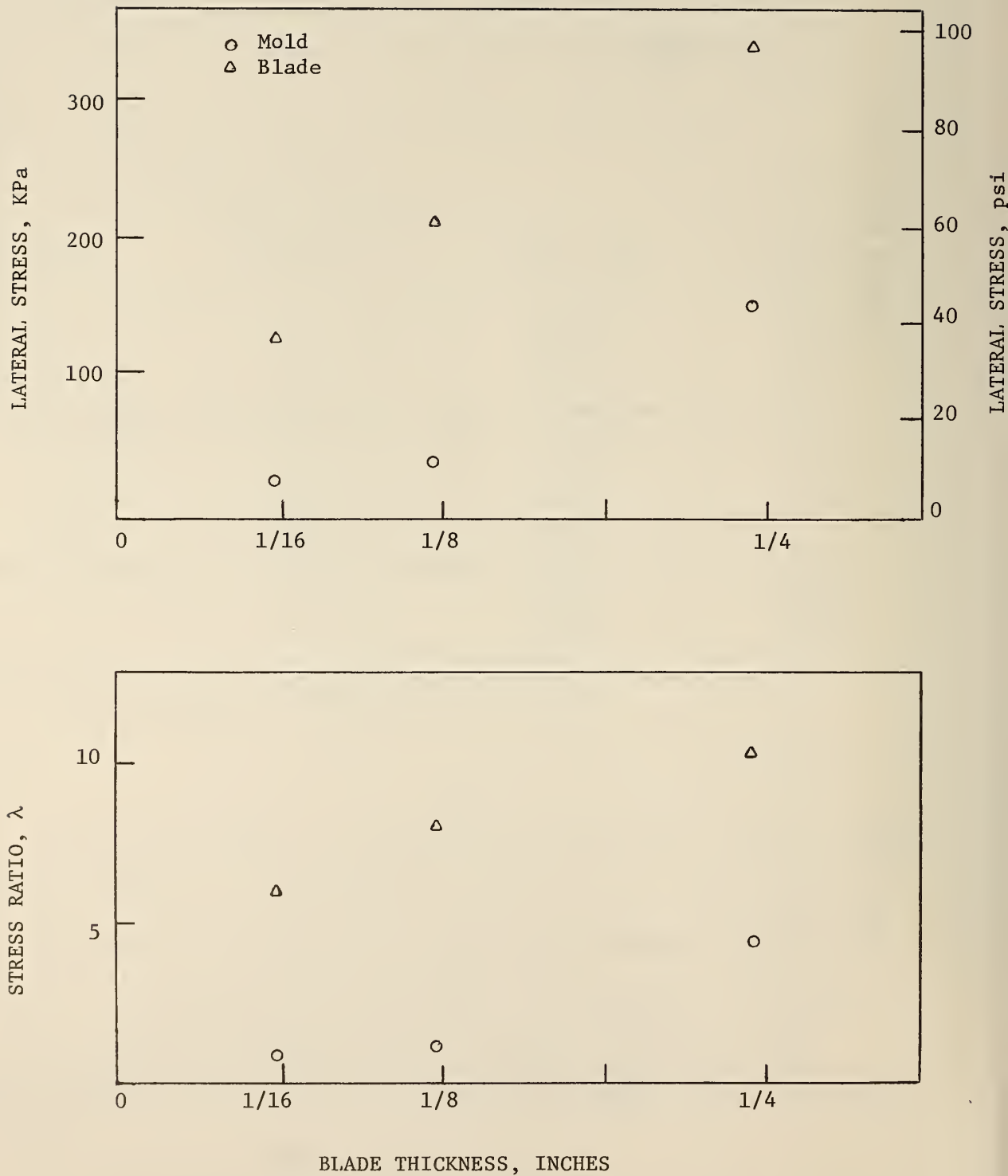
Figure 38. Test results from 2 in. wide rough blades inserted
into low consistency clay specimens.

1 in = 2.54 cm , 1 psi = 70.31 gm/sq cm
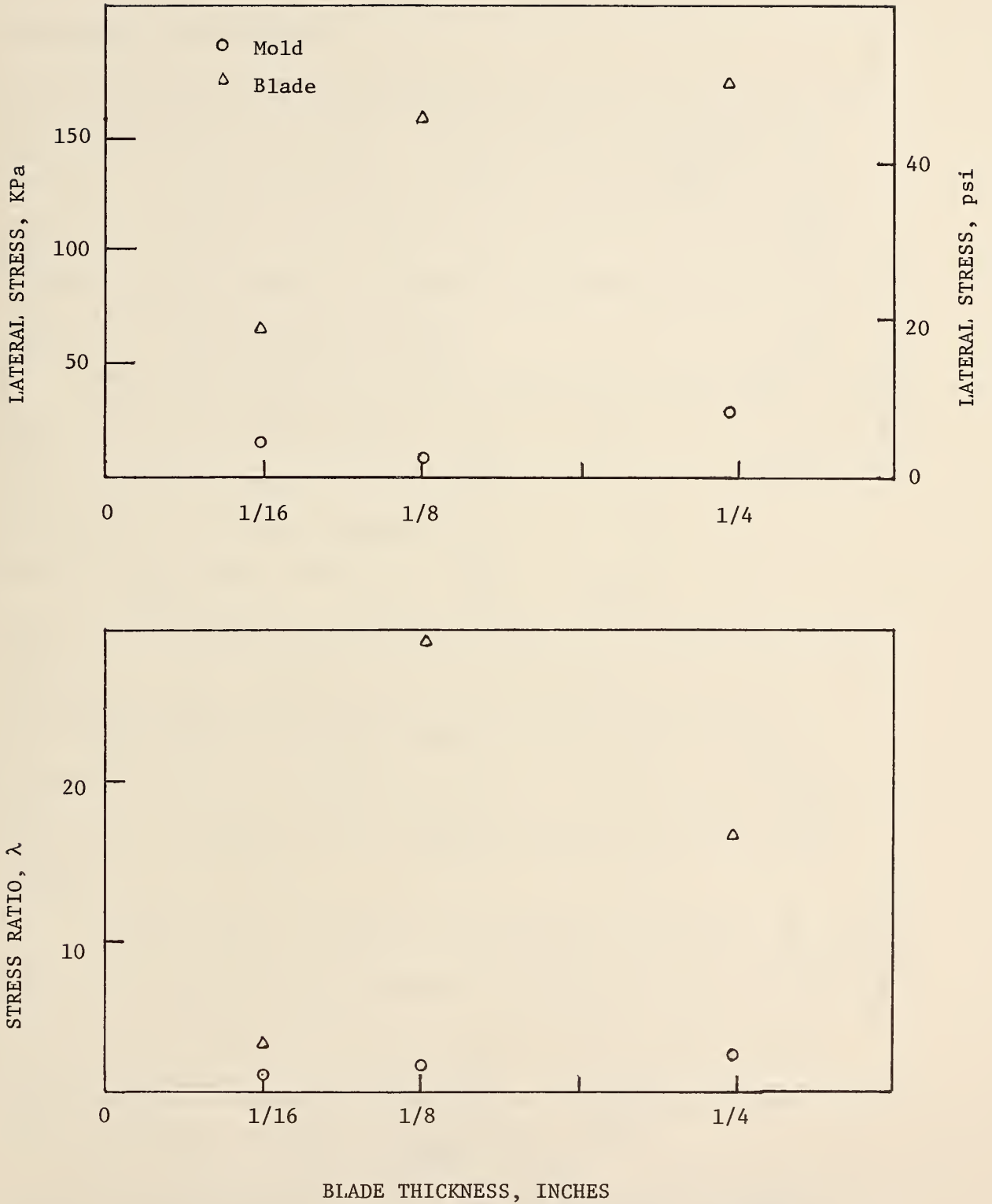
Figure 39.   Test results from 1 in. smooth blades inserted into low
consistency clay specimens.

1 in = 2.54 cm , 1 psi = 70.31 gm/sq cm
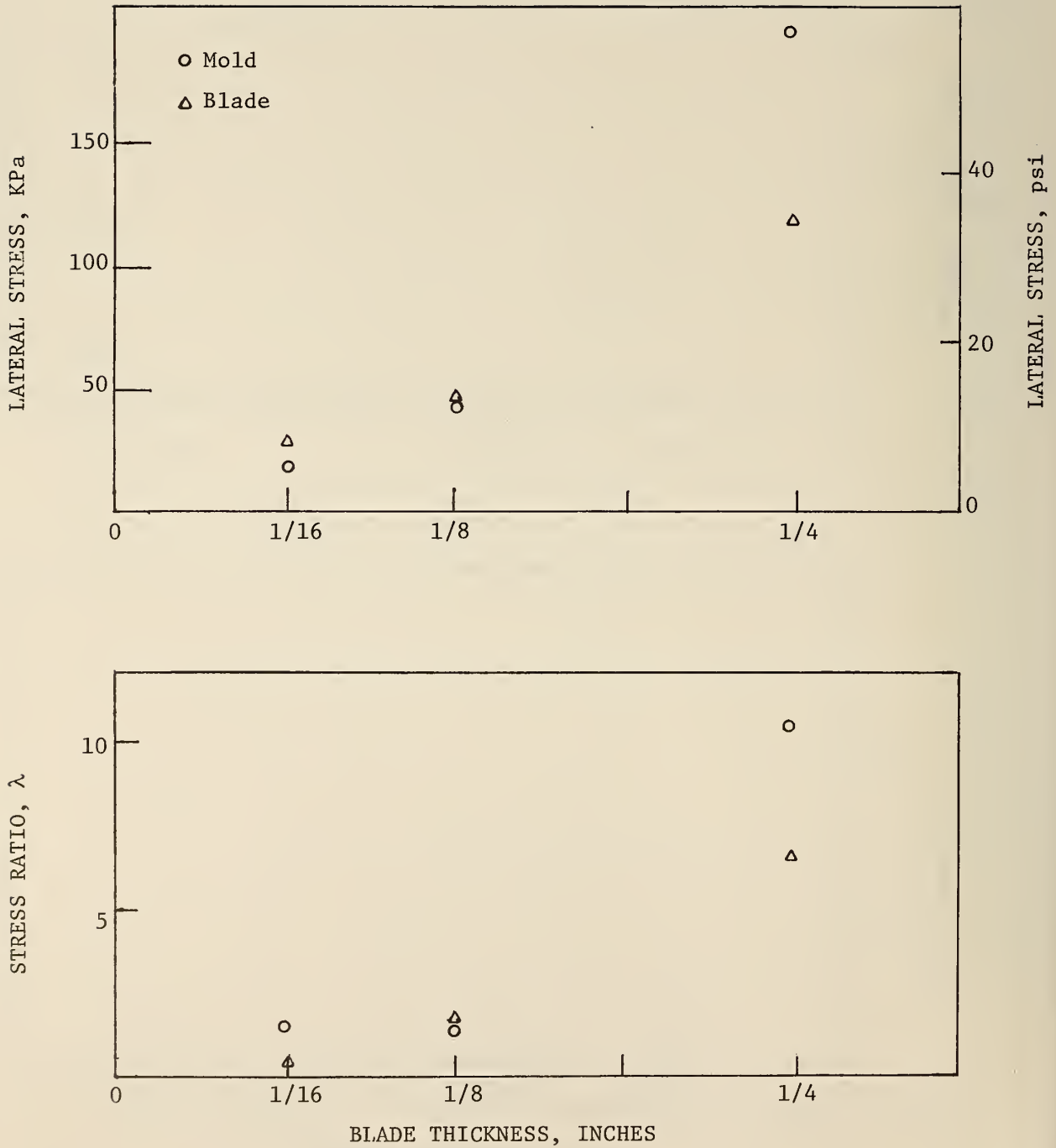
Figure 40. Test results from 2 in. wide smooth blades inserted into high consistency clay specimens.

1 in = 2.54 cm , 1 psi = 70.31 gm/sq cm

Exponential Curve Data Fit

Exponential curves were found to give the best fit to all stress
vs. blade thickness data sets. A justification may be that as the
thickness of the inserted blade increases, densification required to
maintain a constant lateral stress must increase; since soils have a
maximum attainable density, as compaction proceeds, more work will be
needed for additional densification.

A listing of best-fit curves for stress ratio versus blade thickness
data from tests in sand is shown in Table 6, while Table 7 is a listing of
the corresponding curves obtained from tests conducted in clay. All
curves are in the general equation form:

$$\lambda = ae^{bt} \tag{15}$$

where t is the blade thickness (inches) and λ is the same as previously
defined. No curve fitting was done with the lateral stress data because
of the variation in the initial stress. A value of a = 1 indicates
extrapolation to zero thickness does give an accurate undisturbed stress
measurement, and the value of b indicates sensitivity to thickness
changes.

It should be kept in mind while evaluating the strength of relation-
ships, that correlation coefficients of 0.987 and 0.951 would indicate
0.10 and 0.20 levels of significance, respectively. Most r values
were above the 0.10 level of significance, indicating a strong relation-
ship between blade thickness and mold stress ratios.

Interesting results were obtained in the mold stress ratio curve
fits. Actual values of "a" for sand did not vary significantly when

99

Table 6. Summary of Best-Fit Exponential Curves to Stress Ratio Data * (Sand)

1 in = 2.54 cm

Material	Blade Type	σ_3 Blade/σ_{3i}	r	σ_3 Mold/σ_{3i}	r
Sand 40% D_r	2 in. smooth blade	$\lambda = 0.12e^{17.7t}$	0.941	$\lambda = 0.7e^{10.7t}$	0.999
	2 in. rough blade	$\lambda = 0.4e^{12.1t}$	0.927	$\lambda = 1.0e^{9.6t}$	0.991
	1 in. smooth blade	$\lambda = 0.4e^{12.1t}$	0.912	$\lambda = 0.73e^{8.6t}$	0.994
Sand 75% D_r	2 in. smooth blade	$\lambda = 4.5e^{7.8t}$	0.965	$\lambda = 2.6e^{10.5t}$	0.997
	2 in. rough blade	$\lambda = 3.15e^{10.1t}$	0.979	$\lambda = 2.4e^{11.5t}$	0.990

*t in in.

Table 7. Summary of Best-Fit Exponential Curves to Stress Ratio Data * (Clay)

1 in = 2.54 cm

Material	Blade Type	σ_3 Blade/σ_{3i}	r	σ_3 Mold/σ_{3i}	r
Soft Clay	2 in. smooth blade	$\lambda = 1.7e^{6.4t}$	0.980	$\lambda = 0.5e^{11.1t}$	0.979
	2 in. rough blade	$\lambda = 6.2e^{2.3t}$	0.937	$\lambda = 0.5e^{8.7t}$	0.986
	1 in. smooth blade	$\lambda = 5.1e^{6.1t}$	0.561	$\lambda = 0.7e^{5.2t}$	0.999
Hard Clay	2 in. smooth blade	$\lambda = 0.2e^{14.2t}$	0.963	$\lambda = 0.7e^{10.5t}$	0.964

* t in in.

101

compared at like sand densities, and for 40% D_r sands were close to one, which is very encouraging. The 75% D_r sand also had consistent, but higher a-values. The b-values for all sand tests were consistent, with an average of 10.2.

The exponential curves found to best fit the clay test results are also indicated in Table 7. Correlation coefficients were found to be very high when mold stress ratios were related to blade thicknesses in both soft and hard clay. The a-values for these curves closely agreed, averaging 0.6 in magnitude, not far from the ideal value of 1.0. Similarly, b-values were consistent.

Results of curve fits based on blade stress ratio for sand tests show somewhat lower correlation coefficients. This is probably due to the inaccuracies in determining the actual lateral stress on a blade. But even with a lower r value, general trends in "a" and "b" can be noted. A general trend in "a" and "b" coefficients for tests in clay is that a-values were low when smooth blades were used and high when rough blades were used, whereas "b" values showed the opposite trend.

In general terms, it appears that an exponential function does a good job of defining the relationship between stress ratio and blade thickness for tests in both clay and sand. This type of function should theoretically work as well when used with measured lateral stress versus blade thickness data. Unfortunately due to limited testing data, it is impossible to establish an exact prediction equation for the values of either coefficient "a" or "b".

Stress Sensor Tests in K Test Mold

Stress sensor development was pursued simultaneously with simple blade penetration tests in the K Test mold. The next step was to combine these efforts, and use blades with stress sensors. Since it was suspected that the assymetrical, overly stiff elastic confinement supplied by the K Test mold could have contributed error, in this series of tests the Teflon plate that previously was rigidly clamped on the top of the mold was held down with a spring, allowing some volume expansion of the soil upward.

Blades 1/8 and 3/16 in. thick and 2 in. wide were pushed to depths of 3 to 3 1/2 in. in samples held in the K-Test mold. At the end of penetration, the soil stress acting on the blades was determined by the stress sensor incorporated in each. The blades were then pulled and the force necessary to pull was recorded, and a soil stress acting on the blades was then evaluated from the pulling force.

Soils used in these tests included the two consistencies of molding clay previously used, plus three different grades of sand ranging in gravel content from 0 to 26%, and a standard Ottawa sand. The clays were compacted as before, whereas all three sands were compacted to $D_r = 40\%$. Relevant property data from K Tests and from grain-size analyses are presented in Table 8.

Table 8. Physical Properties of Laboratory Test Soils
1 psi = 70.31 gm/sq cm

Material	c, psi	ϕ, Degrees	c_s, psi[a]	ϕ_s, degrees[a]	Clay <.002mm	F. Silt .002 to .020mm	C. Silt .020 to .074mm	F. Sand .074mm to .2mm	M.Sand .2 to .6mm	C.Sand .6 to 2mm	Gravel >2 mm
Soft Clay	4.0	6.0	0.35	5.0	100	-	-	-	-	-	-
Stiff Clay	4.0	8.0	0.4	6.0	100	-	-	-	-	-	-
Standard Sand	0	39.5	0	16.5	0	0	0	8	31	35	26
MS-1	0	39.5	0	16.5	0	0	0	7	38	38	17
MS-2	0	39.5	0	16.5	0	0	0	4	40	56	0
Ottawa Sand	0	35.0	0	16.9	0	0	0	0	2	98	0
Monona Loess[b]	4.7	35.4	n.d.	n.d.	16.8	...92.6...		0.6	0	0	0
Shelby Till[c]	7.0	27.5	n.d.	n.d.	32	...65.....		.........2.6.........			0

[a] Subscript "s" denotes soil-to-steel parameters

[b] Max. dry density, 103.8 lb/ft^3; optimum moisture content, 18.5%; LL = 32%, PL = 26%.

[c] Max. dry density, 100.0 lb/ft^3; O.M.C., 20.9%; LL = 54%, PL = 32%.

104

Results from these tests are given in Table 9. Blade stresses calculated from pulling forces also are included, and as can be seen, the ratio σ_b/σ_s of blade stress determined in this way compared to the readings from the stress sensors varies from 0.22 to 4.53, averaging from 0.56 for Ottawa sand to 1.48 for the other sands, and 1.90 for the hard clay to 3.86 for the soft clay. This large variability makes either the blade data or the sensor data suspect. The value and range of over-stress ratios λ_b and λ_s calculated from the corresponding values are smaller for the sensor data, the mean values and standard deviations being $\lambda_b = 5.0 \pm 5.0$ and $\lambda_s = 2.6 \pm 1.7$. The sensor data therefore appear more reliable, but the problem of the K Test mold influences remains. The inconsistency of λ with regard to blade thickness prevents fitting meaningful curves.

In some of the sand tests, the values of λ determined indirectly or measured directly by the stress sensors are less than one. The probable cause for this is a combination of the shear behavior of sand and the close confines of the K-test mold. As the blades were being pushed into samples in K-test mold, observations were made at regular intervals of stress changes laterally and vertically in the mold as well as the force being applied to push the blade. In the tests on clays all of these values increased with penetration depth, but in some of the sand tests, all of these stresses and loads increased and then decreased at a penetration depth of about 2.5 in. A decrease in the lateral mold stress would necessarily mean a decrease in the stresses acting on the blade. It seems

Table 9. Summary of Single-Blade Laboratory Tests.

Test	σ_{3i}	σ_{1iT}	σ_{1iB}	K_{avg}	σ_s	σ_b	σ_b/σ_s	λ_s	λ_b
Ottawa Sand—40% Dr									
1/8	6.78	13.26	13.50	.51	9.20	6.03	0.65	1.36	0.89
1/8	2.94	12.60	7.50	.29	8.39	4.16	0.60	2.85	1.41
1/8	7.91	–	9.50	.83	10.61	5.63	0.53	1.34	0.71
1/8	6.74	13.26	12.00	.53	11.25	6.30	0.56	1.67	0.93
1/8-.005T	5.81	12.60	6.00	.62	18.26	9.12	0.50	3.14	1.57
1/8-.005T	3.19	13.26	4.00	.37	13.58	7.11	0.52	4.26	2.23
3/16-.005T	2.99	11.94	10.50	.27	13.00	6.17	0.47	4.35	2.06
3/16-.01T	6.78	15.25	6.00	.64	54.66	46.20	0.85	8.06	6.81
3/16-.01T	3.69	5.31	3.00	.89	11.33	5.27	0.47	3.07	1.43
3/16-.01T	5.08	11.94	4.50	.62	12.70	6.17	0.49	2.50	1.21
Standard Sand-40% Dr									
1/8	3.69	–	5.00	.74	5.80	1.29	0.22	1.57	0.35
b1/8	5.02	–	1.00	5.02	7.28	32.69	4.49	1.45	6.51
b1/8	4.27	–	1.50	2.85	11.17	21.77	1.95	2.62	5.10
b1/8	12.09	–	2.00	6.04	13.48	24.22	1.80	1.11	2.00
3/16-.01T	5.02	5.97	4.50	.96	2.80	3.99	1.43	0.56	0.79
3/16-.01T	10.50	13.93	10.50	.86	4.34	8.53	1.97	0.41	0.81
3/16-.01T	5.07	7.96	3.00	.93	5.13	4.29	0.84	1.01	0.85
MS-1									
3/16-.01T	5.64	7.96	3.00	1.03	3.28	2.48	0.76	0.58	0.44
3/16-.01T	7.18	11.94	3.00	.96	2.63	6.77	2.57	0.37	0.94
3/16-.01T	5.67	9.28	5.00	.79	3.45	4.13	1.20	0.61	0.73
MS-2									
1/8-.005T	5.17	7.61	3.50	.93	5.80	3.96	0.68	1.12	0.77
1/8-.005T	5.20	7.94	3.00	.95	3.47	2.81	0.81	0.67	0.54
3/16-.01T	7.64	14.59	6.00	.74	7.68	7.84	1.02	1.01	1.03
3/16-.01T	5.68	9.93	5.00	.76	5.48	5.28	0.96	0.96	0.93

106

Table 9. (continued)

Test	σ_{3i}	σ_{1iT}	σ_{1iB}	K_{avg}	σ_s	σ_b	σ_b/σ_s	λ_s	λ_b
Soft Clay									
a1/8	5.68	11.94	5.00	.67	13.18	58.50	4.44	2.32	10.30
1/8-.005T	4.65	7.29	4.00	.82	11.36	44.52	3.92	2.44	9.57
1/8-.005T	2.49	5.97	1.00	.71	9.87	43.53	4.41	3.96	17.48
1/8-.005T	4.74	11.27	2.00	.71	14.88	50.44	3.39	3.14	10.64
1/8-.005T	4.63	6.30	2.00	1.12	9.30	44.28	4.76	2.01	9.56
b3/16	4.40	14.59	6.00	.43	26.92	73.24	2.72	6.12	16.65
3/16-.01T	5.28	8.62	3.00	.91	13.62	49.54	3.64	2.58	9.38
3/16-.01T	2.57	5.97	2.00	.64	10.14	45.92	4.53	3.95	17.87
3/16-.01T	3.00	5.31	2.00	.82	11.25	45.92	4.09	3.75	15.31
3/16-.01T	7.17	7.29	5.00	1.17	15.30	40.94	2.68	2.13	5.71
Stiff Clay									
a1/8	5.68	11.27	5.00	.70	15.52	47.47	3.05	2.73	8.34
a1/8-.005T	6.67	12.60	8.00	.65	17.62	31.76	1.80	2.64	4.76
1/8-.005T	6.03	12.60	6.00	.65	17.73	32.48	1.83	2.94	5.39
1/8-.005T	7.18	7.29	7.00	1.00	21.18	16.07	0.76	2.95	2.24
3/16	5.54	6.63	5.00	.95	24.03	39.14	1.63	4.34	7.06
3/16-.005T	6.69	10.61	9.00	.68	18.90	28.79	1.52	2.83	4.30
3/16-.01T	3.94	7.29	3.00	.77	12.56	37.26	2.97	7.49	9.46
3/16-.01T	4.96	9.28	4.50	.71	13.40	29.95	2.24	2.70	6.04
3/16-.01T	7.73	14.59	11.00	.60	27.43	34.68	1.26	3.55	4.49

σ_{3i} = initial mold stress

σ_{1iT} = initial top stress

σ_{1iB} = initial bottom stress

$\lambda_s = \sigma_s/\sigma_{3i}$

$K_{avg} = \sigma_{3i}/(\dfrac{\sigma_{1iT}+\sigma_{1iB}}{2})$

σ_s = sensor stress

$\lambda_b = \sigma_b/\sigma_{3i}$

σ_b = blade stress; calculated from

$$\sigma_b = \dfrac{F_s - \alpha A_b}{A_b \tan \phi_s}$$

NOTE: T stands for Teflon, number preceding is the thickness in in. Where there is not thickness and T the diaphragm was stainless steel shim.

a blade pushed 3.25 in.

b blade pushed 3.50 in. All other blades pushed 3.00 in.

*stresses in psi. Conversion to KPa: KPa = 6.895 psi.

likely then that the effect of introduction of the blades in sand is made more severe by the small size of the K-test mold and the rigid confine of the mold base.

The physical properties of modeling clay depend in particular on temperature. A Torvane, a pocket vane shear device, was used to evaluate the shear strength of the clay used in the tests. With a normal shear strength value of 8 psi at 23°C, a one degree F change in temperature caused an 0.7 psi, or 9 percent change in shear strength. This effect would influence test results, since temperature changes were experienced during the testing program.

Stress Sensor Tests in Test Box

In order to examine the inferred limitations of use of the K Test mold, a set of tests was conducted with the vane stress sensors in a large box. In the initial tests the three sensor blades of varying thicknesses were alternately pushed horizontally into compacted soil in the box. In subsequent tests the stepped vane was used. A surcharge load was applied on the box to simulate conditions in a soil mass under overburden pressure.

Soils. Monona loess soil, a uniform silt-sized material, and Shelby till soil (Table 8) were used in the box tests. The soils were mixed with water to the optimum moisture content and compacted to standard maximum density. Three layers with 220 blows of a modified Proctor hammer per layer were found to provide the necessary level of compaction.

Apparatus. The test box has interior dimensions as shown in Fig. 41. One end plate has a 3-in. diameter hole through which the sensors were pushed lengthwise into the box. A removable top plate is supported by a wide-flange beam to minimize bending of the plate. A thin layer of sand separated the soil from the plate.

The entire assembly was placed on a Fairbanks scale with a frame such that a load can be applied to the scale platform. In this manner a surcharge load of 1000 lb was applied to the top plate of the box and transmitted to the loess soil, and 800 lb to the till.

Test Procedure and Results. Following compaction of the soil, it was allowed to cure 24 hours before the surcharge load was applied, and another 24 hour period was then waited to allow the stress to equalize

With the single blades a total of five sets of tests was performed throughout the length of the box. A hole was advanced between sets to enable fresh material to be tested. Each test set consisted of alternately pushing three thicknesses of blades in sequence from thinnest to thickest. Caution was taken to ensure that each blade was pushed in the void left by the preceding thinner blade. Because of its length, with the stepped blade only two depths were tested, and since a pilot hole was not drilled, difficulty was experienced pushing the blade deep enough for the third thickness.

Table 10 summarizes the tests performed in the box. The theoretical stress at each location is calculated as the applied surcharge load distributed over the area of the box less the area of the soil removed by boring. Thus, the theoretical stresses on the single blades increase
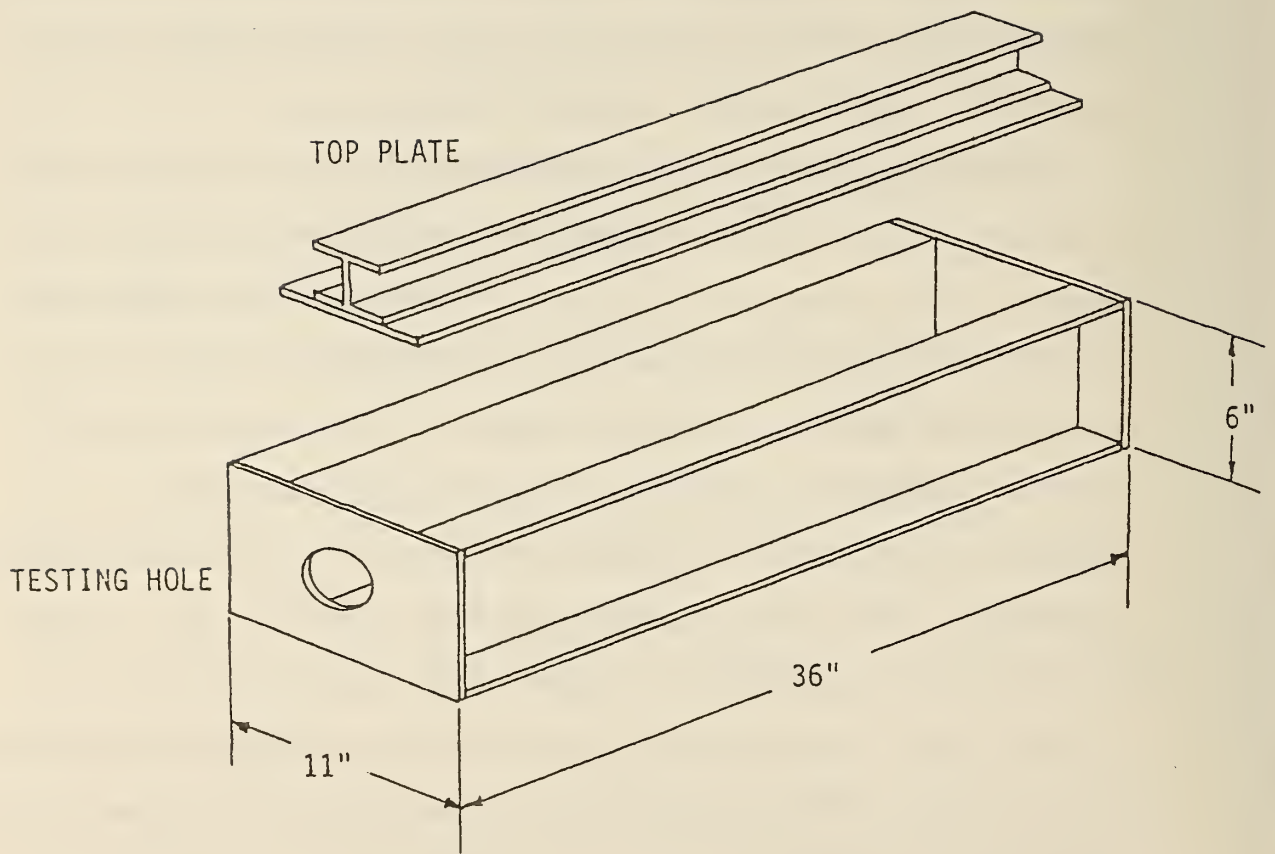
Figure 41. Sketch of test box
1 in = 2.54 cm

110

Table 10. Results of Stress Sensor Tests in Test Box

1 in = 2.54 cm , 1 psi = 70.31 gm/sq cm.

Soil	Blade*	Penetration Distance, in.	Applied σ_o, psi	Measured σ_s, psi	Extrapolated $a\sigma_o$, psi	a	b, mm^{-1}	r
Monona	A	2	4.4	8	5.1	1.2	0.15	0.99
	B			10.7				
	C			12.8				
	A	6.5	4.6	6.3	2.7	0.6	0.26	0.99
	B			8.8				
	C			14.3				
	A	13	5.0	3.0	0.4	0.08	0.66	0.97
	B			13.2				
	C			24.1				
	A	20	5.6	15.1	6.6	1.2	0.27	0.99
	B			25.2				
	C			35.4				
	A	26	6.2	13.0	7.8	1.3	0.16	0.99
	B			17.9				
	C			21.9				
	A$_s$	3.5	4.5	12.4	1.2	0.3	0.73	–
	B$_s$			39.6				
	C$_s$			(21.5)				
	A$_s$	10.5	4.5	17.3	5.8	1.3	0.35	–
	B$_s$			30.0				
Shelby	A$_s$	3.5	3.6	29.5	11.1	3.1	0.31	–
	B$_s$			48.0				
	C$_s$			(12.0)				
	A$_s$	10.5	3.6	18.5	15.1	4.2	0.06	–
	B$_s$			20.5				

*A = 1/8 in. single blade; B = 3/16 in. single blade; C = 1/4 in. single blade; A$_s$, B$_s$, C$_s$ signify the same thicknesses in the stepped blade.

111

with distance from the end since less soil in cross-sectional area is supporting the constant surcharge load. This still does not realistically describe the stresses occurring in soil along the sides of the hole, but may give a reasonable approximation of the stresses in the remaining undisturbed soil, which is of primary importance here.

Exponential regressions were fit using equation (15) plus the definition of λ:

$$\lambda = \frac{\sigma_s}{\sigma_o} = ae^{bt} \tag{15}$$

where σ_s is the sensor stress and σ_o is the initial stress. Hence

$$\sigma_s = a\sigma_o e^{bt} \tag{15a}$$

Extrapolation to t = 0 gives

$$\sigma_o = a\sigma_o$$

It will be noted that in a regression of σ_s vs. t, $(a\sigma_o)$ and b are the regression coefficients.

It can be seen in Table 10 that the values for a vary from 0.08 to 1.3 for the loess soil, averaging 0.85, but with most values falling in the range 1.2 to 1.3. In the stiffer till soil the ratio is much higher, 3.1 to 4.2. No consistent difference was found from pushing successive single blades compared to pushing the stepped blade. All

measurements with the 1/4 inch portion of the stepped blade were
believed to be erroneous since they were lower than values obtained
with the thinner blade sections, and were not used in the analysis.

The value of 1.2 to 1.3 for single blade tests in loess in the test
box compares to a value of about 1.7 for soft clay tests in the K Test
mold, supporting the view that the lower restraint offered by the box
did result in a value for a closer to the ideal value of 1.0. Still,
the close proximity of the blades to the unyielding sides of the box
probably results in a larger stress acting on the sensor than if the
soil were behaving as a semi-infinite mass. The adverse effects of
confinement would be expected to be accentuated in tests on the glacial
till soil, because of its stiffness and included pebbles, so we tend to
disregard that data. If a should equal 1.0, equation (15a) becomes

$$\sigma_s = \sigma_o e^{bt} \tag{15b}$$

Methods and Interpretation

Both single-blade and stepped blade tests were conducted in the field. Preliminary trials of a three-blade stepped vane are reported in the Appendix.

Since the field in situ stress for the most part is unknown, or at best has been measured by another instrument whose accuracy is not known, it is tentatively assumed that the multiplier a in equation (15) equals 1.0, and equation (15b) applies.

This assumption may not be entirely correct even in a semi-infinite soil mass because of dislocations of grains along the extrapolated "zero thickness" plane. Thus a should exceed 1.0, particularly in sands and coarse-grained soils, and some empirical correlation may have to be developed which considers soil particle size. Also, it is expected that any significant departure from the semi-infinite ideal condition such as proximity to a rigid structure or inclusion will boost a and give high readings. This possibility may be analyzed since an inclusion causing a high local value for a also should result in a high value for the stiffness parameter b.

The method for field data evaluation therefore is as follows:

1. If the measured stress σ_s steadily progresses to higher values with larger blade thicknesses, an exponential regression of σ_s vs. blade thickness t is made in accord with equation (15b). This gives the

following:

        (1).   Regression coefficient σ_o.

        (2).   Regression coefficient b.

        (3).   Correlation coefficient r.

If r is below 0.98, the relationship may be invalid, and an alternative

interpretation is made as follows:

    2. Two points may be selected to fit equation (15b). This gives:

        (1).   Regression coefficient σ_o.

        (2).   Regression coefficient b.

If b appears unreasonably high or low for the material tested, the

relationship may be invalid, and the third method for interpretation is

made:

    3. A value for b is selected from adjacent test data and applied

for individual points. In this case equation (15b) is rewritten

$$\sigma_o = \sigma_s e^{-bt} \tag{15c}$$

This gives individual values for σ_o but no other information. This method

is perhaps most appropriate where σ_o truly varies, and the data may be

used to calculate a mean and range in σ_o.

Single-Blade Tests, Overconsolidated Loess

    The first field in situ stress tests were made with three thicknesses

of blades pushed hydraulically into loess soil that had been overconsolidated

by being overrun by a glacier. The test location is a 77-foot (23.5 meter),

approximately 2:1 roadcut extending down through Wisconsin till, the underlying Wisconsin loess, and into pre-Wisconsin till, Fig. 42. The cut is located about 2 miles southwest of Boone, Iowa. Loess density was approximately determined with an Eley Volumeter. The Wisconsin till dry density is known to be fairly uniform, about 1.86 (116 pcf). Loess data are shown in Fig. 43.

The lower center of the 8-foot thick loess layer was bored horizontally for 2 to 2.3 meters, and the blades were pushed hydraulically into undisturbed soil at the bottom of the hole. The blades had circular Teflon-covered penumatic pressure cell which had been calibrated against air pressure. By pushing the blades with the flat sides oriented horizontally, vertical stress could be measured and compared to the calculated overburden stress; by pushing with the blades oriented vertically, horizontal stress could be calculated and used to find the lateral stress ratio K_o.

Results. Data from the Boone site are shown in Table 11. As can be seen, stresses from the thickest blade were lower than those from the intermediate blade, and therefore were omitted from the analysis. The thick blade was fabricated by attaching a removeable back-up plate to the intermediate thickness blade, and had less than the design tip-to-sensor distance. The two-point method outlined above therefore was used, giving σ_o and b, but no correlation coefficient. The values for b are in fairly good agreement, the higher value being horizontally, in the direction of

116
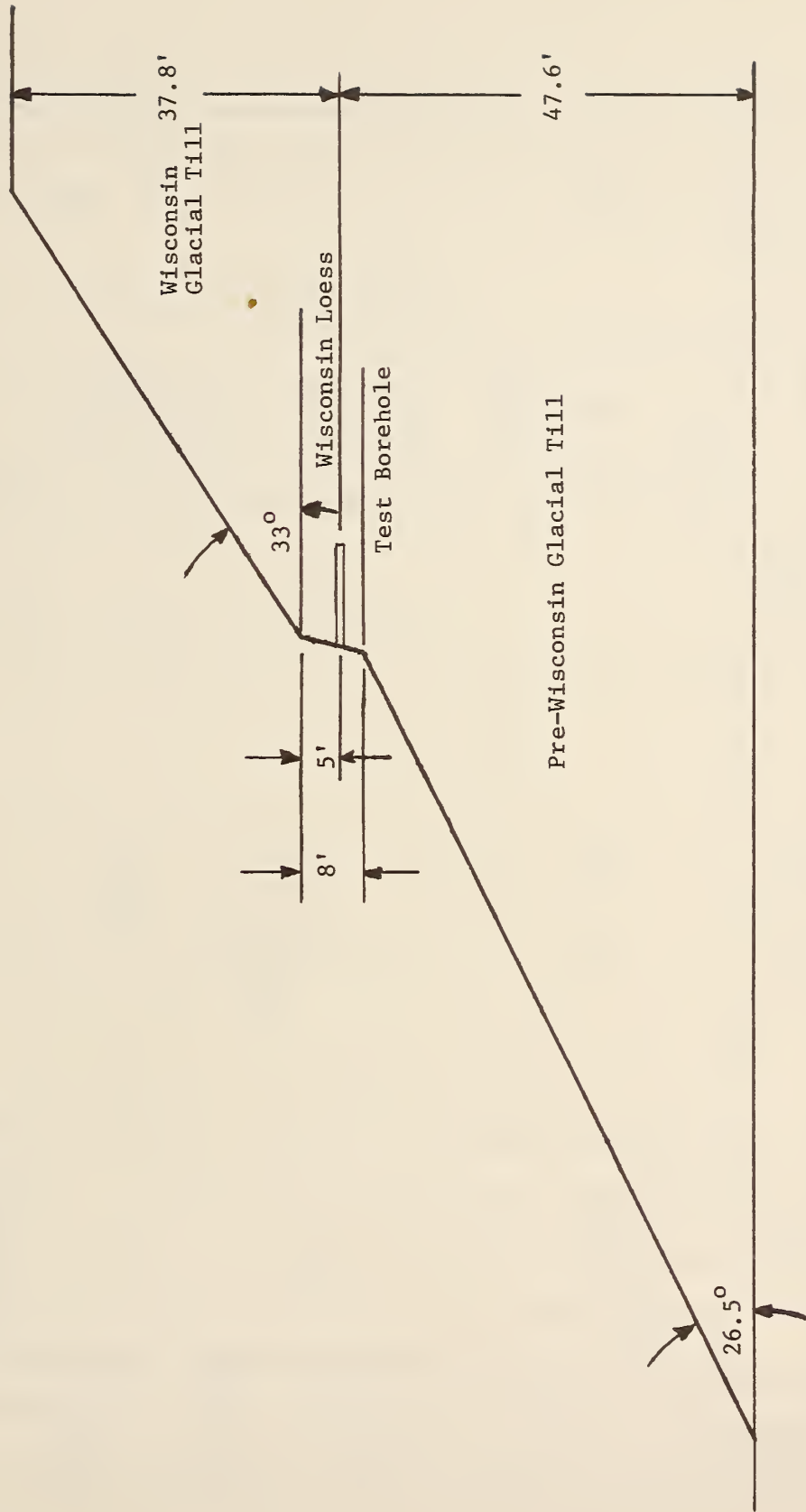
Figure 42. Test site near Boone, Iowa.

1 ft. = 0.3048 meters
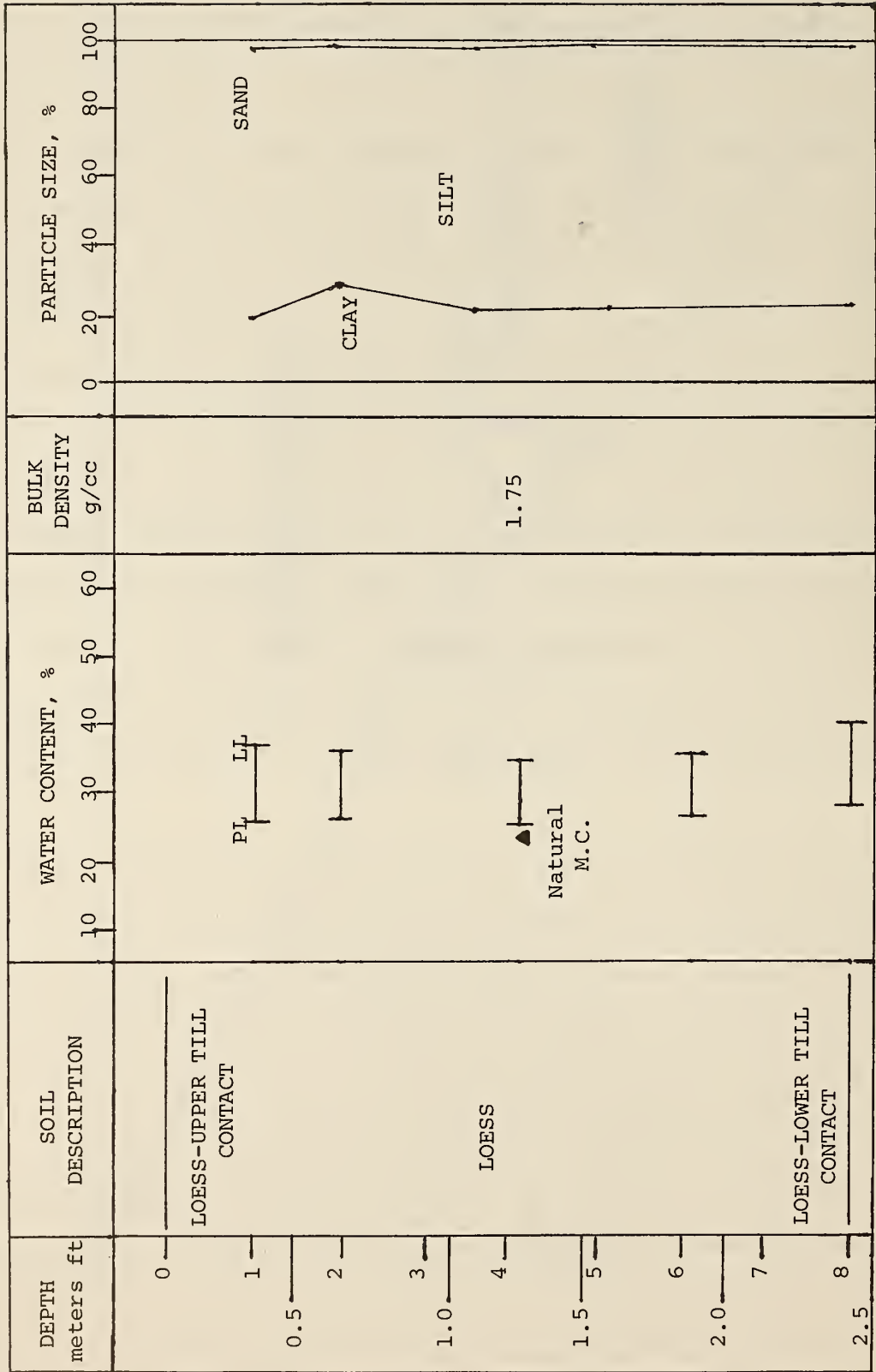
Figure 43. Soil data from the Boone, Iowa, test site.

118

the larger in situ stress. The vertical stress of 15.2 psi (104 KPa) is somewhat higher than the theoretical stress from elastic analysis, which

Table 11. Field stress data, Boone site.
1 ft = 0.3048 meters, 1 psi = 70.31 gm/sq cm

Blade	Horizontal Penetration, ft.	Vertical σ_s, psi	Horizontal σ_s, psi	σ_{o}, psi [*]	b, mm^{-1}
A(1/8 in.)	6.5	38.4		15.2	0.293
B(3/16 in.)	7.0	61.1			
C(1/4 in.)	9.0	(50.4)			
A	8.0		54.3	20.0	0.315
B	7.5		89.5		
C	9.5		(72.0)		

$$K_o = \frac{20.0}{15.2} = 1.32$$

[*] $\underline{a}$ assumed to equal 1.0.

is between 12.4 and 13.0 psi based on an assumed till wet density of 2.16 (135 pcf). If the vertical stress is 12.7 psi it has been over-estimated by a factor of 1.2, and $\underline{a}$ in equation (15a) should be 1.2. This is in close agreement with the test box data on loess.

The value for K_o does not depend on the coefficient $\underline{a}$ which affects both vertical and horizontal stress values. In an overconsolidated material K_o should exceed 1.0. The value of 1.3 therefore appears

reasonable, and to the authors' knowledge represents the first field measurement of this coefficient.

Single-Blade Tests, Underconsolidated Loess

A loess testing site was selected in a 35-foot roadcut 2.2 miles east of Turin, in western Iowa on Iowa Highway 37. The cut is on the north side of the highway, entirely in Wisconsin loess. As at the Boone site, a hole was augered horizontally into the cut, Fig. 44. Blades were pushed by hydraulically jacking against a bearing plate anchored to the soil. The hole was advanced an average of 6 inches between successive tests with the individual blades. Soil data for soil from the testing depth may be briefly summarized as follows:

Dry Density	Liquid Limit, %	Plastic Limit, %	Particle Size Gradation		
			Sand	Silt	Clay
1.60(100 pcf)	30.5	25.5	0.8%	87.4%	11.8%

Results. Turin site stress data are presented in Table 12. The vertical stress data shows a consistently higher stress with thicker blades and an exponential regression gave r = 0.994, indicating acceptable data. Also the value for b is in the range found for the Boone site loess.

The horizontal stress data do not show this consistent trend with blade thickness, and r is too low. The data therefore may be paired for analysis or, since b is known from other tests, analyzed as individual values. These methods for data treatment are shown in the lower part of Table 12. Of the three possible data pairs, AB, BC and

120
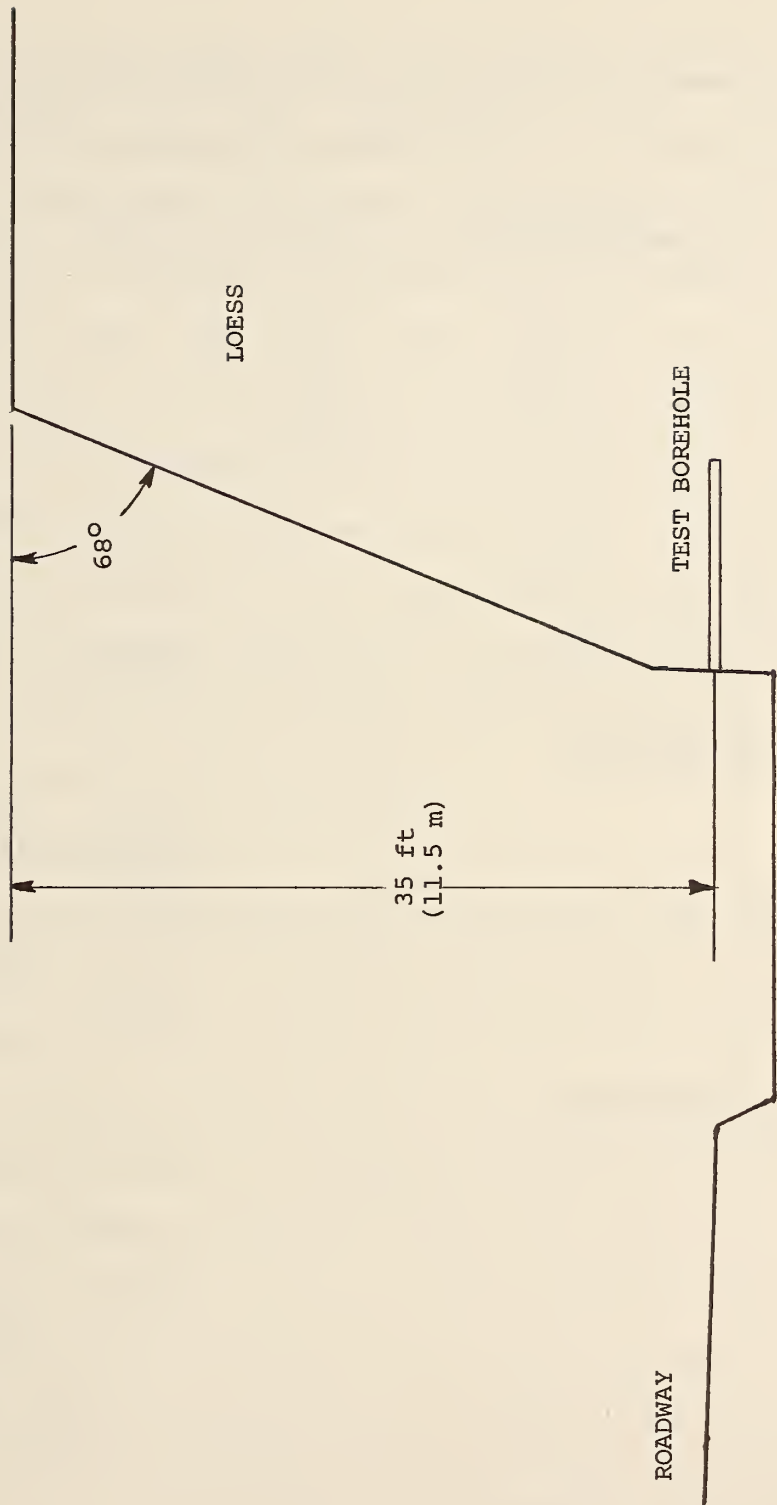
Figure 44.   Test site - Turin, Iowa. N½, NW¼, Se.13,
R44W, T83N.
1 ft = .3048 meters

121

Table 12.   Results of Blade Stress Sensor Tests, Turin Site.
1 ft = 0.3048 meters, 1 psi =70.31 gm/sq cm

Blade	Horizontal Penetration, ft.	Vertical σ_s, psi	Horizontal σ_s, psi	σ_o, psi	b, mm^{-1}	r
A	8.0	7.4		2.72	0.308	0.997
B	8.5	11.3				
C	9.5	19.7				
A	6.5		8.5	(3.8)	(0.211)	(0.800)[*]
B	9.0		7.7			
C	10.5		16.6			

Treatment as Data Pairs

A			8.5	(4.4)	(0.211)[*]	-
C			16.6			
B			7.7	(0.8)	(0.484)[*]	-
C			16.6			

Treatment as Data Points

A			8.5	3.20	0.308	-
B			7.7	1.78	0.308	-
C			16.6	2.35	0.308	-
				2.44 $\pm$ 0.71		

$$\bar{K}_o = 0.897$$

[*]Parentheses indicate rejected values.

122

AC, the first is rejected because it gives a negative value for b. The other pairs also give unlikely values for b, so the third procedure is used where points are evaluated individually with b assumed to be 0.308. This gives a mean horizontal stress of 2.4 psi and $K_o = 0.90$

The vertical stress from elastic theory should be 15.5 to 16.8 psi, almost 6 times higher than measured. This difference probably relates to either inelastic behavior of the material or, more likely, stress relief by erosion and undercutting at the ditch level. This also would explain the relatively high K_o, but it should be emphasized that no other K_o data are available from either field or laboratory determinations, since this is an eolian silt soil that is underconsolidated as a consequence of never having been saturated with water.

Single-Blade Tests, Alluvium

Logan-1. A site designated as Logan-1 is located just southeast of Logan, Iowa. The tests were conducted in a vertical hole on the Boyer River Floodplain.

Soil description and data are in Fig. 45. Alternating layers of silts and clays were encountered throughout, densities and moisture contents being determined on samples sealed at the site and sent to the laboratory. Since all blade tests were run in a vertical borehole, only horizontal stresses were obtained. The hole was advanced between test in order to run each subsequent test in undisturbed material.
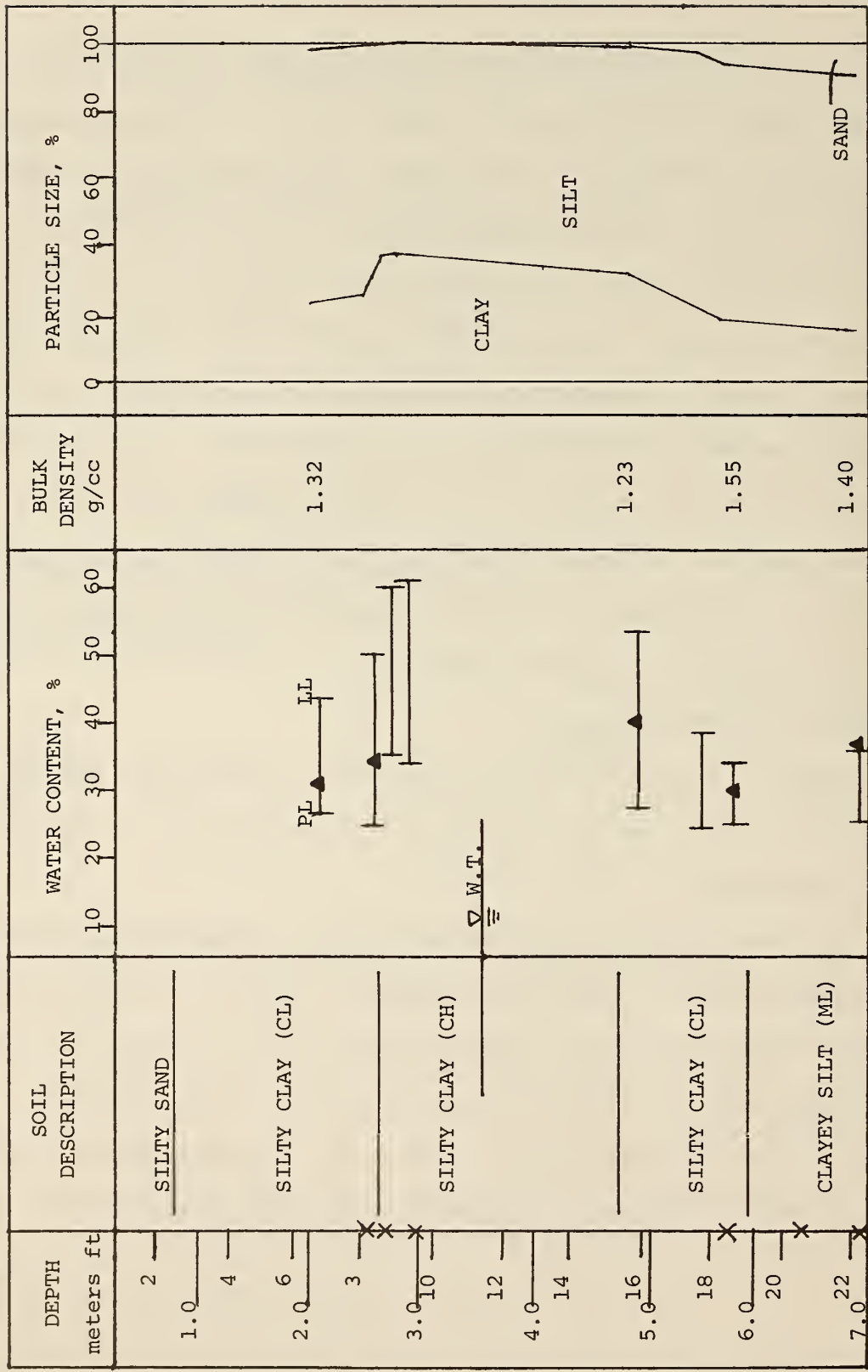
Figure 45. Soil Data, Logan-1 TEST SITE

Results. Results from the Logan-1 tests are shown in Table 13.
In the first set measured stresses decreased with increasing blade
thickness, but as shown in Fig. 45, the tests were conducted in two
different layers. In the second set the C blade gave a low value, and
a two-point fit gave σ_o = 1.9 psi. This cannot be correct since it is
less than the pore water pressure.

Logan-2. The erratic nature of the results was tentatively
attributed to the alluvial stratification and not conducting sequential
tests at the same depth. Since the stepped blade was not ready for field
use at the time, a second site, Logan-2, was selected where tests were
conducted in three different boreholes but at identical depths. Logan-2
also is on the Boyer River floodplain, 5.5 miles southwest of Logan.
Soil data from the three borings was quite consistent; data from one
of the borings are shown in Fig. 46.

Results. Horizontal stress results from Logan-2 also are shown in
Table 13. The data were more consistent than at Logan-1, but again the
thick blade data were suspect. Two-point fit gave stress values as
indicated in Table 13. The values for b vary widely, as might be
expected in a layered deposit. The calculated K_o values range from 0.5
to 1.1, the high value being at a depth of 5 ft. These values are not
unlikely because of the expansive nature of the clay mineral, but there
has been no independent check on these results.

Stepped Blade Tests in FHWA Test Pit

The first "field" tests using the stepped blade sensor were per-
formed in a test pit at the Federal Highway Administration (FHWA) research
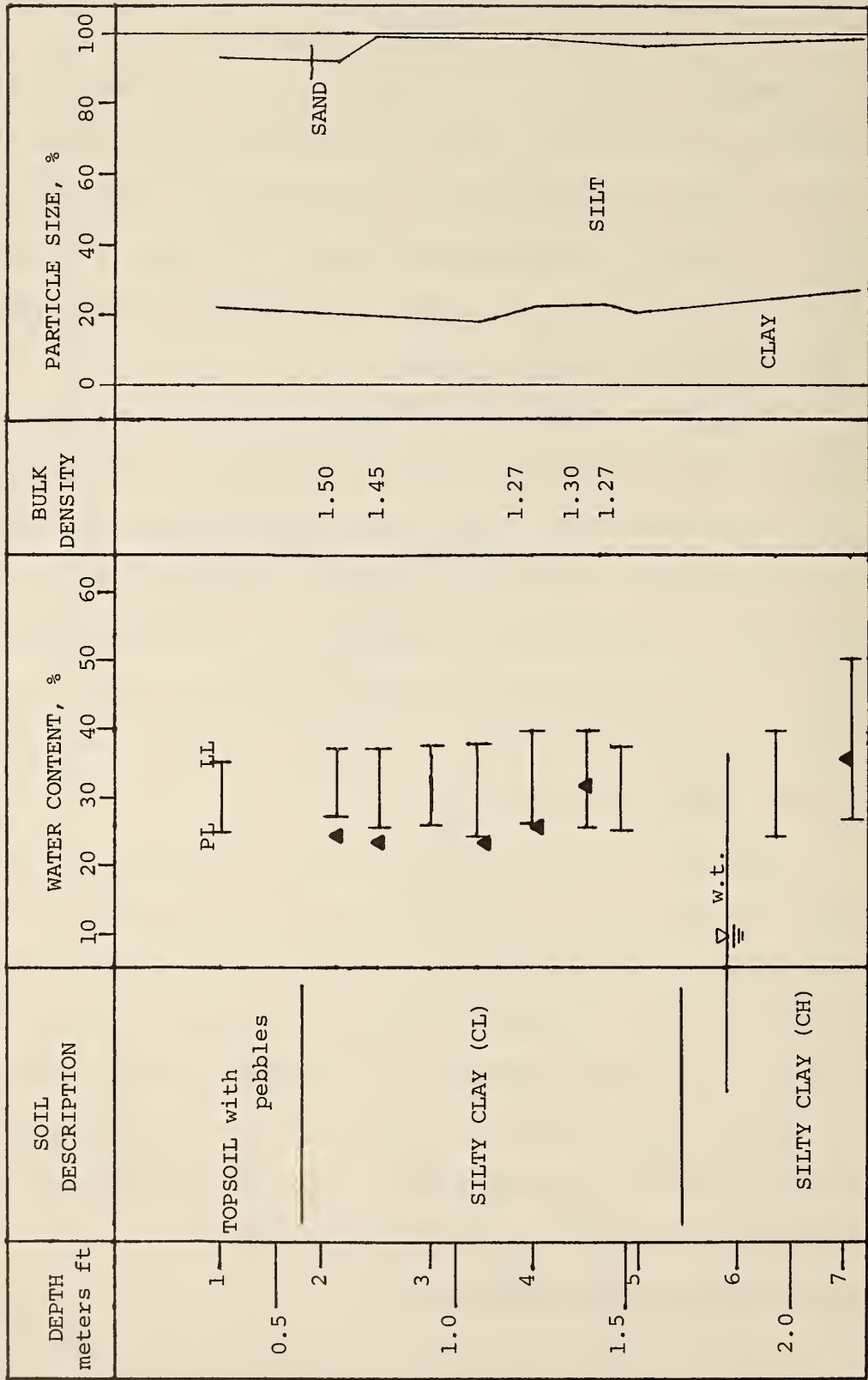
Figure 46. Soil Data, Logan-2 TEST SITE

Table 13. Results of Blade Stress Sensor Tests at Logan 2.
1 ft = 0.3048 meters, 1 psi = 70.31 gm/sq cm

Blade	Depth ft.	Horizontal σ_s, psi	σ_o, psi	b, mm^{-1}	r	Overburden Total Stress psi	Pore Pressure u, psi	K_o *
Logan-1								
A	8.0	15.8	(Negative Slopes)		-			-
B	8.5	15.0			-			-
C	9.0	8.8			-			-
A	20.0	6.7	(1.86)	(0.40)	-	14.5	3.6	-
B	21.0	12.7				16.2	4.4	-
C	24.0	(11.7)	-	-				-
Logan-2								
A	3.0	3.4	1.09	0.358	-	2.40	0	0.47
B	3.0	6.0				2.21	0	
C	3.0	(5.0)						
A	5.0	6.5	3.99	0.154	-	3.04	0	1.1
B	5.0	8.3				3.65	0	
C	5.0	(6.2)						
A	7.0	4.1	3.73	0.030	-	5.28	0.51	0.67
B	7.0	4.3				5.09	0.51	
C	7.0	(17.1)						

*Effective stress basis.

127

facilities in McLean, Virginia. The pit is approximately 10 feet square with concrete sides. Previous studies in the pit by the FHWA were involved with subgrade performance, so there was an asphaltic concrete surface course approximately 4 in. thick covering the soil. A vertical hole was bored into the underlying soil to a depth of 27 in. The stepped blade was pushed into the soil at the bottom of the hole in increments of 6, 7 and 9 in., so the sensor of each successive blade section was at the same point in the soil. Soil properties to the depth of testing are shown in Fig. 47. This was a very firm soil, having been compacted to 100% standard density and subjected to many cycles of loading tests. The moisture content was well below the plastic limit.

Results. Results are in Table 14. The thickest section of the stepped blade gave a lower stress than the intermediate blade. A two-point fit to the other data gave $b = 0.443 \text{ mm}^{-1}$, which appears reasonable for a dense, highly constrained soil, and gave a lateral stress of 11.3 psi. Dividing by the calculated overburden pressure of 2.3 psi gives $K_o = 4.9$, indicative of a highly overconsolidated deposit.

Stepped Blade Tests, Mitchellville Till Site

Horizontal stress evaluations were performed with the stepped blade in conjunction with subsurface exploration for cooperative grain storage bins in Mitchellville, Iowa,[44] approximately 20 miles east of Des Moines. The site is located geologically within the end moraine of the Cary substage of Wisconsin-age glacial till.
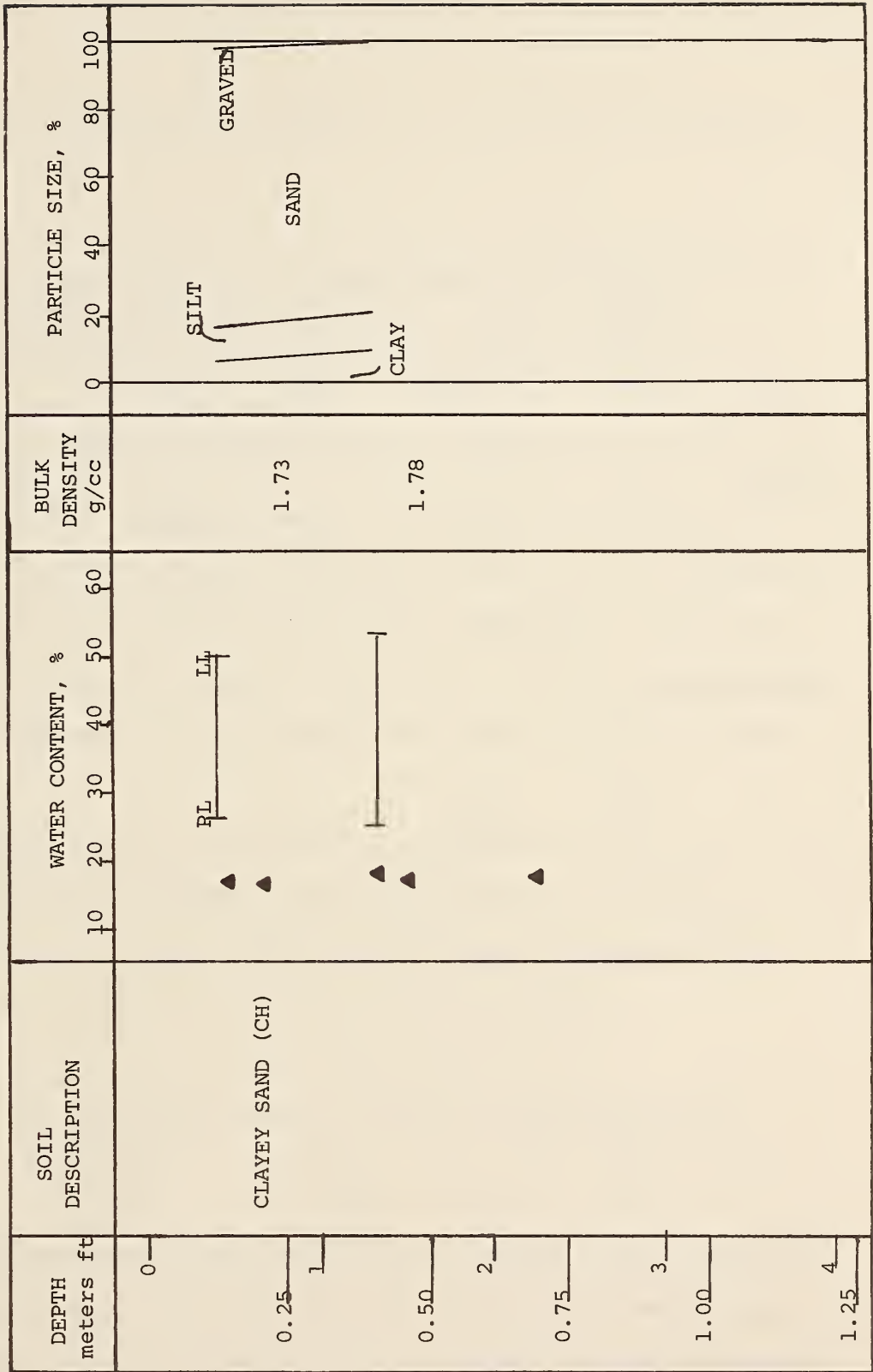
Figure 47. Soil Data, FHWA Test Pit

129

Table 14. Results of Stepped Blade Tests at FHWA Test Pit and Mitchellville Site.

$1 \text{ ft}^2 = 30.71 \text{ cm}^2$, $1 \text{ psi} = 70.31 \text{ gm/sq cm}$

Blade Section	Depth, ft.	Horizontal σ_s, psi	σ_o, psi	$b_{2,1}$ mm	r	Pressuremeter p_o, psi*
FHWA						
A	2.5	46.0	11.3	0.443	–	–
B		92.9				
C		(92.3)				
Mitchellville						
A	16	26.5	18.3	0.120	0.997	19.3
B	(Till)	32.9				
C		38.8				
A	31.5	27.5	17.7	0.133	0.992	16.7
B	(Loess)	32.4				
C		42.0				

*Pressuremeter data courtesy of Michael Feist and Soil Testing Services of Iowa, Inc.

The glacial till therefore should not be heavily overconsolidated . Test borings showed about 18 ft of fill and till-alluvial mixtures, overlying Wisconsin loess to a depth of 45 ft, overlying a paleosol (gumbotil)

developed in pre-Wisconsin glacial till. The soil data are shown in Fig. 48.

Two sets of stepped blade stress sensor tests were conducted to determine horizontal stresses, at depths of 16 and 31.5 feet. In addition, pressuremeter tests were run at the same depths to find corresponding p_o's as a comparison.

Results. The Mitchellville test sets appeared to give valid stress measurements for all blade sections, indicating that the thickest (1/4 in.) blade may perform satisfactorily in sufficiently compressible soils. Three-point regressions gave high correlation coefficients and reasonable values for b and horizontal stress, Table 14. Of particular interest is the close agreement to pressuremeter p_o values, within 1.0 psi.

The value for K_o is calculated on an effective stress basis, which means subtracting pore pressure from both vertical and horizontal stress before finding the ratio. These calculations are as follows based on measured soil densities and depths below the water table:

Depth, ft.	Overburden Total Stress σ_v, psi	Pore Pressure u, psi	σ_v', psi	σ_h', psi	K_o
16(till)	14.6	1.7	12.9	16.6	1.29
31.5(loess)	27.9	8.4	19.5	9.3	0.48

131
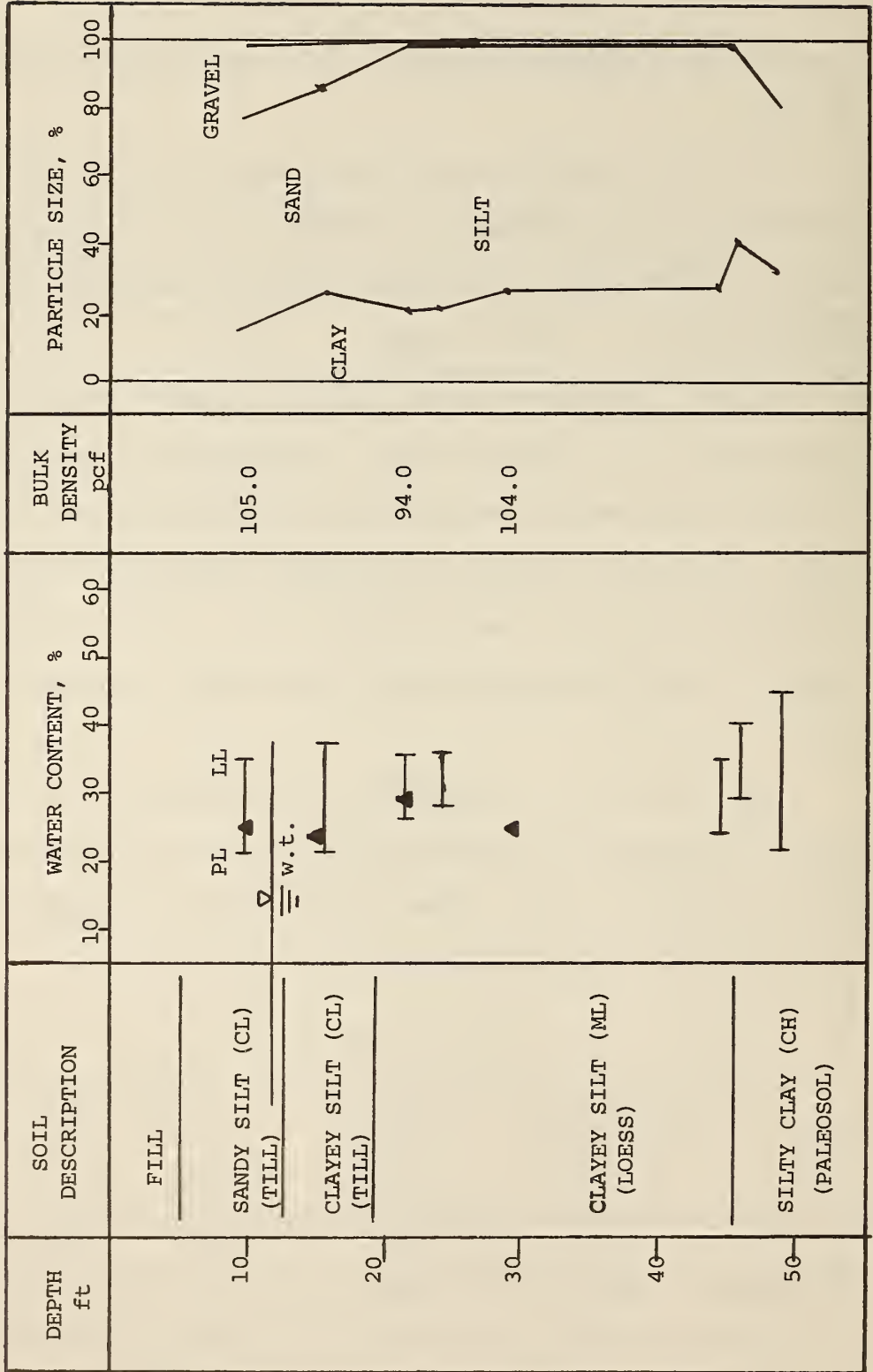
Figure 48.   Soil Data, Mitchellville site.
1 ft = 0.3048 m, 1 pcf = 16.018 Kg/cu m

132

The K_o data suggest a rather surprising inference that the glacial till is preconsolidated whereas the underlying loess is not. The occurrence of soft, even underconsolidated loess underneath till is a fairly common observation, and usually is attributed to the lack of free drainage for the loess while it was under ice pressure, whereas the glacial material contains random sand lenses.

Stepped Blade Tests, Houston Clay

Following the success at the Mitchellville site, stress measurements were made with the stepped blade in the highly expansive, overconsolidated Houston clay on the University of Houston, Texas campus. The clay was not sampled, since the site was previously investigated in connection with on-going pile load test research. A soil description is given in Table 15.

Table 15. Soil Data, University of Houston Test Site.
              1 ft = 0.3048 meters

Depth, ft.	N, Blows/ft.	Description
0 - 9	5	Gray and tan Stiff to very stiff clay w/nodules below 2 meters
9 - 12	10	Gray and tan Very stiff, very sandy clay
12 - 27	12-18	Red and light gray Very stiff slickensided clay with calcareous nodules
27 - 45	7-35	Light gray and tan Very stiff sandy clay with sand pockets

Note: Groundwater at 7.5 ft.
Data courtesy Prof. M.W. O'Neill and Fugro-Gulf, Inc.

Tests were conducted in duplicate at nominal 5-ft depth intervals in two different borings, giving 4 test sequences at each depth. A truck-mounted drill rig was used to wash-bore down to the testing depth and to push the blade hydraulically for three stress measurements at each depth. The two borings, each to 50 feet, required about 6 hours testing time for two technicians and a driller.

Results. Stress data from the Houston tests are given in Table 16. In none of the tests did the C (1/4 in.) section gives reasonable data, so all values of σ_o and b are from two-point determinations. Where by inspection the b values were negative, σ_o's were not calculated, and where calculated b values appear too low or too high, data are put in parentheses.

An aid to determination of whether b is reasonable or not is a plot of b versus depth, Fig. 49. Of interest is that the two borings show different trends, even though they are only a few yards apart in the same clay. Deleted values are usually high, probably reflecting proximity to nodular inclusions noted in Table 15. Stress data still may be salvaged by use of the one-point method with b values obtained from adjacent depths or read from Fig. 49.

Averaged or "normalized" b data also may be used to back-calculate in situ stresses from each data point. This procedure assumes that the horizontal stress is more variable than the soil stiffness parameter b after deletion of extraneous b values; therefore b data are smoothed or averaged. This procedure also is reasonable when we see that variability

134
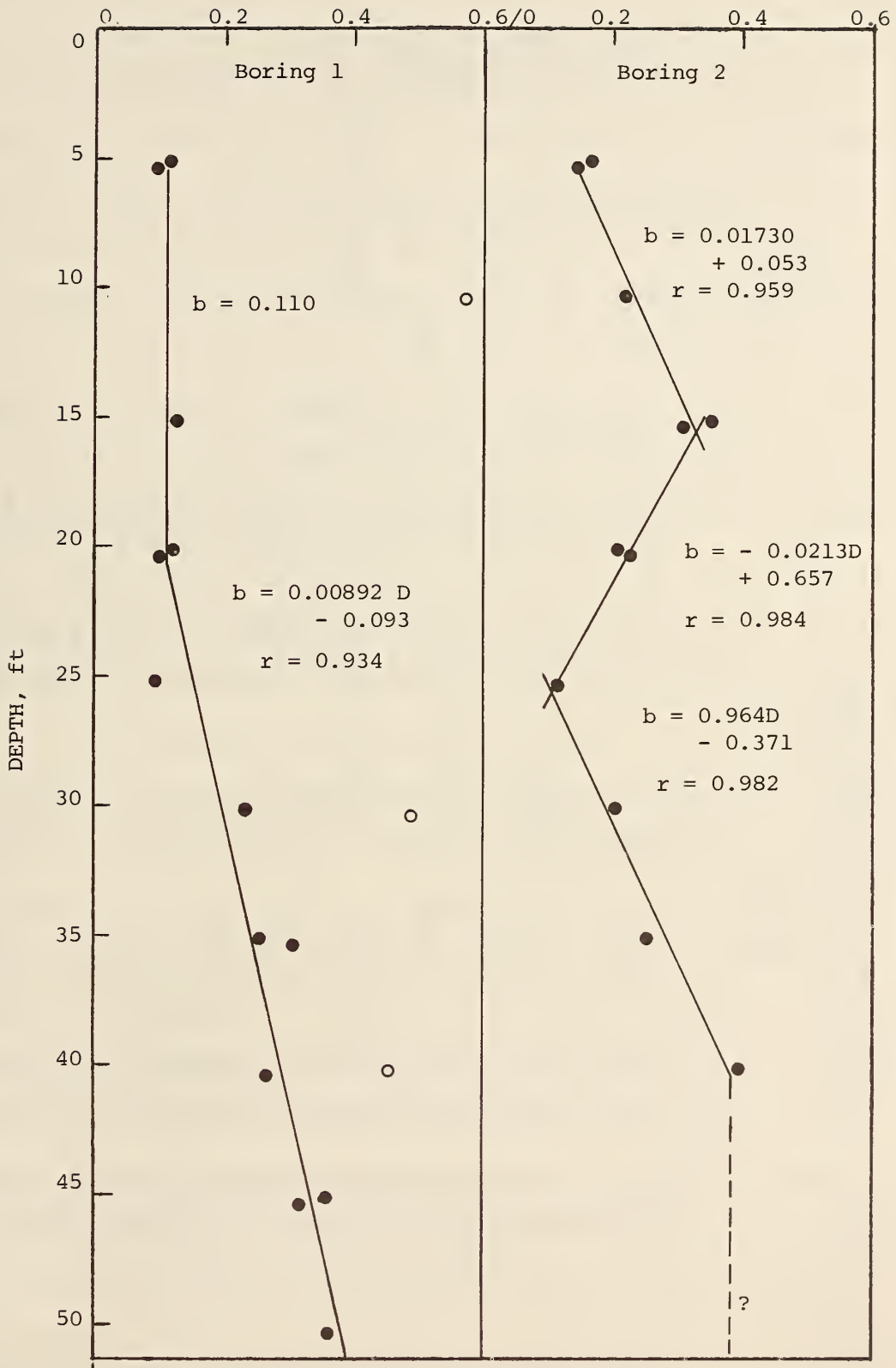
Figure 49. Houston clay stiffness factor "b" versus
depth.
1 ft = .3048 meters

135

Table 16. Results of Stepped Blade Tests, Houston Clay

1 ft = 0.3048 m., 1 psi = 70.31 gm/sq cm

Depth, ft.	Boring 1 σ_s, psi A*	B	C	σ_o, psi	b, mm^{-1}	Boring 2 σ_s, psi A*	B	C	σ_o, psi	b, mm^{-1}
5.25	20.15	24.31	(23.32)	13.8	0.118	28.10	36.38	(29.5)	16.8	0.163
5.83	37.64	43.74	-	27.9	0.094	30.22	37.9	-	19.2	0.143
10.25	16.97	(10.13)	(6.33)	(Negative Slope)	(Negative Slope)	17.5	50.03	(14.05)	(2.14)	(0.662)
10.83	22.27	56.33	-	(3.5)	(0.585)	41.35	58.43	-	20.7	0.218
15.25	71.56	87.31	(59.37)	48.1	0.125	37.64)	65.78	(47.01)	12.3	0.352
15.83	35.52	(35.33)	-	(Negative Slope)	(Negative Slope)	57.78	94.13	-	21.8	0.307
20.25	80.04	96.76	(9.93)	54.8	0.120	90.11	125.11	(81)	46.7	0.207
20.83	78.45	92.03	-	57.0	0.101	58.84	84.16	-	28.8	0.225
25.25	98.06	(81.53)	(11.99)	(Negative Slope)	(Negative Slope)	87.46	(29.03)	....(Negative Slope).....	(Negative Slope)	(Negative Slope).....
25.83	106.54	123.53	-	79.3	0.0932	98.06	117.23	-	68.6	0.113
30.25	31.28	45.31	(42.89)	14.9	0.233	35.52	48.98	-	18.7	0.202
30.83	37.64	81.53	-	(8.0)	(0.487)	46.12)	-	-	-	-
35.25	84.28	125.63	(76.88)	37.9	0.252	75.8	113.03	-	34.1	0.252
35.83	86.4	140.33	-	32.8	0.306	66.26	-	-	-	-
40.25	48.24	98.86	(45.98)	11.5	(0.452)	41.88	78.38	-	12.0	0.395
40.83	62.02	94.13	-	26.9	0.263	68.91	-	-	-	-
45.25	66.79	118.28	(56.28)	21.3	0.360	27.04	94.13	-	-	-
45.83	54.6	89.93	-	20.1	0.314	31.28	-	-	-	-
50.25	48.24	53.18	(45.98)	(39.7)	(0.061)	16.44	(9.04)	-	-	-
50.83	45.59	80.48	-	14.6	0.358	22.8	-	-	-	-

*Section A, 1/8-in.; B, 3/16 in.; C, 1/4 in. thickness.

136

or error in either of two stress readings affects $\underline{b}$, in effect doubling the likelihood of error in $\underline{b}$ compared to error in individual stress readings. Table 17 shows stress data recalculated by the one-point method with $\underline{b}$ values from the regressions in Fig. 49. The stress data of Table 17 were examined for erratic values, which were omitted. In all, 18 of the 75 points were omitted, 6 because of erroneous or unknown $\underline{b}$ values. A plot of stress vs. depth is in Fig. 50.

The plot in Fig. 50 shows a very strong increase in lateral stress at depths between 10 and 25 feet, then an abrupt drop in stress somewhere between 25 and 30 feet depth. This range corresponds with the zone of slickensides noted in Table 15 from 12 to 15 feet. These features are indicative of shearing due to horizontal expansion pressures. The allowable pressure should increase with depth because of the larger restraint to shear by overburden pressure acting as the minor principal stress. It also will be seen that the standard deviation is largest in the transitional stress zone, as might be expected. An increase in lateral pressure also is seen above the water table, probably as a result of desiccation. The cause for the apparent increase at 35 feet is not known, but might be speculated as being due to a relict feature caused by a former low position of the water table, evidenced by the mottled soil colors. Data are erratic at 50 ft., perhaps related to a soil change indicated at 47 ft. Furthermore the measured stress should not be less than the pore water pressure inferred from ground water elevations.
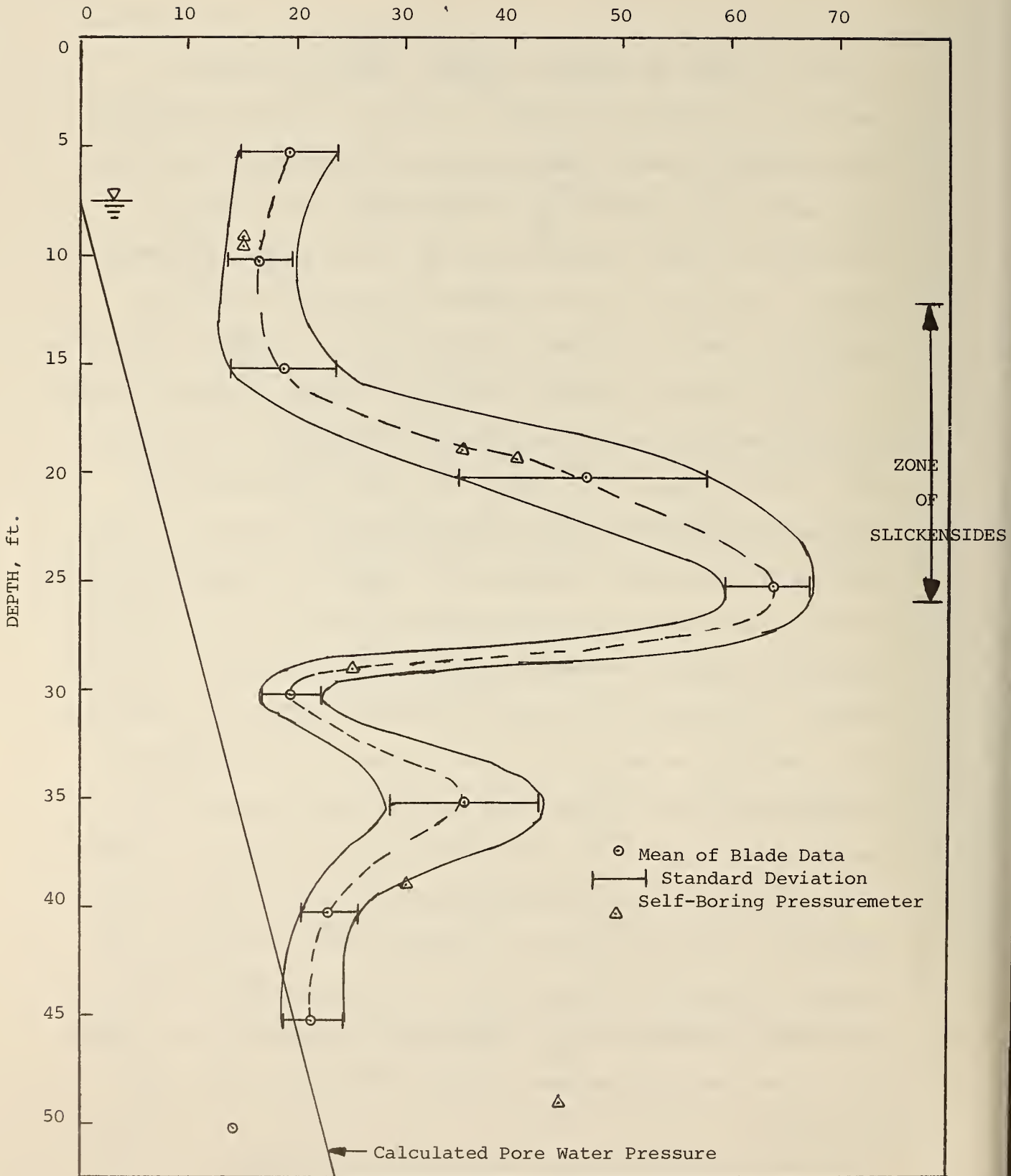
Figure 50.   Horizontal stress versus depth in Houston clay.   Pressuremeter
            data coutesy of Fugro-Gulf, Inc.
                l ft = .3048 meters, l psi = 7031 gm/sq cm

Table 17. Houston Clay Stresses with Linearly Regressed $\underline{b}$ data
$1 \text{ ft} = 0.3048 \text{ m}$, $1 \text{ psi} = 70.31 \text{ gm/sq cm}$

Depth, ft.	Boring 1			Boring 2			σ_o psi
	$b,$ mm^{-1}	A σ_o, psi	B σ_o, psi	$b,$ mm^{-1}	A σ_o, psi	B σ_o, psi	
5.25	0.110	14.2	14.4	0.149	17.5	17.9	19.2 ± 4.6
5.83	0.110	26.5	25.9	0.149	18.8	18.6	
10.25	0.110	12.0	6.0*	0.236	8.3*	16.3	16.5 ± 3.0
10.83	0.110	15.7	33.4*	0.236	19.5	19.0	
15.25	0.110	50.5*	51.7*	0.325	13.4	14.0	18.6 ± 4.9
15.83	0.110	25.1	20.9*	0.325	20.6	20.0	
20.25	0.110	56.4	57.3	0.221	44.7	43.7	46.3 ± 11.7
20.83	0.110	55.3	54.5	0.221	29.2	29.4	
25.25	0.155	59.9	39.0*	0.115	60.7	16.8*	63.4 ± 4.1
25.83	0.155	65.1	59.0	0.115	68.1	67.8	
30.25	0.200	16.6	17.5	0.197	19.0	18.7	19.4 ± 2.8
30.83	0.200	19.9	31.4*	0.197	24.7	n.d.	
35.25	0.244	38.8	39.3	0.290	30.2	28.4	35.3 ± 6.8
35.83	0.244	39.8	43.9	0.290	26.4	n.d.	
40.25	0.289	19.3	25.0	0.383	12.4*	12.6*	22.7 ± 2.6
40.83	0.289	24.8	23.8	0.383	20.4	n.d.	
45.25	0.333	23.2	24.2	(0.385?)	(8.0?)*	(15.2?)*	21.2 ± 2.9
45.83	0.333	19.0	18.4	(0.385?)	(9.3?)*	n.d.	
50.25	0.378	14.5	8.8*	(0.383?)	(4.9?)*	(1.6)*	13.8 ± 0.6
50.84	0.378	13.7	13.3	(0.383?)	(6.8?)*	n.d.	

*Data omitted from calculations of mean and standard deviations.

139

Table 18. Houston Clay K_O Data

1 ft. = 0.3048 m , 1 psi = 70.31 gm/sq cm

Depth, ft.	Pore Water Pressure psi	Total Stress psi		Effective Stress, psi		K_o
		σ_v	σ_h	σ_v'	σ_h'	
5.5	0	4.6	19.2	4.6	19.2	4.2
10.5	1.1	8.8	16.5	7.7	15.4	2.0
15.5	3.5	12.9	18.6	9.4	15.1	1.6
20.5	5.6	17.1	46.3	11.5	40.7	3.5
25.5	7.8	21.3	63.4	13.5	55.6	4.1
30.5	10.2	25.4	19.4	15.2	9.2	0.61
35.5	12.1	29.6	35.3	17.5	23.2	1.3
40.5	14.3	33.8	22.7	19.5	8.4	0.43
45.5	16.5	37.9	21.2	21.4	4.7	0.22
50.5	18.6	42.1	(13.8)	23.5	(-4.8)	-

Table 19. Soil Data, FHWA Fairbank Highway Research Station, McLean, Virginia Test site.

1 ft = 0.3048 m , 1 psi = 70.31 gm/sq cm

Depth, ft.	Description	N, blows/ft
0 - 5	Clayey micaceous clay	
5 - 22	Micaceous silt	8 - 18
22 - 30	Micaceous silt	19 - 26
30 - 42	Micaceous silt	>27

Note: Groundwater at 18.5 feet

140

Also shown in Fig. 50 are P_O data, courtesy of Fugro-Gulf, Inc., obtained from tests with a self-boring pressuremeter. Except at 50 feet depth, the data are closely comparable. The pressuremeter p_O is read only to the nearest 5 psi, and in all cases except at 50 ft the agreement is within this range. Due to the larger test depth intervals, the pressuremeter apparently missed the peak stress zone at 25 feet.

The stress data of Fig. 50 also may be plotted in terms of K_O, or the ratio of horizontal to vertical effective stress. The latter was done by assuming a uniform soil dry bulk density of 1.92 (120 pcf). Calculations are presented in Table 18 and shown graphically in Fig.51. The maximum value of K_O is 3.5 to 4.0, at depths of 20 to 25 feet.

In summary, the stepped blade data give reasonable values for horizontal in situ stress, and are closely comparable to self-boring pressuremeter data.

Stepped Blade Tests at Fairbank Highway Research Station, McLean, Virginia

Tests were conducted in two adjacent boreholes in a micaceous, silty residual soil at the FHWA Fairbank Highway Research Station, McLean, Virginia. A drill rig was used, the hole being advanced by augering. Soil data are presented in Table 19.

Stress measurements made with the stepped blade at Fairbank are presented in Table 20. These data are averages of two or three pressure gauge readings, often by different operators interested in learning the technique. No usable data were obtained from the thick (1/4 in.) blade section due to firmness of the soil, so data are not included.

141
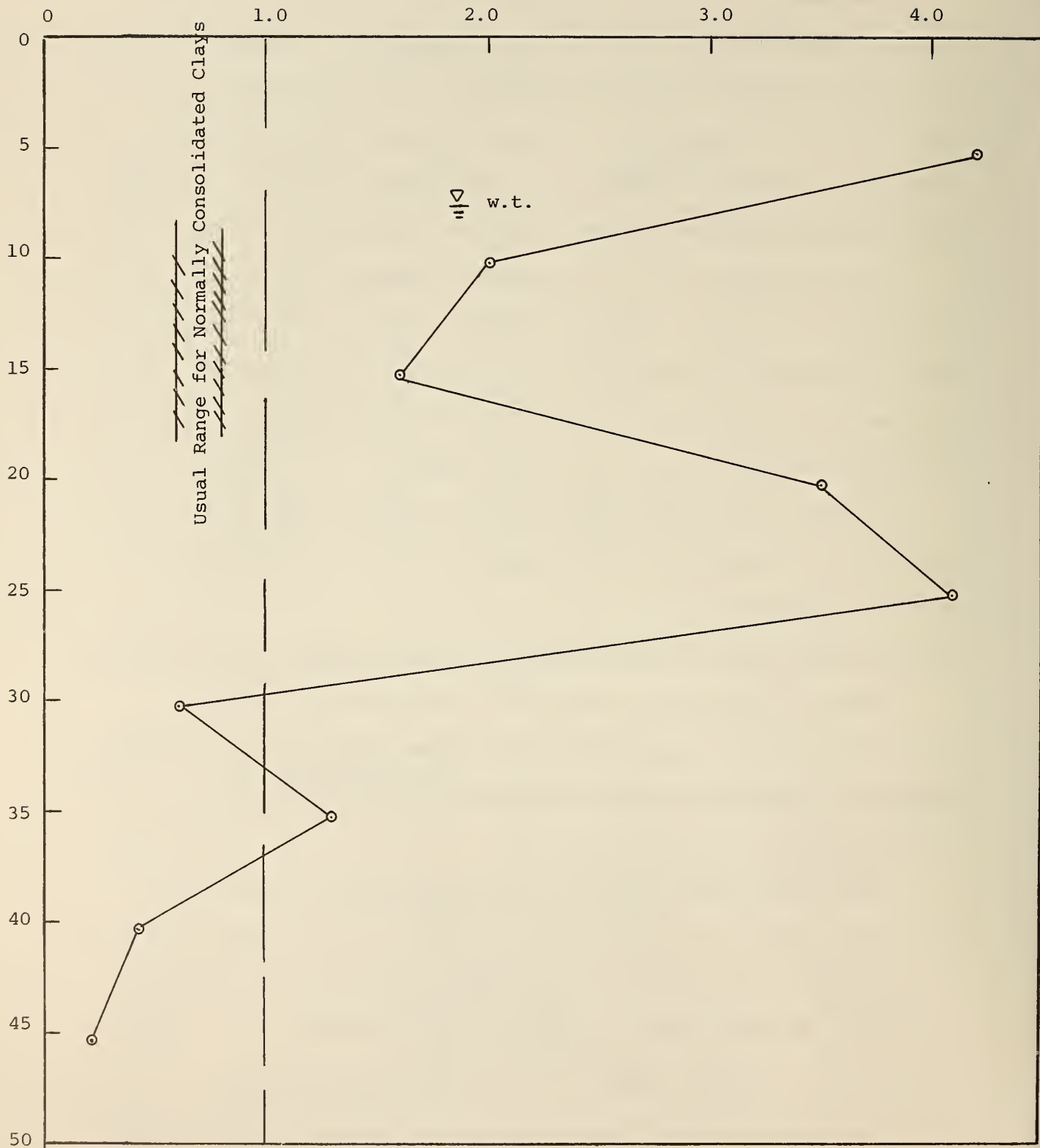
Figure 51. K_o versus depth for Houston clay.
            1 ft = .3048 meters

Table 20. Results of Stepped Blade Tests, FHWA Fairbank Highway Research
Station, McLean, Virginia Test Site.

1 ft = 0.3048 m , 1 psi = 70.31 gm/sq cm

Depth ft.	Boring 1 σ_s, psi A	B	σ_o, psi	b, mm^{-1}	Boring 2 σ_s, psi A	B	σ_o, psi	b, mm^{-1}
4.25					15.0	30.8	3.6	0.453
4.83					15.0	36.0	2.6	0.551
5.25	26.8	39.8	12.2	0.249				
9.25					28.0	54.0	7.5	0.414
10.25	30.7	52.0	10.7	0.332	36.0	53.5	16.3	0.250
10.83	32.0	51.5	12.4	0.300				
14.25					42.5	77.5	12.8	0.378
14.83					36.0	62.5	11.9	0.347
15.25	40.7	59.0	19.4	0.234				
15.83	42.3	65.5	17.6	0.275				
19.25					44.0	47.5	37.8	(0.048)
19.83					50.8	81.2	19.9	0.295
20.25	35.7	68.0	9.84	0.406				
20.83	31.7	83.0	4.62	0.606				
24.25					38.5	83.5	8.2	0.488
24.83					83.2	123.0	38.0	0.246
29.25					103.2	126.0	69.2	0.126
29.83					83.0	164.0	21.3	0.429
30.25	40.0	n.d.	-	-				
30.83	41.0	43.0	37.3	0.030				
35.25	90.7	127.5	45.9	0.215				
35.83	97.3	122.5	61.4	0.145				

A plot of $\underline{b}$ values from Table 20 versus depth shows a wide scatter with no consistent trend. As previously discussed, the variability of $\underline{b}$ values is greatly magnified by their determination from stress measurements. In order to reduce this variability, data from the same approximate depths were grouped as shown by horizontal lines in Table 20, and regressions performed on the grouped data, Table 21. This gave much more consistent values for $\underline{b}$ which show consistent trends, Fig. 52. Low correlation coefficients do not necessarily indicate erroneous $\underline{b}$ values because of the data pairing, a high A blade stress normally with a high B blade stress, etc. The low $\underline{r}$ in the range 29.25 - 30.83 feet is contributed to by Boring 1 data in a "soft zone," but omitting that data did not appreciably alter the $\underline{b}$ value.

Stresses recalculated with $\underline{b}$ values from Fig. 52 are presented in Table 22 and plotted in Fig. 53, the $\pm$ values and plotted ranges indicating standard deviations. Fig. 53 shows a uniform tendency for horizontal stress to increase with depth, as might be anticipated in a residual soil due to volume expansion on weathering although other factors, such as tectonic compressive stresses in the underlying rock, may have an influence. Two exceptions are noted -- an apparent discontinuity in the vicinity of the ground water table, and a low stress zone at 30.5 feet depth. The latter was described in the field notes as a "soft and soupy," possibly due to water concentration along a fracture or fault.

144
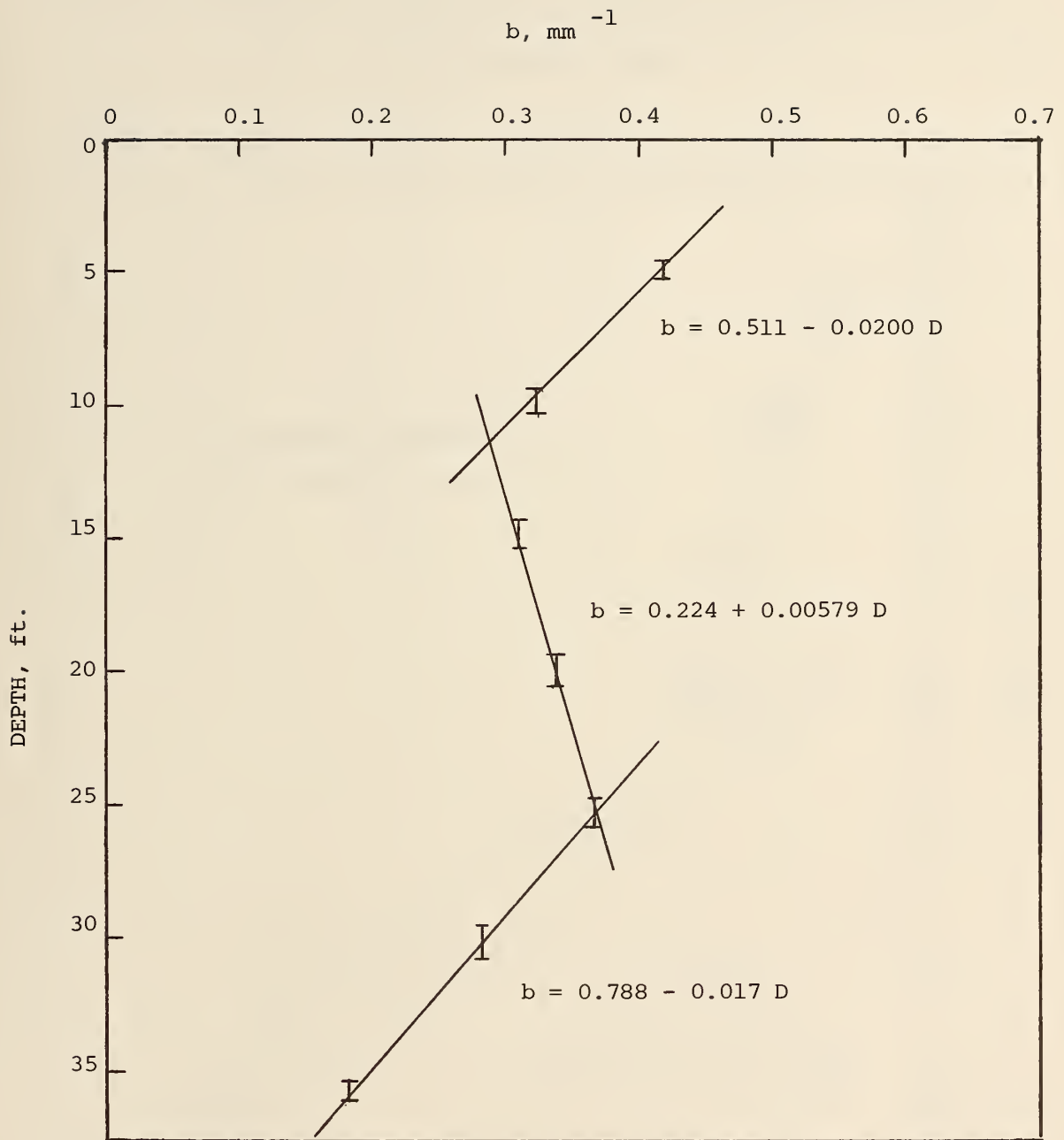
Figure 52. Fairbank Highway Research Station, McLean, Virginia site "b" values from grouped data.

1 ft = 0.3048 meters

145
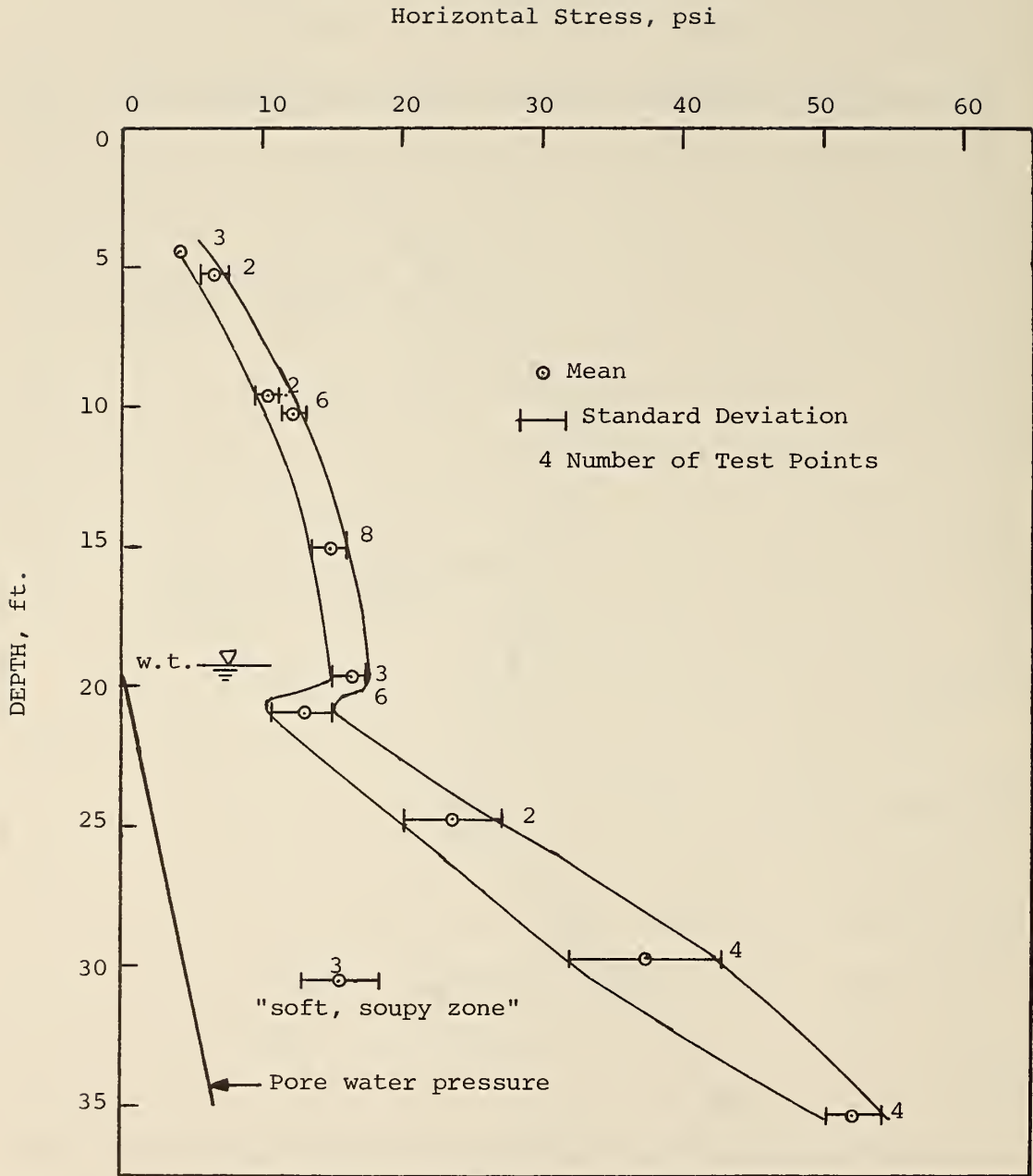
Figure 53. Horizontal stress versus depth, Fairbank site.
1 ft = 0.3048 meters, 1 psi = 70.31 gm/sq cm

146

Table 21. Grouped Data Calculation of $\underline{b}$ Values for Fairbank Site.
1 ft = 0.3048 m., 1 psi = 70.31 gm/sq cm.

Depth Range, ft.	σ_o, psi	b, mm^{-1}	n	r
4.25 – 5.25	4.8	0.418	6	0.85
9.25 – 10.83	11.3	0.324	8	0.97
14.25 – 15.83	15.1	0.309	8	0.94
19.25 – 20.83	13.6	0.339	8	0.80
24.25 – 24.83	17.7	0.367	4	0.69
29.25 – 30.83	24.8	0.284	7	0.41
35.25 – 35.83	53.1	0.180	4	0.98

Table 22. Fairbank Soil Stresses with Linearly Regressed b Data
1 ft = 0.3048 m

| Depth, ft. | Calculated b, mm^{-1} | Horizontal Stress, psi | | | | | |
| | | Boring 1 | | Boring 2 | | Aver. | n |
		A	B	A	B		
4.25	0.428			3.9	4.0	4.0±0.1	3
4.83	0.416			4.0	(9.6)		
5.25	0.408	7.3	5.7			6.5±1.1	2
9.25	0.330			9.8	11.2	10.5±1.0	2
10.25	0.310	11.5	11.9	13.5	12.2	12.3±0.67	6
10.83	0.299	12.4	12.4				
14.25	0.307			16.0	18.0	15.0±1.5	8
14.83	0.310	13.5	14.3				
15.25	0.313	15.1	13.3				
15.83	0.316	15.5	14.5				
19.25	0.336			15.1	(9.6)	16.2±1.1	3
19.83	0.339	17.3	16.2				
20.25	0.341	12.1	13.4			13.1±2.0	6
20.83	0.345	10.6	16.1				
24.25	0.370			11.9	14.3		
24.83	0.367			25.9	21.4	23.7±3.2	2
29.25	0.290			41.1	31.7	37.5±5.4	4
29.83	0.281			34.0	43.0		
30.25	0.273	16.8				15.6±3.0	3
30.83	0.264	17.7	12.2				
35.25	0.188	50.5	52.1			52.5±1.9	4
35.83	0.179	55.1	52.2				

The data in Fig. 53 also can be expressed in terms of K_o based
on calculated overburden stresses. A dry bulk density of 1.50 (94 pcf)
was assumed, and uniform moisture contents of 20% and 30% above and
below the water table, respectively. These calculations are shown in
Table 23, and results are plotted versus depth in Fig. 54. The soil
for the most part appears to be overconsolidated, perhaps from reduction
of overburden pressure through erosion. This would not explain the low
K_o just below the water table elevation. Other possible explanations
previously mentioned include expansion on weathering and relict tectonic stresses.

Table 23.   Fairbank Soil K_O Data

1 ft = 0.3048 m , 1 psi = 70.31 gm/sq cm.

| Aver. Depth, ft. | Pore Water Pressure, psi | Total Stress, psi | | Effective Stress, psi | | K_o |
		σ_v	σ_h	σ_v'	σ_h'	
4.75	0	3.7	4.0	3.7	4.0	1.1
5.25	0	4.1	6.5	4.1	6.5	1.6
9.25	0	7.2	10.5	7.2	10.5	1.5
10.5	0	8.2	12.3	8.2	12.3	1.5
15.0	0	11.8	15.0	11.8	15.0	1.3
19.5	0.4	15.3	16.2	14.9	15.8	1.1
21.8	1.4	17.3	13.1	15.9	11.7	0.7
24.8	2.7	19.8	23.7	17.1	21.0	1.2
29.5	4.8	23.8	37.5	19.0	32.7	1.7
30.5	5.2	24.7	15.6	19.5	10.4	0.5
35.5	7.4	28.9	52.5	21.5	45.1	2.1
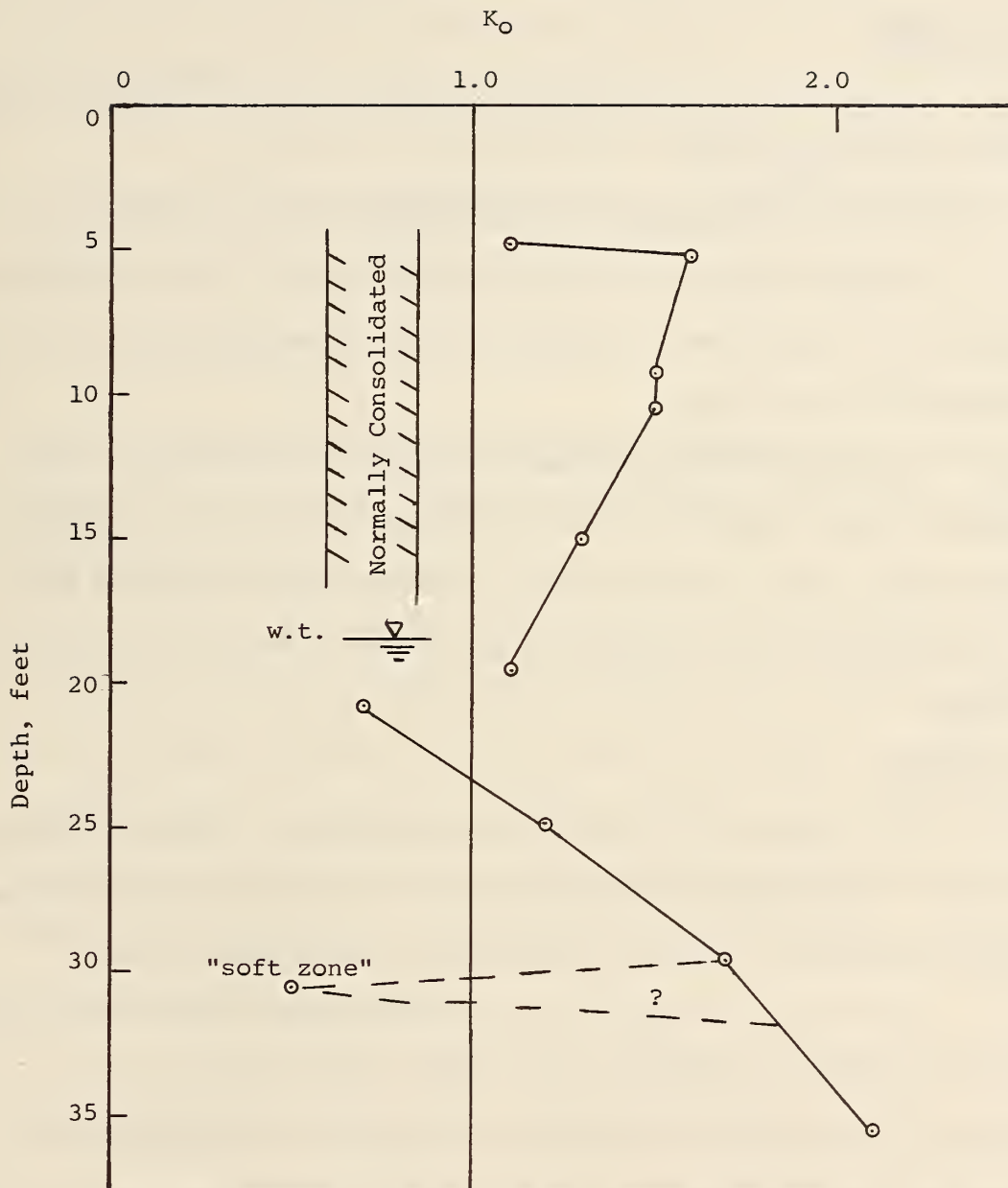
Figure 54. Ko versus depth for Fairbank site.

1 ft = 0.3048 meters

CONCLUSIONS

Blade Design:

1. A 60 degree apical wedge angle minimizes stress increases in soil caused by blade insertion.

2. Smooth blades produce less disturbance than rough blades.

3. The sensor should be located approximately 15 blade thicknesses from the end of the blade to minimize effects of the active shear zone developed around the blade.

4. The Teflon-diaphragm pneumatic stress cell developed in this research is thin, precise, accurate, sensitive, and simple in operation. The fabrication costs for thin blades to carry several cells are high, and consideration should be given to use of an electrical strain-gaged diaphragm.

Test Results:

5. Soil stresses on the blade are an exponential function of blade thickness. Thus measuring stresses with two different blade thicknesses allows extrapolation to give the stress on a zero-thickness blade.

6. In hard soils the thick (1/4 inch) blade consistently gave lower stresses than did the thinner blades. This is not in keeping with the exponential relationship, and indicates a change in soil behavior with the thicker blade. Future instruments therefore should omit the 1/4-inch blade if it is to be used in hard soils.

7. Tests with the stepped blade sensor are rapid and produce replicated data that is highly advantageous for statistical treatment. The following tentative procedure was developed for interpretation of test results:

a. Each data set incorporating results from different blade thicknesses at a given position is fit to an exponential equation of the form

$$\sigma_s = \sigma_o e^{bt}$$

where σ_s is the blade stress, t the blade thickness, and σ_o and b the regression coefficients. The σ_o also represents an initial estimate of zero-blade-thickness stress.

b. The "b" slope data are examined for consistency, trends, and relation to soil type. Tests made to date indicate that b usually will be in the range 0.120 mm^{-1} for soft soils to 0.480 mm^{-1} for hard, dense, compact soils. If b values are highly variable or fall outside of this range or do not agree with observations relative to the soil, data within depth intervals should be pooled and exponentially regressed to obtain better estimates of b.

c. The b values obtained by regression are placed with individual stress readings to give a revised estimate of insitu stress:

$$\sigma_o = \sigma_s e^{-bt}$$

d.   The in situ stresses may be graphed and treated statistically by depth increments, plotted versus depth, and/or used to calculate the coefficient of earth pressure, K_o.

Comparative Data:

8.   Pressuremeter data from two of the test sites, one in glacial till and loess, and the other in expansive clay, indicate very close agreement with blade stress results.   The blade is easier to use than the pressure-meter, particularly in the self-boring versions, and because of its statistical advantage is more precise.

Future Designs:

9.   Based on results described in this report, a three-bladed stepped vane with 9 pressure cells has been successfully designed, built and tested in preliminary trials.   Results with that device are appended to this report.

10. For future blades it is recommended that a piezometer be installed to allow monitoring of pore water pressure, in order that effective stresses may be calculated instead of being inferred from the depth below the observed ground water table.

FIELD TESTING PROCEDURES

(1)   A hole is advanced to approximately one foot above the desired testing depth.

(2)   The blade is pushed hydraulically until the first section has fully penetrated the soil mass, a distance of 9 inches. The drill rod is then lifted to remove load from the blade by means of a slip-joint inserted between the drill rod and the blade.

(3)   The gas supply valve is opened to the first blade section.

(4)   The pressure regulator is turned slowly to provide a uniformly increasing pressure.

(5)   When significant return flow is indicated by the flow meter, the pressure reading is noted and the system depressurized.

(6)   Steps (2) through (5) are repeated for successive blade sections.

REFERENCES

1. Alpan, I. "The Empirical Evaluation of the Coefficient Ko and Kor." Soil and Foundation, 7, No. 1 (1967), 31-40.

2. American Society for Testing and Materials. 1969 Annual Book of ASTM Standards. Part II. Philadelphia, Pa.: American Society of Testing and Materials, 1969.

3. Baguelin, F., J. F. Jezequel, E. LeMee, and A. Lemehaute. "Expansion of Cylindrical Probes in Cohesive Soils." Journal of the Soil Mechanics and Foundation Engineering Division, 98, No. 11 (1972), 1129-1142.

4. Baguelin, F., J. F. Jezequel, and A. Lemehaute. "Self-Raising Placement Method of Soil Characteristics Measurements." Proc. ASCE Speciality Conference on Subsurface Explorations for Underground Excavation and Heavy Construction, Henniker, N. H., 1974, pp. 312-332.

5. Baguelin, F. and J. F. Jezequel. "Further Insights on the Self-Boring Technique Developed in France." Proc. ASCE Speciality Conference on In Situ Measurement of Soil Properties, Raleigh, N. C., 2 (1975), 231-243.

6. Baligh, Mohsen M. and Ronald F. Scott. "Quasi-Static Deep Penetration in Clays." Journal of the Geotechnical Engineering Division, 101, No. 1 (1975), 1119-1133.

7. Bishop, A. W. "Test Requirements for Measuring the Coefficient of Earth Pressure at Rest." Proc. Brussels Conf. on Earth Pressure Problems, (1958), 2-14.

8. Bjerrum, L., J. K. Nash, R. Kennard, and R. S. Gibron. "Hydraulic Fracturing in Field Permeability Testing." Geotechnique, 22, No. 2 (1972), 319-332.

9. Broms, B. B. and J. O. Silberman. "Skin Friction Resistance to Piles in Cohesionless Soils." Sols-Soils, No. 10 (1964), 33-43.

10. Brooker, Elmer W. and Herbert O. Ireland. "Earth Pressures at Rest Related to Stress History." Canadian Geotechnical Journal, 2, No. 1 (1965), 1-15.

11. Carroll, Dorothy. Clay Minerals: A Guide to Their X-ray Identification. Geological Society of America, Boulder Colo., Special Paper 126, 1974.

12. Clark, J. I. and G. G. Meyerhof. "The Behavior of Piles Driven in Clay. II. Investigation of the Bearing Capacity Using Total and Effective Strength Parameters." Canadian Geotechnical Journal, 10, No. 1 (1973), 86-100.

13. Fox, Nathaniel S. "Plan, Program, and Feasibility Study: Determination of the In Situ State of Stress in Soils." Proposal HCP-12, 1976. Marietta, Ga.: Soil Systems, Inc., 1977.

14. Fox, Nathaniel S., Richard D. Barksdale, Richard L. Handy, and Gary D. Trott. "Measuring and Testing Techniques for Determination of the In Situ States of Stress in Soils." Interim Report DOT-FH-11-9172. Marietta, Ga.: Soil Systems, Inc., 1977.

15. Kezdi, Arpad. "Pile Foundations." In Foundation Engineering Handbook, Chap. 19, H. P. Winterkorn and H. Y. Fang, Eds. New York: Van Nostrand Reinhold Company, 1975.

16. Ladanyi, B. and W. J. Eden. "Use of the Deep Penetration Tests in Sensitive Clays." Proc. 7th International Conference on Soil Mechanics and Foundation Engineering, 1 (1969, 225-230.

17. Lambe, T. William and Robert V. Whitman. Soil Mechanics. New York: John Wiley and Sons, Inc., 1969.

18. Lutenegger, Alan James. The Iowa Continuous K-Test: A Laboratory Test for Measuring Lateral Stresses in Soils Induced by Vertical Applied Loads. Unpublished M.S. Thesis. Ames, Iowa: Iowa State University, Library, 1977.

19. Massarsch, K. Rainer. "New Method for Measurement of Lateral Earth Pressure in Cohesive Soils." Canadian Geotechnical Journal, 12, No. 1 (1975), 142-146.

20. Massarsch, K. R., R. D. Holtz, B. G. Holm, and A. Fredriksson. "Measurement of Horizontal In Situ Stresses." Proc. ASCE Specialty Conference on In Situ Measurement of Soil Properties. Raleigh, N.C., 1 (1975), 266-286.

21. Massarsch, K. Rainer and Bengt B. Broms. "Lateral Earth Pressure at Rest in Soft Clay." Journal of the Geotechnical Engineering Division, 102, No. 10 (1976), 1041-1047.

22. Meyerhof, G. G. "The Ultimate Bearing Capacity of Foundations." Geotechnique, 2 (1950), 301-331.

23. Meyerhof, G. G. "Compaction of Sands and Bearing Capacity of Piles." <u>Journal of the Soil Mechanics and Foundations Division</u>, 85, No. 6 (1954), 1-30.

24. Meyerhof, G. G. "The Ultimate Bearing Capacity of Wedge Shaped Foundations." <u>Proc. 5th International Conference on Soil Mechanics and Foundation Engineering</u>, 2 (1961), 105-109.

25. Meyerhof, George Greffrey. "Bearing Capacity and Settlement of Pile Foundations." <u>Journal of the Geotechnical Engineering Division</u>, 102, No. 3 (1976), 197-228.

26. Robinsky, E. I. and C. F. Morrison. "Sand Displacement and Compaction Around Model Friction Piles." <u>Canadian Geotechnical Journal</u>, 2, No. 1 (1964), 81-93.

27. Robinsky, E. I., W. L. Sagar, and C. F. Morrison. "Effects of Shape and Volume on the Capacity of Model Piles in Sand." <u>Canadian Geotechnical Journal</u>, 1, No. 4 (1964), 189-204.

28. Sanglerat, G. <u>The Penetrometer and Soil Exploration</u>. Amsterdam: Elsevier Publishing Company, 1972.

29. Spangler, Merlin G. and Richard L. Handy. <u>Soil Engineering</u>. New York: Intext Educational Publishers, 1973.

30. Taradash, Samuel. "Structural Supports." <u>Tunnel Construction State of the Art and Research Needs</u>. Mildred Clark, Ed. Transportation Research Board, Special Report 171, 1977.

31. Tavenas, F. A. "In Situ Measurement of Initial Stresses and Deformation Characteristics." Proc. ASCE Specialty Conference on In Situ Measurement of Soil Properties, Raleigh, N.C., 2 (1975), 263-271.

32. Tavenas, F. A., G. Blanchette, S. Levoueil, M. Roy, and P. La Rochelle. "Difficulties in the In Situ Determination of K_o in Soft Sensitive Clays." <u>Proc. ASCE Specialty Conference on In Situ Measurement of Soil Properties</u>, Raleigh, N.C., (1975), 450-476.

33. Terzaghi, Charles. "Old Earth Pressure Theories and New Test Results." Engineering News Record, 85, No. 14 (1920), 132-637.

34. Terzaghi, Karl. <u>Theoretical Soil Mechanics</u>. New York: John Wiley and Sons, Inc., 1943.

35. Terzaghi, K. and R. B. Peck. Soil Mechanics in Engineering Practice, New York: John Wiley and Sons, Inc., 1967.

36. Tschebotarioff, Gregory P. Foundations, Retaining and Earth Structures. New York: McGraw-Hill Book Company, 1975.

37. Vesic, Aleksandar B. "Bearing Capacity of Deep Foundations in Sand." Highway Research Board, 20 (1963), 112-153.

38. Vesic, Aleksandar S. "Ultimate Loads and Settlements of Deep Foundations in Sand." Bearing Capacity and Settlement of Foundations. A.S. Vesic, Ed. Durham, N.C.: Duke University Press, 1965.

39. Vesic, Aleksandar Sedmark. "Expansion of Cavities in Infinite Soil Mass." Journal of the Soil Mechanics and Foundations Division, 98, No. 3 (1972), 265-290.

40. Vesic, Aleksandar S. "Bearing Capacity of Shallow Foundations." In Foundation Engineering Handbook, Chap. 3, H.F. Winterkorn and H.Y. Fang, Eds. New York: Van Nostrand Reinhold Company, 1975.

41. Wissa, Anwar E. Z., R. Torrence Martins and John E. Garlanger. "The Piezometer Probe." Proc. ASCE Specialty Conference on In Situ Measurement of Soil Properties, Raleigh, N.C., 1 (1975), 536-545.

42. Wroth, C. P. "In Situ Measurement of Initial Stresses and Deformation Characteristics." Proc. ASCE Specialty Conference on In Situ Measurement of Soil Properties, Raleigh, N.C., 2 (1975), 181-230.

43. Marchetti, Silvano. "In Situ Tests by Flat Dilatometer." Journal of the Geotechnical Engineering Division, 106, No. GT3, (1980), 299-321.

44. Feist, Michael. "Pressuremeter vs. Laboratory Testing for Deep Foundation Settlement Analysis." Unpubli. M.S. Thesis, Iowa State Univ. Library, Ames, Iowa, 1980.

Appendix A

Vane Stress Test Procedure

Preliminary

The final vane developed in this project consists of three blades, each blade with three thicknesses and cells, giving a total of 9 stress cells. The blades and cells each are numbered 1, 2, and 3. Gas lines and selector valves are numbered with two-digit numbers, the first digit designating the blade, and the second the cell, from thinnest to thickest. Thus line 11 comes from the thinnest section of the first blade; 12 from the middle thickness of the first blade, etc., up to 33, from the maximum thickness of the third blade.

In addition each blade carries a manifolded exhaust line marked "E".

Set-up Procedure

1. Open the console lid and back off the pressure regulator so the handle is loose (Fig. A-2). This is to prevent surge when the gas bottle is turned on. Failure to do this could result in rupture of sensors.

2. Lift console plate by removing the middle thumb screw (Fig. A-2, A-3), and open the gas bottle valve (Fig. A-4). Replace console plate and screw.

3. Connect marked lines to appropriate quickconnects in the console, 11 to 11, etc., (Fig. A-5). Be sure all valves are in the closed (down) position.

4. Connect exhaust line manifold which connects to 3 lines, to the flow gauge desiccator chamber held in the lid of the case (Fig. A-6). Open the flow gauge valve several turns. (This valve is kept closed during storage to preserve the silica gel desiccant.)

5. If not previously attached, connect numbered gas lines to corresponding numbered fittings on the blade (Fig. A-7).

6. Drill a 6-inch diameter hole in soil, to just above the first desired testing depth.

7. Connect vane to the slip connector (Fig. A-8) which in turn connects to A (or AW) drill rod with an adapter. Orient the vane in the hole and note the orientation on a sketch. Lower vane to rest on the bottom of the hole, being careful not to stretch or foul the gas lines.

8. Mark off a 9-inch increment for hydraulic pushing of the vane by the drilling machine, and push the vane 9 inches. Then lift the drill rod about 1 inch, to remove rod weight from the vane. The slip connector is included between the vane and the drill string for this purpose.

First-Position Readings

9. All toggle valves in the console normally are closed (handles horizontal), and the pressure regulator handle is unscrewed to be loose. Open one valve (Fig. A-9) and slowly screw in the pressure regulator (Fig. A-10) while watching the gauge and the flowmeter ball. When the ball jumps (Fig. A-11) read the pressure gauge (Fig. A-12) and immediately back off the regulator. Repeat this procedure one or two more times. Record all readings. Readings should agree to ± 1 psi. An excessive flow "blow-by" usually damages the sensor diaphragm and it must be replaced; see below.

10. Back off the regulator until the gauge reads zero pressure, close the open valve and open the next valve (Fig. A-13) and repeat the test. Continue until all valves have been read.

<u>Advance Readings</u>

11.   Push the vane 7 inches for the second set of readings, lift off the rod weight and repeat the test for valves 11, 21, 31, and 12, 22, 32.

12.   Push the vane 9 inches for the third set of readings, and repeat the test for valves 12, 22, 32, and 13, 23, 33.   Care should be taken not to overpush the device on the last test as this can cause a stress increase.

13.   Close all selector valves, back off the regulator, pull the vane, and clean it off.   Auger bore to the next testing depth and repeat starting with step 6.

<u>Interpretations</u>

The above testing sequence gives pressure data at two depths 9 inches apart: The first is 6 inches below the bottom of the hole and is read on 3 sensors on three blades.   The second depth is 13 inches below the bottom of the hole and is tested on three blades but with only sensors 1 and 2. This procedure may be diagramed as follows:

```
First push, read:  11, 21, 31.⤶┐◄─── Data combinations
Second push, read: 11, 21, 31. │ ⤶┐   for 6-inch depth.
                   12, 22, 32.◄┤ ├◄──Data combinations
Third push, read:  12, 22, 32. │ ⤶┘   for 13-inch depth.
                   13, 23, 33.◄┘
```

An abbreviated procedure may be used wherein only a single depth is tested:

```
First push, read:  11, 21, 31.⤶┐     Data combinations
Second push, read: 12, 22, 32.◄┤     for 6-inch
Third push, read:  13, 23, 33.⤶┘     test depth.
```

Note that in each performance sequence only the first digit changes, i.e. the blade number changes but the thickness remains the same.

Replacing the Sensor Diaphragms

Sensor diaphragms are preformed Teflon discs. They may become cut or perforated through use, especially if sharp rocks or dense sharp sand are encountered.

Improper diaphragm seating is indicated by consistently low readings.

Cut or damaged diaphragms give no return and no reading.

To replace a diaphragm:

1. Insert the special punch into one of the three holes in the back of the blade opposite the damaged sensor, and tap lightly with a hammer (Fig. A-14). Move to the second and third holes and repeat. This forces out the diaphragm retainer ring.

2. Clean off the perforated sensor face and wipe with light oil.

3. Position the new diaphragm and retainer ring (Fig. A-15) and push into place with the C-clamp vise. Be sure the ring is fully seated and the diaphragm has not been cut by the ring edge. Full seating is important in that no part of the retainer ring should protrude above the face of the blade.

It is a simple matter to replace the sensor diaphragm. When in doubt, replace the diaphragm!

Manufacture of Sensor Diaphragms

1. Place Teflon sheet on the punch anvil (Fig. A-16) and set on guide ring (Fig. A-17).

2. Drive special punch (Fig. A-18) to cut out disc (Fig. A-19).

3. Place disc on the forming anvil (Fig. A-20).

4. Place forming die on top (Fig. A-21), hammer sharply (Fig. A-22), and remove the formed disc (Fig. A-23).
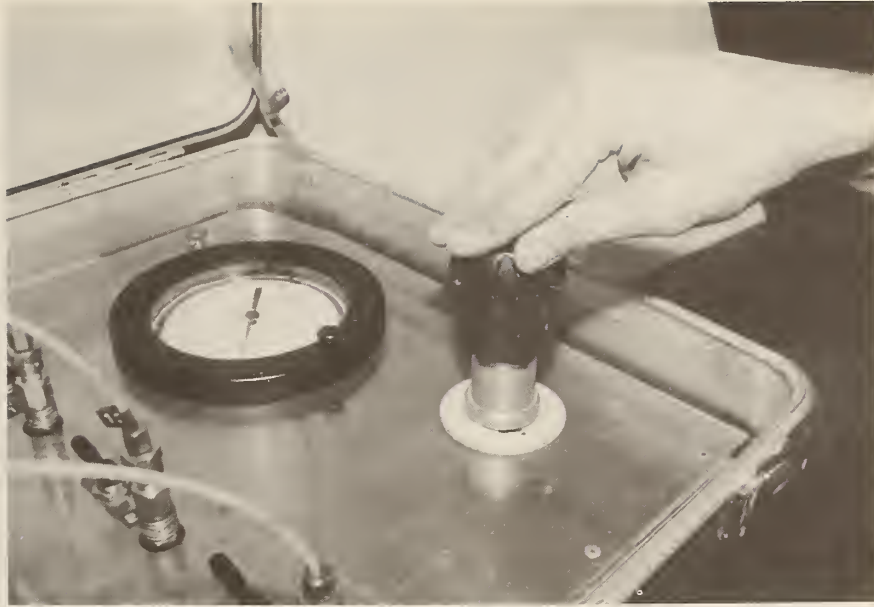
Fig. A-1. <u>Assembly</u>: Console pressure regulator is turned counterclock-
wise so knob is loose, so no pressure will be applied during
hook-ups.

Fig. A-2. Remove middle screw to open console deck.
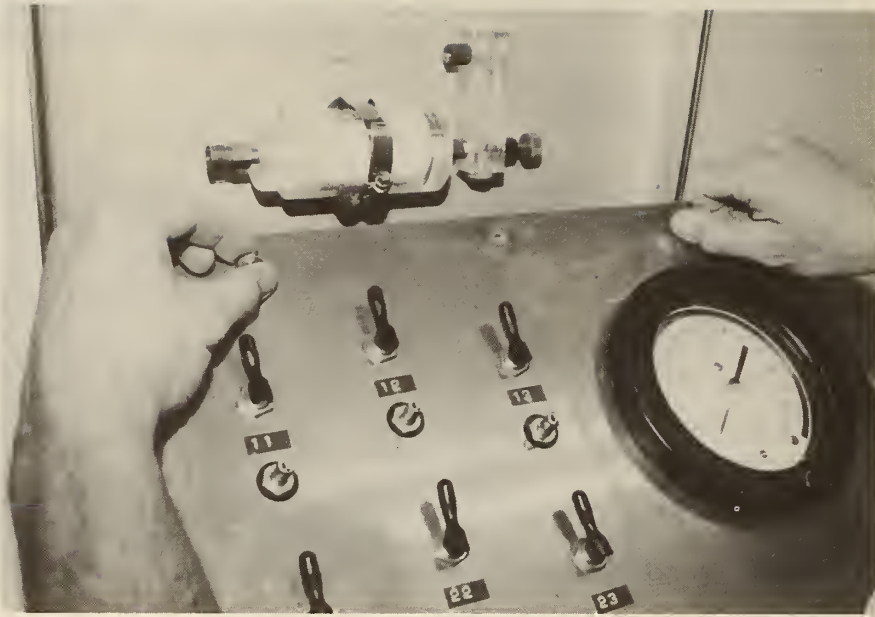
Fig. A-3. Deck is lifted for access to CO_2 gas cylinder.

Fig. A-4. Turn on gas.
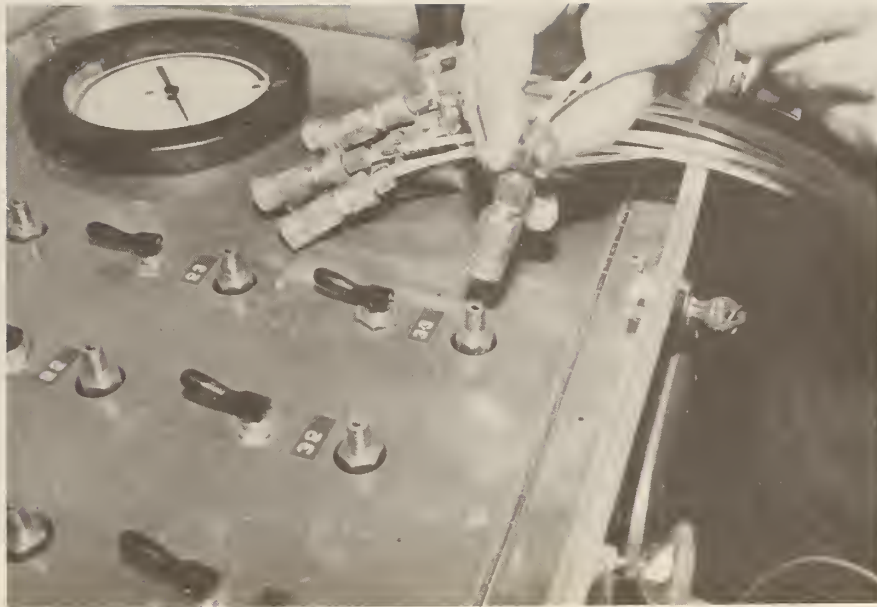
Fig. A-5. Connect numbered lines to appropriately numbered quick-disconnects.
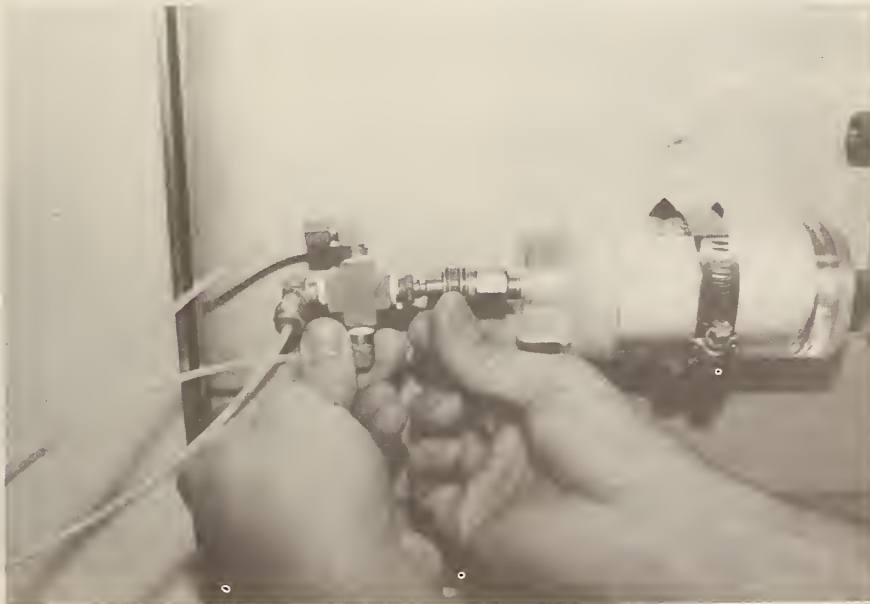
Fig. A-6. Connect return line manifold to desiccator.

Fig. A-7. If not previously done, connect numbered lines to appropriately numbered elbows on the vane.

Fig. A-8. Vane is fastened to an special connector which allows drill rod weight to be lifted off the vane. Assembly is then attached to any conventional rotary exploration drilling machine.

168

Fig. A-9. Measurement: Toggle valve is opened to transmit gas pressure
to a pressure cell.

Fig. A-10. Pressure is slowly
increased to the selected cell
while the return flow is
monitored on the flow gauge.
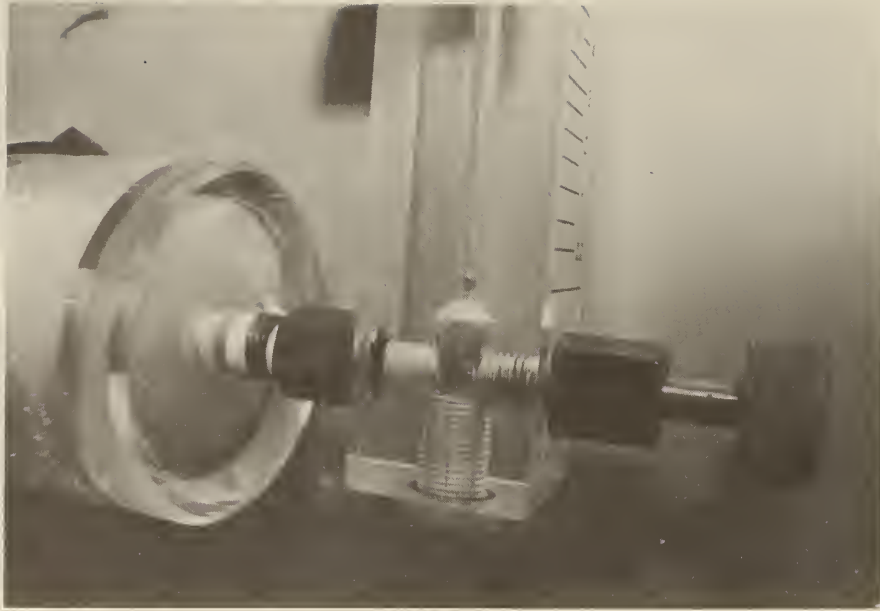
Fig. A-11.   A rising ball indicates return flow.

Fig. A-12.   The pressure gauge is immediately read and the reading recorded.

Fig. A-13. Procedure is repeated for the next pressure cell.

Fig. A-14. <u>Diaphragm replacement</u>: Remove press ring by carefully driving
a small punch through three holes on the back of the blade.

Fig. A-15.   Hold a new diaphragm and the press ring in place.   The ring
             is pushed down with a special C-clamp (not shown).

Fig. A-16.   <u>Diaphragm manufacture</u>:   Teflon sheet is laid on the punch anvil.

Fig. A-17. Guide is placed on top.

Fig. A-18. Punch is driven.
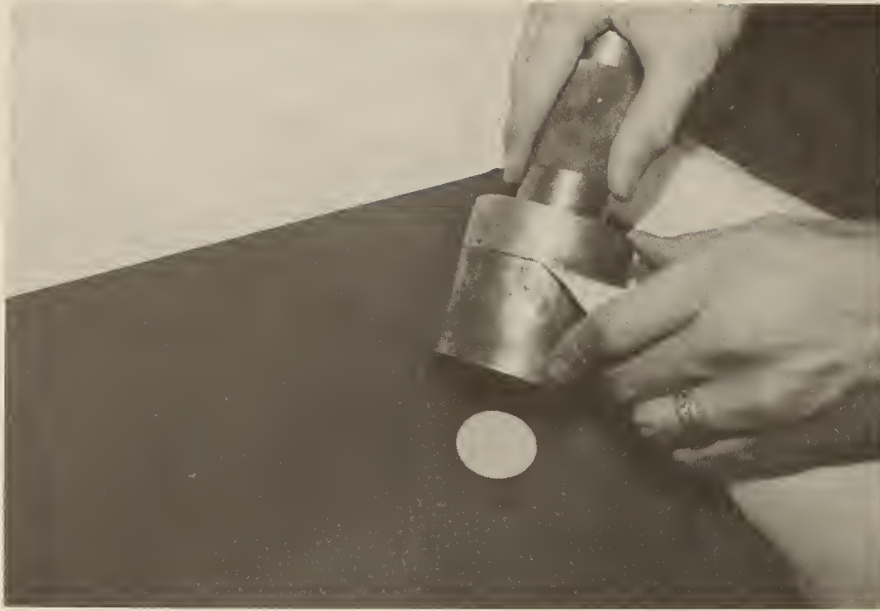
Fig. A-19. Diaphragm disc falls through.

Fig. A-20. Disc is placed on a special forming die.

Fig. A-21. Top of die is put in place.

Fig. A-22. Die is hit gently with a hammer.

Fig. A-23. Disc, now cupped at the edge, is removed.

Appendix B

Data Interpretation--Three-Bladed Vane

1. As discussed in the Report, in situ stresses are evaluated by means of exponential least-squares regression of the type

$$\sigma = \sigma_o e^{bt}$$

where

σ = measured blade stress, FL^{-2}

t = blade thickness, L

b = a constant indicative of soil stiffness, L^{-1}

σ_o = in situ stress for zero blade thickness, FL^{-2}

The regressions are readily performed with a hand-held advanced programmable calculator or any of the more sophisticated computational devices. Tentative on-the-spot interpretations are possible, but the results should be carefully reviewed before final acceptance.

2. The most important part of the interpretation is the evaluation of the constant $\underline{b}$, which may be examined for reasonableness and consistency. The value of $\underline{b}$ varies from 0 for soft, plastic silts to about 0.4 mm^{-1} (10 $in.^{-1}$) for compact, dense soils, and even higher if the blade is pushed close to a rigid inclusion. A tentative procedure to evaluate $\underline{b}$ from three-blade data is as follows:

(a) Perform exponential regressions on each blade data set.

(b) Examine the resulting correlation coefficients. Reasonable b
data with high r values should be averaged.

(c) Use the averaged b with individual cell pressure readings
to obtain individual extrapolated zero-thickness pressures:

$$\sigma_o = \sigma e^{-bt}$$

(d) Examine the resulting calculated stresses for trends. Data
not showing directional or depth trends may be averaged to obtain mean
stresses and standard deviations.

3. This procedure is based on the assumption that the soil response
to variable thickness blades, indicated by the stiffness parameter b
(which is the slope of the exponential relationship), is more likely to
be uniform than the individual cell pressure readings, which are readily
influenced by nonhomogeneity in the soil. Enough data are generated at
each testing depth that valid sets should be obtained to give b. Finally,
the value of b should be examined to see if it is in the correct range
for the soil tested. This gives a two-way check of data reliability:
Is b reasonable; is σ_n reasonable and/or possible? (For example, a σ_n
less than the pore water pressure is highly improbable.)

Example Calculations

Data Sheet

Location: <u>Anita Iowa Elevator</u> By: <u>Handy, Lutenegger, Saye</u> Date: <u>7-8-80</u>

Soil: <u>Alluvium; stratified</u>

Time	Hole Depth	Blade Orientation	Push Distance	Blade Segment	Pressure Readings, psi, Blade No.		
					1	2	3
4:00 pm	10.5'	#1N	9"	1	20,20	20,20	20,20
			7"	1	12,12	12,12	12,12
				2 — A	16,16	16,17	17,17
			9"	2	12,11	15,15	16,16
				3	17,17	22,22	19,20

(bracket B spans segments 1, 2, 2)

4:25 pm

(Data Sheet will repeat for subsequent tests)

Note that only two readings were taken at each cell position, since each data pair was in substantial agreement. The entire set required 25 minutes, which included drilling to the new depth; thus to test a 50-foot hole at 5-foot depth increments should require about 5 hours plus set-up time, or essentially one working day.

The first step in interpretation is to identify data sets, that is, test data that were obtained at essentially the same depth with sequential blade segments. These are shown as A and B above, and should be noted on the field notes. Set A has three tests at 9 in. below the bottom of the

hole; set B has two points at 9 + 7 = 16 in. = 1.33 ft. below the bottom of the hole.

The second step is to draw a table of data for regression analyses, with average data readings reported for the data sets:

Data Set	Blade Segment	x = thickness, in. (mm)	y = average pressure, psi; Blade No. 1	2	3
A	1	1/8 (3.18)	(20)	(20)	(20)
	2	5/32 (3.97)	16	16.5	17
	3	3/16 (4.76)	17	22	19.5
B	1	1/8 (3.18)	12	12	12
	2	5/32 (3.97)	(11.5)	15	16

Inspection of the data is made to insure that sequential blade segments give consistently higher readings, and suspect data are set in parentheses and omitted from the analysis.

The third step is to perform regression analyses with individual sets and blades or arbitrarily pooled data. Inspection indicates a consistent increase in stress from blades 1 through 3, but sets A and B are in fairly close agreement. Since statistical reliability is enhanced by pooling data, sets A and B in this case will be combined for each blade. Results are as follows:

	Blade 1	2	3
r^2	(0.88)	0.97	0.94
r	(0.94)	0.99	0.97
n	3	4	4
σ_0, psi	(6.2)	3.5	4.7
b, mm^{-1}	(0.22)	0.38	0.31

The values for b are inspected for reasonableness and consistency, the b values being indicative of a stiff soil. The low values for b and r for blade 1 indicate the data should be reexamined. Since 2 out of 5 blade 1 points have already been omitted, this test is aborted. It will be seen that the high value for intercept a for blade 1 relates to the relatively low slope b, which in turn relates to the low value, 17 psi, for segment 3.

Results may be reported as follows:

Blade:	1	2	3
Orientation	N	SW	SE
Stress direction	N90E	N30W	N30E
Total Stress, psi	n.d.	3.5	4.7

Blades are numbered counterclockwise, and stresses are normal to blade directions. Thus blade 1, pointed N, measures stress in an EW direction, blade 2, pointed N120W, measures stress N30W, etc. With readings from three orientations, principal stress directions can be determined as for rosette strain gage data.

Calculation of K_o. In order to calculate the coefficient of earth pressure at rest, K_o, the vertical stress must be measured or calculated, and vertical and lateral stresses converted to an effective stress basis. The water table at the above site was at a depth of 12.1 feet, or below the test depth, so total and effective stresses are assumed to be the same.

If the soil unit weight is 120 lb/ft^3,

$$\sigma_v = 120 \times (10.5 + 1) = 1380 \text{ psf} = 9.6 \text{ psi},$$

the average test depth for sets A and B being 1 foot below the bottom of the hole. Values for $K_o = \sigma_h'/\sigma_v'$ are:

	N30E	N30W
K_o:	0.36	0.49

Appendix C

Test Report: 3 Bladed Vane

1. <u>Calibrations</u>. Cells were calibrated after the field tests by
use of a clamp-on chamber and air pressure. Cells operating correctly
show a 1:1 calibration.

Cell	Applied Pressure, psi	Blade			Av. Ratio of Meas: Applied
		1	2	3	
1	10	10	13	10	1.10
	20	18.8	22.3	20.5	1.03
	30	31.2	29.3	30.7	1.01
	40	41.5	40	41.5	1.02
2	10	9	11.2	*	1.01
	20	17 ≠	21	*	1.05
	30	23.5≠	29	*	0.97
	40	28.5≠	35.7	*	0.89
3	10	9.5	11	*	1.02
	20	19.3	21	*	1.01
	30	30	31	*	1.02
	40	40	41.2	*	1.02
			Wtd. Average		1.02

*Return line plugged; no calibration

≠Leaky seal; data not included.

Blade 1 cell 2 gave a low, curvilinear calibration characteristic of a
leaky seal, and a correction graph was prepared for these readings.

Scatter in the other data is attributed to experimental error and non-uniform calibrating pressure. The average calibration constant is 1.02, or nominally 1.0.

2. <u>Blade Thickness</u>. It should be emphasized that the three sections of the vane blades are in equal steps from 1/8 to 3/16 in. (3.175 to 4.762 mm) thick, rather than 1/8 to 1/4 in. (3.175 to 6.35 mm) for the single stepped bladed discussed in the body of this report. The reason for this was the frequent failure of the 1/4 in. (6.35 mm) section to give meaningful results in stiff soils.

3. <u>Soils.</u> The 3-bladed stepped vane was tested in the field in three soils, an soft alluvial silt, a soft loess, and a hard, clayey paleosol (buried soil) underneath the loess. The first was selected for having a known anisotropic loading condition. The soils and sites are as follows:

Location	Site	Soil	Depths	Comments
Anita, Ia.	1	Alluvial Silt	10', 15', 20'	Av. 50' from loaded grain bins.
	2	Alluvial Silt	5, 10, 15, 20'	9.3' from edge of loaded grain bin
	3	Alluvial Silt	5, 10, 15'	Away from bins
Menlo, Ia.	–	Loess	5, 10'	Very soft
Menlo, Ia.	–	Paleosol	17'	Hard, expansive clay

4. Menlo paleosol data.   Since the paleosol, a stiff, heavy,
montmorillonitic clay, is closer in properties to previous soils tested,
these results are presented first.   Data are as follows, parentheses
indicating corrected values for cell 1-2.   Pressures are in psi.   All
data represent averages of 3 readings.

Depth	Cell	Blade		
		1	2	3
17'	1	39.5	29.5	34.0
	2	(41.5)	35.0	41.0
	3	43.0	44.0	55.0
17 1/2'	1	45.5	30.0	44.0
	2	43.0	44.5	51.5

Exponential regressions gave r^2 and slopes $\underline{b}$ as follows:

Depth	Blade		
	1	2	3
17'	1.36; 0.99	6.40; 0.99	7.70; 0.98
17 1/2'	- ; -	6.20; -	5.04; -

Dashes indicate negative slopes or insufficient data.   (A minimum of 3
points is needed for a correlation coefficient.)   The slope data from
blade 1 is dismissed as unrealistic for a dense clay, leaving average

185

<u>b</u> values as follows:

Depth	b, in.$^{-1}$ (mm^{-1})
17'	7.05 (0.278)
17 1/2'	5.62 (0.221)

Exponential extrapolations based on these slopes give the following pressures:

Depth	Cell	Blade Orientation			Aver.
		1 NW-SE	2 E-W	3 NE-SW	
17'	1	<u>16.4</u>	12.2	14.1	14.2
	2	<u>13.8</u>	11.6	13.6	13.0
	3	11.5	11.7	<u>14.7</u>	12.6
		----	----	----	----
	Aver.	13.9	11.8	14.1	σ_h = 13.3$\pm$1.7
17 1/2'	1	<u>22.5</u>	14.9	21.8	19.7
	2	17.9	18.5	<u>21.4</u>	<u>19.3</u>
		----	----	----	
		20.2	16.7	21.6	σ_h = 19.5$\pm$2.9

High values in each set are underlined and show no consistent trend. The data indicate that the lateral pressure is higher and more variable at 17 1/2' than at 17' depth, probably reflective of changes in clay content in the buried soil profile.

Approximate K_o values were calculated based on a water table at
7.5' depth and γ = 125 pcf:

| Depth, ft. | Stress, psi | | | $\sigma_v{'}$ | K_o |
	σ_h	u	$\sigma_h{'}$		
17	13.3	3.2	10.1	10.9	0.9
17 1/2	19.5	3.2	16.3	10.9	1.5

In this table, σ_h represents the measured total stress, u the
calculated neutral stress or pore water pressure, $\sigma_h{'}$ the effective
horizontal stress, and $\sigma_v{'}$ the estimated effective vertical stress.
These values of K_o, while >1, are low for an overconsolidated expansive
clay, but may be relict from when the soil was buried by eolian loess
silt, 20,000 years ago.

This is the first and only known measurement of insitu horizontal
stress in a buried expansive clay paleosol.

5. Menlo loess data. The loess at Menlo in west-central Iowa is
moderately clayey and very soft due to a moisture content well above
the plastic limit, hole closure indicating a close proximity to the
liquid limit. This is the first time such a soft soil has been tested
by the vane stress device, and it may be anticipated that the stiffness
parameter b will be very low and perhaps even zero. The data are as
follows:

Depth, ft.	Cell	Blade		
		1	2	3
5	1	25.5	24.5	21
	2	(28)	20	21
	3	23	23	20
5.5	1	25.5	23.5	22
	2	(38)	18.5	25
10	1	13.5	11	12
	2	(13.5)	11.5	15
	3	17	16	16
10.5	1	16	12.5	12
	2	(23)	18	18.5

Regressions of data sets gave the following values for $\underline{b}$ and (r^2):

Depth, ft.	Blade			Aver.
	1	2	3	
5	-1.65(0.27)	-1.01(0.09)	-0.78(0.75)	1.0 ± 6.9
5.5	12.8 (-)	-7.66(-)	4.09 (-)	
10	3.69(0.75)	6.00(0.84)	4.60(0.91)	4.76 ± 1.16
10.5	11.61(-)	11.67 (-)	13.85 (-)	12.4 ± 1.3

At 5 and 5.5 feet depth the b̲ values often are negative and regression coefficients are very low, indicating that the soil is yielding and not building up stress as a result of blade insertion. The data therefore can be averaged without extrapolation.

At 10 feet depth the average b̲ is 4.76 in^{-1} (0.187 mm^{-1}), not unreasonable for a silt. At 10.5 feet b̲ is phenomenally high, 12.4 in^{-1} (0.488 mm^{-1}), and the data are suspect. However, the data will be processed as if nothing were wrong.

| Depth | Cell | Blade/Orientation | | | Aver. |
		1/E-W	2/NW-SE	3/NE-SW	
5-5.5	All	28.0 ± 5.9	21.9 ± 2.5	21.8 ± 1.9	
		24.7 ± 1.4			
		(omitting 1-2 data)			
10	1	7.4	6.1	6.6	
	2	6.4	5.5	7.1	6.6 ± 0.6
	3	7.0	6.6	6.6	
10.5	1	3.4	2.7	2.5	2.9 ± 0.4
	2	3.3	2.6	2.7	

The E-W readings are consistently higher, so these data are treated separately. Summary values for σ_h and K_o are as follows:

Depth	σ_v	u^*	σ_v'	E-W			N-S		
				σ_h	σ_h'	K_o	σ_h	σ_h'	K_o
5-5.5	4.6	0	4.6	24.7	24.7	5.4	21.8	21.8	4.7
10	8.9	1.2	7.7	6.9	5.7	0.7	6.4	5.2	0.7
10.5	8.9	1.2	7.7	3.4	2.2	0.3	2.6	1.4	0.2

*w.t. at 7.5'. Assumed γ = 125 pcf.

The K_o values at 5-5.5 feet are high, indicative of preconsolidation in spite of the low stiffness. Possible reasons for the high values are as follows:

(a) The location is a field used by county road maintenance for aggregate storage, in which case the soil very well may be preconsolidated. A K_o of 5 suggests the equivalent of about 20 feet thickness of material. More likely, the preconsolidation is from heavy equipment.

(b) The test was conducted in an overconsolidated B horizon. The low stiffness suggests this is unlikely.

(c) The high total stress values are caused by sudden loss of the loess structure and excessive pore water pressures. Successive readings (averages are reported in the tables) did show a slight tendency to decrease with time. A pore pressure transducer integral with the device would help answer this question.

(d) The high stresses are caused by inaccurate determination of stiffness parameter b , perhaps due to the smothering effect of pore water pressure.

The K_o values at 10 feet depth are realistic for a normally consolidated silty clay, indicating that preconsolidation of the upper layer must have been from equipment with limited contact area rather than stockpiled aggregate.

As previously mentioned, the K_o values at 10.5 feet are suspect because of the abnormally high values of b. The cause is not known, but may relate to pore water pressure.

K_o values are slightly higher in an E-W direction, as could easily occur if preconsolidation was from heavy equipment.

6. Anita grain elevator data. The first trials with the new blade were at the Anita grain elevators site, and included some "debugging" and loss of data, especially in Boring 1. Boring 2, adjacent to a loaded grain bin, and Boring 3, at some distance away, were selected for this preliminary analysis. Only the tests at 20 feet depth in each hole are analyzed, selected to be within the zone of influence of the 42-foot diameter loaded bin, but below any major preconsolidation effect from heavy equipment.

Averaged data are as follows:

Boring	Depth	Cell	Blade 1	Blade 2	Blade 3
2	20'	1	24.5	23*	25
		2	(27)	26	22.5
		3	25	28	26
	20.5'	1	37.5	25	35
		2	35	36.5	28
3	20'	1	21.5	17.5	20
		2	(23.5)	20	20.5
		3	28	21.5	25
	20.5'	1	24.5	18	19.5
		2	23.5	22	25

*Blade 2 in Boring 2 faced the grain bin.

Regressions give the following b and r^2 values:

Boring	Depth	Blade 1	Blade 2	Blade 3
2	20'	0.32(0.04)	3.15(0.98)	0.63(0.07)
	20.5'	– (–)	12.11(–)	– (–)
3	20'	4.23(0.97)	3.29(0.97)	3.57(0.83)
		– (–)	6.42(–)	7.95 (–)

Averaging for four underlined values gives $\bar{b} = 3.56 \pm 0.48$ in.$^{-1}$ (0.14 $\pm$ 0.02 mm^{-1}), which appears to be reasonable. Application of this

$\underline{b}$ value gives the following pressures:

Boring	Depth	Cell	Blade		
			1	2	3
2	20'	1	15.7	14.7	16.0
		2	15.4	14.9	12.9
		3	14.4	14.4	13.3
			Av. 15.2	Av. 14.7[*]	Av. 14.1 14.6 $\pm$ 1.0
	20.5'	1	24.0	16.0	22.4
		2	20.1	20.9	16.1
			Av. 22.0	Av. 18.5[*]	Av. 19.2 19.9 $\pm$ 3.3
3	20'	1	13.8	11.2	12.8
		2	13.5	11.5	11.7
		3	14.4	11.0	12.8
	20.5'	1	15.7	11.5	12.5
		2	13.5	12.6	14.3
			Av. 14.2	Av. 11.6	Av. 12.8 12.8 $\pm$ 1.4

[*]Blade 2 was oriented facing the closest grain bin. $\pm$ entries indicate standard deviations.

The data show that the highest stress in Boring 2 is not on Blade 2, facing the close grain bin, but on Blade 1, which is at an angle but facing another bin farther away. The difference is not appreciable, and less than the anisotropy of the Boring 3 data, presumed to be away from the influence of the bins. The full bins exert a nominal floor

load of 13.5 psi and had a footing design pressure of 13.8 psi.
Settlements in excess of 6 inches were predicted and appear to have
occurred. Thus any directional stress anisotropy ordinarily predict-
able from theory of elasticity may be lost due to plastic deformations
of the relatively soft alluvial silt.

Comparison of the Boring 2 and Boring 3 data show a significant
difference in average horizontal stress, and some stress variations
with depth in Boring 2. This also is shown in the calculated values
for K_o:

Boring	Depth	σ_v	u^*	σ_v'	σ_h	σ_h'	K_o
2	20'	17.6	0.8	16.8	14.6	13.8	0.82
	20.5'	17.6	0.8	16.8	19.9	19.1	1.14
3	20–20.5'	17.6	3.5	14.1	12.8	9.3	0.66

*Water table at 18.5' in Boring 2; 12.1' in Boring 3. Assumed
$\gamma = 125$ pcf.

We may conclude that the silt adjacent to the grain bin is over-
consolidated but shows no significant directionality in horizontal
stress. The value of K_o in Boring 3 away from the bin is character-
istic of a normally consolidated fine-grained alluvium. At 20' depth
10 feet from a 20' radius surface load, the elastic solutions of Foster
and Ahlvin indicate influence coefficients $I_u \approx 0.13$ and $I_h \approx 0.13$,
which suggests the loaded bin increases both horizontal and vertical
stresses by about 1.8 psi. Since this was not taken into account for

calculation of the vertical stress, it may be subtracted from σ_n'
(assuming u from the standing water level is a valid measurement) to
give pre-load Boring 2 stresses:

Depth 20', σ_n' = 13.8 - 1.8 = 12.0 psi

20.5', σ_n' = 19.1 - 1.8 = 17.3 psi

The first value is very close to the 12.8 psi measured away from
the bin. The second is high, perhaps reflecting an uneven layer
transmission of horizontal stress, i.e. a stiffer layer. This also is
indicated by the b values in a preceding table.

7. Conclusions of Trials with the 3-Blade Stepped Vane.

(a) Properly functioning pneumatic pressure cells calibrate with a
factor of 1.0 against air pressure.

(b) The thinner blade thicknesses in this vane successfully avoid
problems of bad readings from the thicker (1/4 in.) blades. Yet the
thin blades have sufficient structural strength because of integration
into a 3-bladed vane. (The thicker single blade experienced some
bending with resulting error.)

(c) Horizontal stress data and stiffness values b with the new
vane were reasonable from tests of stiff, overconsolidated clay, soft
loess soil, and alluvial silts. With the soft loess soil the stiffness
parameter b appears to be zero, and stresses may be appreciably in-
fluenced by excess pore water pressure developed from pushing the blade.

(d)   A theoretically correct stress increase was measured next to a recently loaded structure, but no appreciable directional stress anisotropy. This is believed due to non-elastic behavior from large settlement of the structures.

8.   <u>Recommendations for future research</u>.

(a)   More field trials, preferably with comparative data, are needed.

(b)   Pore pressure transducer(s) should be added to the device.

(c)   Because of the high costs of fabrication, consideration should be given to an all-electrical measurement system using diaphragm strain gages.

(d) $\underline{b}$ values should be related to soil data such as penetration test data, etc. It appears likely that empirical relationships exist, based on preliminary observations that higher $\underline{b}$ means stiffer soils.

(e)   Finally, it should be emphasized that since until now the available methods for in situ stress determination have been elaborate, time-consuming, and almost prohibitively expensive, virtually every new test is a research report, because it gives new insight into soil behavior relevant to soil mechanics solutions, soil genesis, and understanding of soils.

Appendix D

Disassembly of the 3-Bladed Vane

1. Extreme care should be used not to allow foreign material to get into the gas lines in the blade. If a line (usually the return line) does become plugged, try blowing it out with gas pressure. If this does not clear the line, repair must be done in the machine shop:

a. Pry out the inner porous disc from the plugged cell. This ruins the disc, which must be replaced. Sometimes the plugging material collects in the manifold part under this disc.

b. Try introducing a thin, flexible wire through the plugged line.

c. If these measures fail, the blade will have to be re-opened on a milling machine for repair. This is about a 1-2 day job for a skilled machinist. Lines in the blade are stainless steel hypodermic needle stock.

2. To replace a blade or remove it for repair, the following procedure is used:

a. Unscrew and remove the tip.

b. Remove 6 screws holding the three hardened steel lead blades, and remove the lead blades.

c. Remove the axial center screw from the upper end. The head of this screw is inside of the female recepticle for the drill rod.

d. Remove six downward-oriented screws holding the blade cap.

e. Remove six laterally-oriented screws holding the three rectangular blade head pieces just under the cap.

f. Remove all screws from the gusset strips between the blades.

g. Pull the blades free from the central spine.

3. Reassembly requires some extra steps in order that all components be axially tight against each other:

a. Install the three hardened steel lead blades on the spine. Leave the screws slightly loose.

b. Line up the three main blades on the spine, install gusset strips and screws, and leave the screws slightly loose.

c. Screw on the tip and tighten.

d. Tighten all screws previously left loose.

e. Install blade head pieces, cap, and center screws.
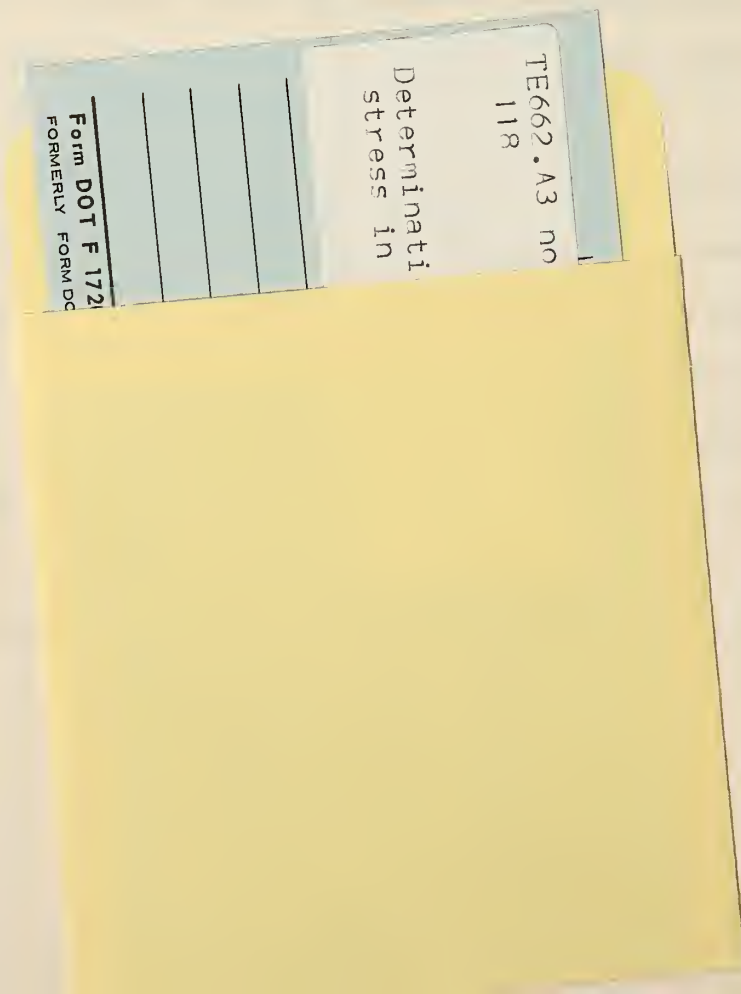
FEDERALLY COORDINATED PROGRAM (FCP) OF HIGHWAY RESEARCH AND DEVELOPMENT

The Offices of Research and Development (R&D) of the Federal Highway Administration (FHWA) are responsible for a broad program of staff and contract research and development and a Federal-aid program, conducted by or through the State highway transportation agencies, that includes the Highway Planning and Research (HP&R) program and the National Cooperative Highway Research Program (NCHRP) managed by the Transportation Research Board. The FCP is a carefully selected group of projects that uses research and development resources to obtain timely solutions to urgent national highway engineering problems.*

The diagonal double stripe on the cover of this report represents a highway and is color-coded to identify the FCP category that the report falls under. A red stripe is used for category 1, dark blue for category 2, light blue for category 3, brown for category 4, gray for category 5, green for categories 6 and 7, and an orange stripe identifies category 0.

FCP Category Descriptions

1. **Improved Highway Design and Operation for Safety**

   Safety R&D addresses problems associated with the responsibilities of the FHWA under the Highway Safety Act and includes investigation of appropriate design standards, roadside hardware, signing, and physical and scientific data for the formulation of improved safety regulations.

2. **Reduction of Traffic Congestion, and Improved Operational Efficiency**

   Traffic R&D is concerned with increasing the operational efficiency of existing highways by advancing technology, by improving designs for existing as well as new facilities, and by balancing the demand-capacity relationship through traffic management techniques such as bus and carpool preferential treatment, motorist information, and rerouting of traffic.

3. **Environmental Considerations in Highway Design, Location, Construction, and Operation**

   Environmental R&D is directed toward identifying and evaluating highway elements that affect

the quality of the human environment. The goals are reduction of adverse highway and traffic impacts, and protection and enhancement of the environment.

4. **Improved Materials Utilization and Durability**

   Materials R&D is concerned with expanding the knowledge and technology of materials properties, using available natural materials, improving structural foundation materials, recycling highway materials, converting industrial wastes into useful highway products, developing extender or substitute materials for those in short supply, and developing more rapid and reliable testing procedures. The goals are lower highway construction costs and extended maintenance-free operation.

5. **Improved Design to Reduce Costs, Extend Life Expectancy, and Insure Structural Safety**

   Structural R&D is concerned with furthering the latest technological advances in structural and hydraulic designs, fabrication processes, and construction techniques to provide safe, efficient highways at reasonable costs.

6. **Improved Technology for Highway Construction**

   This category is concerned with the research, development, and implementation of highway construction technology to increase productivity, reduce energy consumption, conserve dwindling resources, and reduce costs while improving the quality and methods of construction.

7. **Improved Technology for Highway Maintenance**

   This category addresses problems in preserving the Nation's highways and includes activities in physical maintenance, traffic services, management, and equipment. The goal is to maximize operational efficiency and safety to the traveling public while conserving resources.

0. **Other New Studies**

   This category, not included in the seven-volume official statement of the FCP, is concerned with HP&R and NCHRP studies not specifically related to FCP projects. These studies involve R&D support of other FHWA program office research.

---

* The complete seven-volume official statement of the FCP is available from the National Technical Information Service, Springfield, Va. 22161. Single copies of the introductory volume are available without charge from Program Analysis (HRD-3), Offices of Research and Development, Federal Highway Administration, Washington, D.C. 20590.